Chapter 9

REACTIVE TRANSPORT MODELING OF ACIDIC METAL-CONTAMINATED GROUND WATER AT A SITE WITH SPARSE SPATIAL INFORMATION

Pierre Glynn

U.S. Geological Survey
432 National Center,
Reston, Virginia 22091 U.S.A.

James Brown

U.S. Geological Survey
375 S. Euclid Avenue
Tucson, Arizona 85719 U.S.A.

INTRODUCTION

The construction of a multispecies reactive transport model used to predict the future evolution and movement of ground-water contaminants requires, at a minimum, three separate but related elements: (1) an understanding of the ground water flow system and its possible transients, (2) an understanding of the dispersive processes and other processes causing observed dilution or "mixing" of different water types, and (3) an understanding of the primary processes controlling the reactions of the various contaminants, not only across various phases but also within the ground water itself. The degree of understanding of all three of these elements, and perhaps more importantly an appreciation for the remaining knowledge gaps, will be essential in determining not only the usefulness of the constructed model but perhaps also its purpose. Indeed, even though a ground-water model may not adequately predict the future evolution of a contaminant plume, the construction of the model and its use may often result in an improved understanding of contaminant transport at the site.

Most ground-water contamination sites have less geochemical and hydrogeologic information known about them than may be desirable for predictive modeling of reactive contaminant transport. Detailed hydrogeologic and geochemical studies are usually much too expensive to consider*. The resulting lack of knowledge, on the operative chemical and hydrologic processes at a given site, means that investigations should try to use, as efficiently as possible, all tools and knowledge available. It is our belief that a combination of inverse and forward modeling of ground-water flow, inverse and forward modeling of advective/dispersive transport, and inverse and forward modeling of the geochemical evolution of the contaminated ground waters may often provide the greatest knowledge gains for the least amount of money and time. In particular, geochemical inverse modeling should be used first, prior to forward geochemical modeling, both to explain the currently observed ground-water chemistry in the aquifer system, and to make predictions on the future chemical evolution of the ground waters.

* Studies at the Cape Cod (LeBlanc, 1984) and Borden sites (Mackay et al., 1986) are examples of what we would consider detailed studies. On the order of 10^3 to 10^4 sampling points were installed to study plumes on the order of 10^2 meters to a few kilometers long. However, even at these sites many questions remain regarding the operative geochemical and hydrogeologic processes, and even after more than a decade, studies continue to refine and improve the existing knowledge.

0275-0279/96/0034-0009$05.00

This paper focuses on geochemical modeling and will show how both inverse and forward geochemical modeling approaches were used to better understand the evolution of acidic heavy-metal contaminated ground waters in the Pinal Creek basin, near Globe Arizona. The Pinal Creek basin is a site with sparse spatial information (30 wells distributed in a 15 km long and 10^2 to 10^3 m wide sulfate plume) and with significant temporal variations in both chemical and hydrological characteristics (water-table movements of more than 15 m during a three month period, ground-water velocities on the order of 3 to 5 m/day; Brown and Harvey, 1994). The Pinal Creek site is therefore eminently suited to test our modeling philosophy.

INVERSE GEOCHEMICAL MODELING: BASIC THEORY

Inverse geochemical modeling uses existing ground-water chemical and isotopic analyses, which are assumed to be representative of the chemical and isotopic evolution of a ground-water along a given ground-water flow path, and attempts to identify and quantify the reactions that may have been responsible for the chemical and isotopic evolution of the ground water along the flow path. Although an aqueous speciation code may be used to identify thermodynamically possible (or impossible) reactions and to determine the dissolved inorganic carbon content and the redox state (RS) of the ground waters, the inverse modeling approach does not require that reactions proceed to thermodynamic equilibrium. Indeed, mass-balance constraints and the judgment of the user concerning the possibly occurring reactions are the only constraints posed in the inverse modeling approach.

Mathematical formulation: Inverse modeling with the NETPATH computer code

The following discussion is based on Parkhurst and Plummer's (1993) excellent review of geochemical modeling in ground-water environments. Inverse geochemical modeling codes (BALANCE, Parkhurst et al., 1982; NETPATH, Plummer et al., 1991; PHREEQC, Parkhurst, 1995) solve a system of mass balance equations. For the simple case of chemical evolution between an initial and a final water, the mass balance equation for any component i can be written:

$$\Delta(i^{total}) = \sum_{p=1}^{P} b_{p,i}\alpha_p \qquad (1)$$

where $\Delta(i^{total})$ is the change in the total molality of element i between the initial and final waters, $b_{p,i}$ is the stoichiometric coefficient of element i in phase p; α_p is the mass transfer of phase p in moles per kilogram of pure water; and P is the total number of phases. The $\Delta(i^{total})$ concentration changes for each element are known or can be calculated; the reacting phases and stoichiometric coefficients $b_{p,i}$ are postulated by the user; the reaction mass-transfers α_p therefore constitute the unknowns to be solved for. The simulated reactions can include mineral dissolution/precipitation reactions, gas dissolution/exsolution reactions, ion exchange reactions or any other heterogeneous reaction (the NETPATH code, however, does not keep a mass balance on hydrogen or on oxygen, and therefore those elemental mass balances will be ignored if the user, for example defines an H^+/Na^+ exchange reaction).

The mass transfer amounts calculated for the postulated heterogeneous reactions in an inverse geochemical model represent the *net* mass transfer amounts between the initial and final waters chosen for that particular model. An inverse geochemical model does not calculate the specific reaction mass transfers that may be occurring at points along the flowpath in between the final and initial waters chosen for the model.

If the inverse modeling problem requires that several chemically or isotopically different waters be mixed together to form the observed final water, the mass balance equations will instead be stated as follows:

$$(i_{final}^{total}) = \sum_{j=1}^{J} \alpha_j (i_j^{total}) + \sum_{p=1}^{P} b_{p,i}\alpha_p \tag{2}$$

where J is the total number of initial waters to be mixed together to form the final water; and α_j are the fractions of each initial solution j. The α_j and α_p values are the unknowns to be solved for. The number of initial waters used in inverse geochemical modeling is usually less than 2.

Because total dissolved inorganic carbon (TDIC) is not usually measured in most ground-water sampling programs, TDIC concentrations must typically be calculated with a speciation program into which alkalinity and pH data have been entered along with other relevant analytical data.

The total element concentrations referred to in Equations (1) and (2) include all oxidation states of any given element in solution. Therefore, an additional "redox state" (RS) mass balance equation is required to ensure that electrons are conserved during any postulated redox processes. The redox state RS of a solution is defined as

$$RS = \sum_{k=1}^{K} \nu_k(k) \tag{3}$$

where K is the total number of redox species, and ν_k is an operational valence assigned to each aqueous species k. The convention introduced by Parkhurst et al. (1982) defines the operational valence of a species as the charge on the species minus the number of hydrogen atoms in the species plus two times the number of oxygen atoms in the species. Plummer et al. (1983) used the additional convention that all redox-inactive species are assigned an operational valence of zero. Similarly to aqueous species, mineral and gas phases can also be assigned an operational valence μ_p. A few examples of operational valences for aqueous species and mineral and gas phases follow: Ca^{2+}, $\upsilon = 0$; Fe^{2+}, $\upsilon = 2$; SO_4^{2-}, $\upsilon = 6$, $H_2S_{(g)}$, $\mu_p = -2$; $FeSO_{4,(s)}$, $\mu_p = 8$. Consequently, the redox mass-balance equation that can be solved along with the element mass-balances represented by Equation (1) is (for a no-mixing problem):

$$\Delta RS = \sum_{p=1}^{P} \mu_{p,i}\alpha_p \tag{4}$$

where ΔRS is the change in redox state between the final and initial solutions.

Although the equations above relate to chemical mass-balances, isotopic mass-balances can also be used to further constrain the amounts and types of different reactions responsible for the chemical evolution of the ground water, as well as solve for the fractions of various initial waters involved in some "mixing" process that may also contribute to the observed chemical and isotopic composition of the final water.

Given a set of I mass-balance equations to solve, a set of P reactant phases can be postulated by the user. The number of reactant phases must necessarily be greater or equal to the number of mass-balance constraints imposed. If $P > I$, NETPATH and PHREEQC will test all possible subsets of I reactions (within the set of P reactions) and will determine whether or not a solution exists for each subset. A solution represents a set of mass-transfer amounts for each of the I reactions present in each subset of P. The user must use his judgment in postulating the possible reactions responsible for the chemical evolution of the ground water. This judgment may be based on knowledge of the mineralogy of the aquifer system, on speciation calculations predicting thermodynamically possible reactions

for the initial and final ground-water compositions, and on a judgment of the kinetics of these reactions in the ground-water environment. More specifically the user must estimate the ground-water travel time between the initial and the final water sampling points and judge whether the travel time will be sufficient for any significant reaction mass-transfers.

NETPATH and PHREEQC will allow the user to place constraints on the direction of the reaction mass transfers, that is the user may specify whether a given phase should be allowed to only dissolve or only precipitate. The user may also force NETPATH to consider only solutions, i.e. mass-transfer models, that incorporate specific reactions [a capability absent in earlier versions of PHREEQC]. In so doing, the user shows his conviction that those specific reactions must be occurring and must be at least partially responsible for the chemical/isotopic evolution of the ground water. Placing such restrictions as well as limiting the total number of specified possible reactions is often essential to narrowing down the number of possible models, and also has the effect of forcing the user to think about the reaction processes that may be causing the chemical and isotopic evolution of the ground-water system. Ideally, the user will be able to narrow the number of possible models down to a single one, that quantifies and best represents, at least from the user's view, the various chemical reactions responsible for the chemical and isotopic evolution of the ground water.

Inverse modeling accounting for uncertainties, water and proton mass-balances: the PHREEQC code

In addition to solving the element and redox state (RS) mole-balance equations used in NETPATH (Eqns. 1-4), PHREEQC solves mole-balance equations for (1) the individual valence states of redox-active elements, (2) alkalinity, (3) water and also solves a charge balance equation for each aqueous solution. In its solution of this expanded set of equations, PHREEQC solves for the mixing fraction α_q of each aqueous solution, the aqueous mole transfers α_r between valence states of each redox element, the heterogeneous mole transfers α_p of minerals and gases and a set of analytical adjustments $\delta_{m,q}$ that account for uncertainties in the analytical data. Parkhurst (1995) provides a complete description of the equations solved by PHREEQC. The generalized mole-balance equation used in PHREEQC (Parkhurst, 1995, 1996) can be written:

$$\sum_{q}^{Q} c_q \alpha_q (T_{m,q} + \delta_{m,q}) + \sum_{r} c_{m,r} \alpha_r + \sum_{p} c_{m,p} \alpha_p = 0 \qquad (5)$$

where $T_{m,q}$ is the total number of moles of element or element valence state m in an initial aqueous solution q; Q is the final aqueous solution number; q = 1 to q = Q - 1 are any number of initial solutions; $\delta_{m,q}$ is the analytical error adjustment to the number of moles $T_{m,q}$ (this analytical adjustment is computed based on the maximum analytical uncertainties specified and the total charge imbalance of the solution); $c_{m,r}$ is the coefficient of the element or element valence state m in the redox reaction r; $c_{m,p}$ is the coefficient in the dissolution reaction p; α_r and α_p are the redox reaction and dissolution reaction mass transfer amounts and α_q is the mixing fraction of solution q. The c_q coefficients are defined so that c_q = 1.0 for $q < Q$ and c_Q = -1.0 for $q = Q$.

By optionally allowing mass-balances on individual element valence states, PHREEQC (in both its inverse and forward geochemical modeling modes) allows the user to specify multiple redox couples and to appropriately select which redox couples (or an Eh measurement) will control redox equilibria for given elements. For example, the user may have measured dissolved Fe(II) instead or in addition to total dissolved Fe, and dissolved sulfide in addition to dissolved sulfate, and may have made many other possible measurements of redox-active species. Several of those measurements will typically

indicate redox disequilibrium in a given water. Those measurements represent valuable information that is often lost when an inverse modeling code like NETPATH or a forward modeling code like PHREEQE or PHREEQM are used. Indeed, those codes normally specify a single redox potential (which may be based on an Eh measurement or on a specific single redox couple, such as the SO_4^{2-}/S^{2-} couple) that applies to all redox-active elements.

The electron balance equation used in PHREEQC can be written:

$$\sum_r c_{e^-,r}\alpha_r + \sum_p c_{e^-,p}\alpha_p = 0 \tag{6}$$

where $c^-_{e,r}$ and $c^-_{e,p}$ represent the number of electrons released/consumed in each redox or phase dissolution reaction.

The alkalinity-balance equation is similar to the general mole-balance equation:

$$\sum_q^Q c_q\alpha_q(T_{Alk,q} + \delta_{Alk,q}) + \sum_r c_{Alk,r}\alpha_r + \sum_p c_{Alk,p}\alpha_p = 0 \tag{7}$$

When alkalinity has not been measured, PHREEQC will determine the alkalinity of a solution from the following equation:

$$T_{Alk,q} = \sum_i c_{Alk,i} m_{i,q} \tag{8}$$

where $c_{Alk,i}$ is the alkalinity contribution of aqueous species i and $m_{i,q}$ is the number of moles of species i in solution q. The alkalinity contribution values, $c_{Alk,m}$, for the master species (also known as basis specis or component species) are chosen such that the reference state for each element of element valence state is the predominant aqueous species at a pH of 4.5. The alkalinity of a solution is determined from a speciation calculation.

The charge imbalance $T_{z,q}$ in an aqueous-solution q is corrected by specifying the analytical error adjustments such that:

$$\sum_m z_m^{tot}\delta_{m,q} = -T_{z,q} \tag{9}$$

$T_{z,q}$ is determined from an aqueous-speciation calculation. For an element or element valence state, z_m^{tot} is the sum of the charge on the master species for that element or valence state plus the alkalinity assigned to the master species, $z_m^{tot} = z_m + Alk_m$. For alkalinity however, z_m^{tot} is -1.0.

The water mole-balance equation used by PHREEQC is:

$$\sum_q^Q \frac{W_{aq,q}}{gfw_{H_2O}} c_q\alpha_q + \sum_r c_{H_2O,r}\alpha_r + \sum_p c_{H_2O,p}\alpha_p + \delta_{H_2O,Q} = 0 \tag{10}$$

where gfw_{H2O} is the gram formula weight of water. $c_{H2O,r}$ and $c_{H2O,p}$ are the stoichiometric coefficients of water in the aqueous redox reactions and in the phase dissolution reactions. $\delta_{H2O,Q}$ is the error adjustment for the number of moles of water in the final aqueous solution Q, but actually accounts for all the uncertainty in the moles of water everywhere in the system.

The analytical error adjustments, $\delta_{m,q}$, computed by PHREEQC are constrained to be smaller than the specified uncertainties $u_{m,q}$:

$$|\delta_{m,q}| \le u_{m,q} \tag{11}$$

Finally, the aqueous-solution mixing-fractions are also constrained to be positive:

$$\alpha_q \geq 0 \tag{12}$$

In its search for possible mass-transfer solutions, PHREEQC solves all the mole-balance and charge-balance equations given above, subject to the inequalities given by Equations (11) and (12).

The most important difference between NETPATH and PHREEQC is that PHREEQC allows each analytical datum for each aqueous solution to be adjusted within an uncertainty range specified by the user. PHREEQC will determine sets of phase mass-transfers, solution mixing fractions, and adjustments to the analytical data that satisfy the mass-balance constraints, are consistent with the specified uncertainties, and minimize the sum of the adjustments to the analytical data. As an option, PHREEQC will also determine mass-transfer models that minimize the number of phases involved. The constraints used by PHREEQC inverse modeling are automatically specified by providing a list of the potentially reactive phases. For example, if tremolite ($Ca_2Mg_5Si_8O_{22}(OH)_2$) is identified as a potential reactant, PHREEQC will automatically use mass-balance constraints on Ca, Mg, Si, as well as on alkalinity and water. The water and alkalinity mole-balance equations are always solved, irrespective of postulated phases or reactions. In addition to the mass-balance constraints defined by specifying a list of potential reactants, PHREEQC also lets the user specify additional mass-balance constraints that may be used in determining the mixing fractions for two or more solutions that mix to form a final solution. Unlike NETPATH, PHREEQC includes a charge-balance constraint, which specifies that the sum of the deviations from the analytical data for a given solution must equal the charge imbalance present in that solution. PHREEQC also uses a water mass-balance constraint to account for mixing, water derived from mineral reactions, and water evaporation or dilution. PHREEQC will therefore account for water gained by the dissolution of hydrated minerals. The charge-balance and water mass-balance constraints used by PHREEQC are equivalent to including a mass balance on hydrogen or oxygen. During the inverse modeling simulation, PHREEQC will adjust not only the analytical element concentrations, it will also adjust the pH of the waters. The adjustment to total dissolved inorganic carbon is constrained to be consistent with the adjustments to pH and alkalinity.

Assumptions used in inverse modeling

A model is by definition a construct of assumptions that is meant to help understand some facet(s) of reality. Inverse geochemical modeling of ground waters requires the user to make many assumptions concerning (1) the types of geochemical reactions postulated to be present, (2) the rates of reaction relative to the movement of the water and its mobile constituents, (3) the present distribution of chemical constituents in the aquifer system studied and the prior evolution of this distribution. The last 2 sets of assumptions require that the user have some presumptive knowledge of the ground-water flow and transport system and of its prior evolution. The present discussion addresses some of the common assumptions that need to be made regarding flow and transport processes in inverse geochemical modeling of ground-water systems.

Knowledge of flowpaths and the assumption of a steady-state ground-water flow field. These are the most important and possibly the most tenuous assumptions used in inverse modeling of the chemical and isotopic evolution in a ground-water system. The user often does not have enough hydrologic knowledge to precisely determine the flow paths in a ground-water system. Furthermore, even if there is sufficient refined knowledge of the hydrogeologic system, already-existing wells must often be used. One rarely has the luxury of emplacing new sampling wells. When analyses are available from several wells, the spatial array of chemical and isotopic information may itself be used

to decide the most likely flowpath. In most cases, the user will pick a direction that shows the least amount of dilution for the more conservative solutes characterizing the flowpath and the greatest chemical evolution for the more reactive solutes.

Most groundwater systems are likely to experience some seasonal and multi-year fluctuations in hydraulic heads. Therefore, flowlines and groundwater velocities are likely to change at least seasonally, and steady-state conditions may not apply during the time scale of interest. The time scale of interest will normally be the time required for ground-water flow between the wells used in the inverse modeling simulation. The user typically assumes a steady-state ground-water flow field over the time scale of interest, or at the least assumes that any fluctuations in ground-water flow directions and velocities can be averaged out to the ground-water flow field observed at the time of sampling.

The assumption of chemical steady-state. The ground-water analyses used in an inverse model usually represent samples taken concurrently or near-concurrently. The inverse modeling approach assumes that the parcel of water sampled from a final well (well B in Fig. 1) used to have the same composition as that of the water sampled concurrently at the initial well (well A in Fig. 1). This assumption will certainly be reasonable if the ground-water system has remained in chemical (and isotopic) steady-state at least during the travel time required for the water to move from the initial well to the final well. The assumption of chemical and isotopic steady-state simply states that although chemical and isotopic composition may vary spatially, they may not vary in time at any given point in the ground-water system. In ground-water systems with spatially varying chemical and isotopic compositions, the assumption of chemical steady-state will also imply a steady-state ground-water flow field, flow lines and ground-water velocities that have not varied in time at any given point in the system.

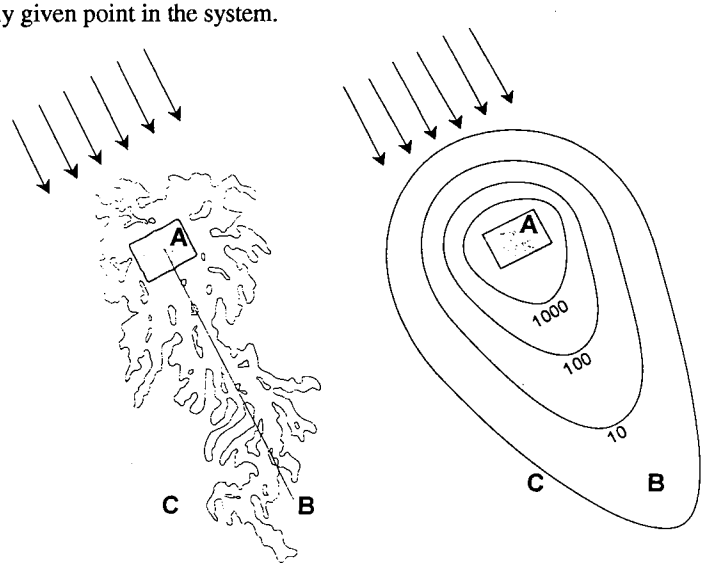

Figure 1. Two map views of a ground-water contaminant plume. Left: actual layout of the plume, drawn with a single concentration contour of concern. A is a well emplaced near or in the source of the contamination (stippled) and B and C are wells further downgradient. Right: Results of a transport model for the same ground-water contaminant plume based on a fit of concentration data obtained from several observation wells. Additional concentration contours are drawn. The large transverse and longitudinal dispersion of the modeled plume results not only from the mixing that actually occurs in the ground but also occurs during pumping at the observation wells, but is also caused by the inability to obtained a sufficiently detailed time-dependent representation of the contaminant plume and of the transient ground-water velocity field.

Most ground-water contamination cases involve dynamically evolving contaminant plumes, for which there can be no assumption of chemical steady-state throughout the ground-water system (steady-state plumes, in which the rate of diffusive/dispersive loss of solute balances the rate of solute influx, are possible but must considered the exception rather than the rule). Fortunately, although it may be desirable, the assumption of chemical and isotopic steady-state is not really required for the inverse geochemical modeling exercise to be meaningful in such situations. Indeed, the less stringent constraint is that the ground-water composition (chemical and isotopic) at the initial sampling point (well A on Fig. 1) must be the same at the time of sampling (t_s) as it was t years ago (at time t_0) when the parcel of water sampled at the final well was near the initial well. (This also assumes that there was a pathline responsible for the transport of water from well A to well B). This less stringent constraint allows the ground-water compositions at points in between the initial and final wells (A and B) to have varied with time, as long as the chemical composition of waters from the initial well has remained invariant. Strictly from a mass-balance point of view, it could be argued that the constraint could be reduced further to require only that the *changes in composition* between waters from well A (at time t_0) and B (at time t_s), rather than the actual compositions of waters from wells A (at time t_0) and B (at time t_s), should have remained constant. A uniform dilution or concentration of the waters sampled at the initial and final wells, however, could lead the user to conclude from his inspection of the mineral saturation indices and general speciation of the waters that some other set of reactions was responsible for the evolution of water A into water B.

How does "mixing" occur in ground-water systems? The U.S. Geological Survey inverse geochemical modeling codes (BALANCE, NETPATH, and the general geochemical code PHREEQC) have the capability of calculating the proportions of two or more initial solutions postulated to have "mixed" together and reacted with themselves and with the surrounding solid and gas phases in their chemical evolution towards the composition of the final water. Clearly in most ground-water environments, "mixing" of ground waters should really be modeled as a continuous process rather than as a discrete process where a small number of specified water compositions are mixed together. Unfortunately, the inverse geochemical codes presented here can not replicate a "continuous" mixing process. Forward transport modeling codes can replicate a continuous mixing process such as dispersion, but even then their results and the very basis of their conceptual models are usually fraught with uncertainty. In using a set of discrete initial water compositions, inverse geochemical models inherently assume that the initial waters chosen encompass the range of intermediate waters that are actually involved in the real, continuous mixing process.

Although the location and timing or sequencing of the mixing and reaction processes is of no mathematical significance in the solution of the mass-balance equations, the user should try to determine where, when and why such mixing processes may have occurred in the ground-water environment. The "mixing" of initial waters by dispersion for example may well have led to heterogeneous mass-transfers in areas that are not on directly on the flowpath between a principal initial water and the final water. The inverse models will, nevertheless, implicitely incorporate those mass transfers in their solution of *net* mass-transfer amounts.

The premise of inverse geochemical modeling is that the "final" and "initial" ground-waters used in a model should be related to each other. Ideally, they would represent very small volumes of water sampled from a unique flow-line or path-line. If it were indeed possible to do so (it is not), then the "final" ground water sampled could only have experienced "mixing" as the result of two different processes:

(1) diffusion of chemical and isotopic constituents (and possibly of water) to or

from the flow line (or path line) to neighboring flow lines or to stagnant water zones.

(2) sampling from the path line for more than an infinitesimally small amount of time, in the case of a system not in chemical steady-state. Although most ground-water analyses do not require large samples, and the samples are therefore typically collected over usually small time periods, this may be important in the case of contaminated ground-water evolution. If the system is not in chemical steady-state, the concentration of various constituents may be changing as a function of time at the final well and therefore a sample may in fact represent some ground-water composition averaged out in time and therefore in space.

From a more practical point of view sampling an instantaneous punctual ground-water composition is impossible and unwarranted considering the many sources of other uncertainties. Therefore "mixing" often results from:

(3) the sampling of multiple flow lines that have undergone different chemical and isotopic evolution. This will occur particularly in regions of converging flow, and also when sampling from wells screened across large and/or multiple intervals. Flow convergence may occur naturally or may be the direct result of pumping.

Using the "mixing" option in an inverse geochemical model may also of course be needed because the "initial" and "final" ground waters may not be truly related despite the belief of the user. Just as excessively high values of dispersivity are often used in ground-water transport modeling because of a lack of precise spatial and temporal information (Fig. 1), the use of the "mixing" option in NETPATH or in PHREEQC can often be the result of insufficient information on a ground-water system. For example in Figure 1 if the final well used in the inverse model (well C for example) was off to the side of the path line of heaviest contamination (on which wells A and B are) and if well A was used as the initial well, the inverse model defined by the user would probably require a significant contribution of "background" water to explain the extent of "dilution" between well A and the final well. Similarly pumping a large amount of water from the final well chosen (well B or C) and using the average composition of this water as the final water composition in the inverse model could also lead to a serious misrepresentation of the amount of mixing between the initial most heavily contaminated water (well A) and less contaminated, or even clean, "background" water used as the diluting water. An error in the mixing fractions of initial waters could result in significant errors in the amounts of reaction mass transfers calculated by the inverse model. Furthermore, using water compositions averaged out over a large volume by the sampling process could also mislead the modeler into thinking that certain reactions were thermodynamically impossible, when in fact proper sampling, and location, of the initial and final waters would have indicated that these reactions were in fact possible.

FORWARD GEOCHEMICAL MODELING: THE PHREEQM AND PHREEQC REACTIVE TRANSPORT CODES

Because the concepts of forward geochemical modeling are widely known (at least much more than those of inverse modeling), this discussion will limit itself to a brief description of the reactive transport capabilities of the PHREEQM and PHREEQC geochemical codes.

PHREEQM is a geochemical code developed by Appelo and Willemsen (1987). PHREEQM adds several subroutines to the U.S. Geological Survey geochemical speciation and mass-transfer code PHREEQE (Parkhurst et al., 1980). These subroutines allow PHREEQM to simulate the transport of aqueous-solutions by advection, dispersion

and diffusion in a 1-dimensional column (made up of a sequential series of "cells") and to simulate the reaction of those solutions with minerals and surfaces inside the column. PHREEQM has all the chemical reaction simulation capabilities of PHREEQE (it can even be run in a non-transport mode), but in addition PHREEQM is also able to simulate ion exchange processes. Because it is based on the equilibrium mass transfer code PHREEQE, PHREEQM typically uses the local equilibrium assumption in its modeling of reactive transport. Irreversible, zero-order kinetic reactions can be specified, however, and the code can be easily modified to account for first-order element decay or production (Glynn, unpublished work).

The transport algorithm in PHREEQM uses an operator splitting technique. Advection is modeled by shifting cell contents from one cell to the next at every time step or "shift". Dispersion and/or diffusion is simulated by mixing the aqueous contents of each cell with that of its adjacent cells. This algorithm gives PHREEQM the advantage (over most typical finite-difference and finitie-element codes) of being able to simulate not only an advective-dispersive transport process or a diffusive transport process, but also a purely advective, albeit one-dimensional, transport process. The mixing factors f calculated are a function of both aquifer dispersivity α and molecular diffusivity D^*:

$$f_i = \frac{\alpha_i + \alpha_{i+1}}{l_i + l_{i+1}} + 4D^* \frac{\Delta t}{(l_i + l_{i+1})^2} \tag{13}$$

where i is a given cell number and Δt is the time step. Equation (13) can be derived from a finite difference approximation (ignoring advection) centered in space and forward in time. Because its simulation of dispersion is centered in space, PHREEQM shows no numerical dispersion error for conservative constituents when simulating advection-dispersion processes. Numerical dispersion does occur, however, in the case of non-conservative dispersing constituents and is dependent on the amount of retardation experienced by each constituent and on the cell lengths chosen (the maximum numerical dispersivity equals 1/2 the cell length). PHREEQM does not show any numerical dispersion in simulations with only diffusion as a transport process. The lack of sequential iterations between PHREEQM's solution of the chemical equilibrium equations and its simulation of the transport processes at every time step can theoretically generate some error, although our comparisons (Glynn et al., 1991, for example; see Figs. 9 and 10 discussed later) with the sequential iteration finite difference code MST1D (Engesgaard and Kipp, 1992) lead us to believe that the error is typically small as long as an appropriate discretization is used. Finally, operator splitting in itself can also generate error, although our comparisons of PHREEQM with the MST1D code and results by Steefel and MacQuarrie (this volume) suggest that this error is usually minor. A much more complete description of the PHREEQM code and its capabilities can be found in Appelo and Postma (1993).

The recently published geochemical code PHREEQC (Parkhurst, 1995) has the capability of doing both inverse and forward geochemical modeling. Its inverse modeling capabilities have been described in the previous section. PHREEQC also includes all the forward geochemical modeling capabilities of PHREEQE and adds the capability to simulate (1) ion-exchange reactions, (2) sorption processes (using Dzombak and Morel's (1990) diffuse double-layer surface-complexation model and associated thermodynamic data for hydrous ferric oxide), (3) gas bubble formation and (4) advection in a 1-dimensional column. Unlike PHREEQE, PHREEQC also keeps track of mineral amounts, an essential requirement for any reactive-transport simulation. A newer version of PHREEQC has been developed by Tony Appelo (written communication, December 1995) that incorporates all of the features of the PHREEQM transport simulation into PHREEQC, as well as several additional capabilities (including some reaction kinetics). This newer, still

unpublished, version of PHREEQC uses essentially the same transport algorithm as PHREEQM, and includes dispersion and diffusion processes. In contrast, the recently published version of PHREEQC includes only pure advection, although dispersion and diffusion can be simulated to some extent through a cell-mixing option (Parkhurst, 1995; Brown, 1996). Unless mentioned otherwise, all PHREEQC simulations referred to in this paper were performed with the published version of the code.

The forward geochemical modeling approach (using the PHREEQE, PHREEQM or PHREEQC codes) is conceptually different from the inverse modeling approach. The inverse modeling approach uses *existing* aqueous-solution data and calculates the mass-transfer amounts for various reactions suspected of accounting for the chemical and isotopic evolution of an "initial" water into a "final" one. The user is responsible for determining that the "initial" and "final" waters are truly related. In contrast, forward modeling allows the *prediction* of aqueous-solution chemical composition given an initial solution and given certain postulated reactions, some of which are usually considered to go to thermodynamic equilibrium. Forward modeling is most suitable and most useful, when the amount of chemical and isotopic data available for a given ground-water system is limited, and also when the objective is to predict the future evolution of the system. Inverse modeling is most useful when abundant chemical, isotopic, hydrologic and mineralogic data are present and all that is desired is a possible explanation of the past chemical evolution of the ground-water system. Of course, just as understanding the past is a key to understanding the future, inverse modeling can also provide some understanding of the reactions that may control the future chemical evolution of a ground-water system.

Forward modeling codes can also be used for the purpose of inverse modeling in a series of trial and error simulations attempting to simulate some real observations (Van Cappellen and Gaillard, Steefel and MacQuarrie, this volume). Although this latest approach can be extremely time consuming, it does have the distinct advantage over simpler inverse geochemical codes of offering a potentially more accurate representation of ground-water mixing as a continuous (rather than discrete) process. This latest approach also does not require the assumption of chemical steady-state. The disadvantages of this approach over that of a non-transport-oriented inverse geochemical modeling approach are essentially the computer time requirements, the significantly greater number of adjustable parameters (flow and transport related) and the consequently greater number of possible solutions that may explain the actual observations. Further references in this paper to inverse modeling will generally not refer to the use of forward codes as part of an inverse modeling approach, although many of the statements made may apply equally well to this latter more sophisticated approach.

The Pinal Creek Toxics Program investigation site, a site of ground-water contamination by acidic metal-laden sulfate-rich wastewater near Globe, Arizona provides a good example of the improved understanding of the chemical reaction and transport processes that may be gained through the combined use of both inverse modeling and forward modeling approaches. The site is described below.

THE PINAL CREEK BASIN SITE: BRIEF DESCRIPTION

The Pinal Creek basin is located in central Arizona, about 100 km east of the Phoenix (Fig. 2). The surface drainage area of the basin occupies 516 km^2, of which 170 km^2 is covered by alluvium and basin fill, which form the regional aquifer. 27 km^2 are covered by mine tailings. Mining, mainly for copper, began in the late 1870s and has been the largest economic activity in the basin.

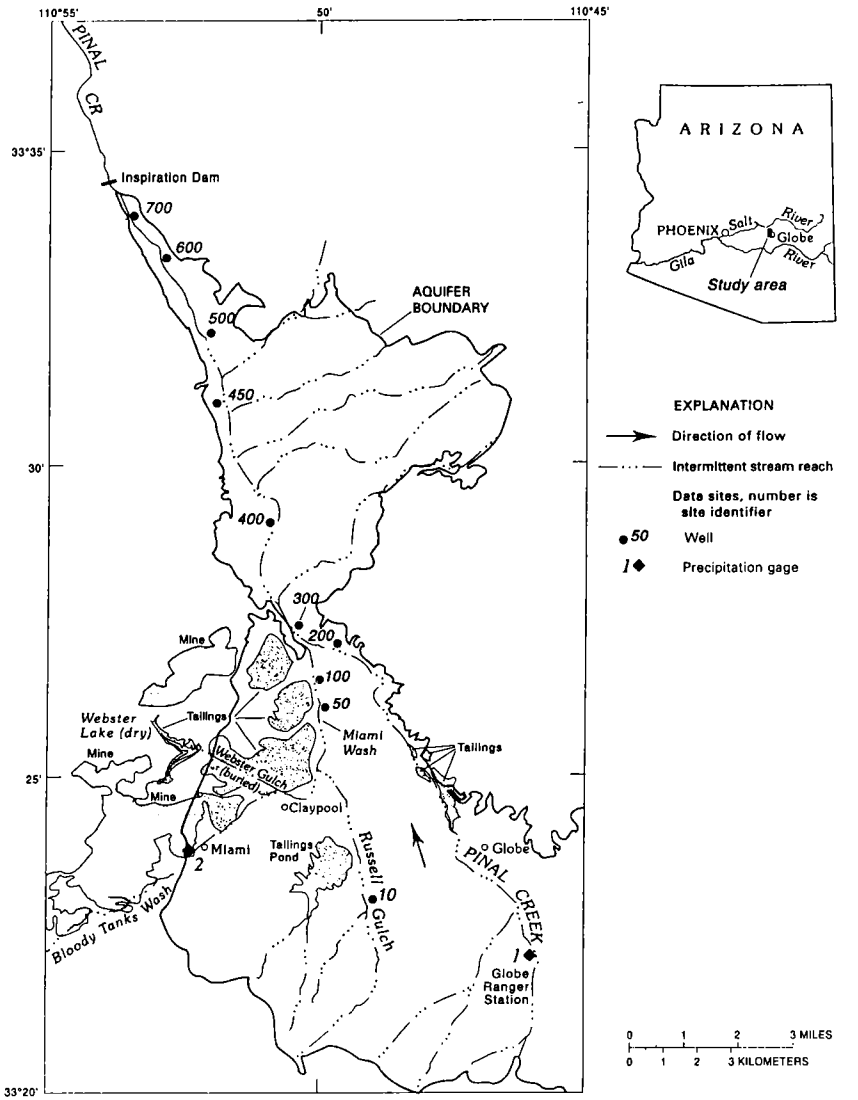

Figure 2. Location of study area, Pinal Creek Basin, Arizona. Several wells screened at different depths actually exist at each well site.

Because of the long history of mining in the basin, there are many potential sources of contamination to the regional aquifer (Eychaner, 1991; Brown and Harvey, 1994). Pyrite is the most abundant sulfide mineral in the tailings. Following significant rainfall, oxidation of pyrite and subsequent runoff into permeable streambeds could represent a significant source of acidity, iron, and sulfate to the regional aquifer. Unlined impoundments of water used in mine processing are a likely source of contamination. In mineralized areas, runoff and ground-water flow may be mineralized naturally, though the amount of this flow is small in relation to flow from unmineralized areas.

The largest suspected single source of contamination in the basin was Webster Lake, an unlined surface water impoundment that existed from 1940 to 1988, when it was drained at the order of the U.S. Environmental Protection Agency (Tolle and Arthur, 1991). Maximum volume of the lake was more than 7 million m^3. In 1988, a sample of water from the lake had a pH of 2.7. Concentrations of iron and sulfate were 6 g/L and 20 g/L, respectively. Aluminum, copper, cobalt, nickel, and zinc were present at concentrations greater than 20 mg/L.

The present U.S. Geological Survey investigation began in 1984 with the drilling of monitor wells along the length of the 15 km-long plume in the stream alluvium. In all, more than 30 wells have been drilled since 1984 to determine the location, chemistry, and movement of the contaminant plume. These wells have been sampled on a regular basis, usually biannually, since November 1984.

Geology

Peterson (1962) describes in detail the geology and mineral deposits of the area. Rocks in Pinal Creek basin range in age from Precambrian to Holocene. Rocks of Precambrian age include schist, diorite, granite, conglomerate, quartzite, limestone, and basalt, which are widely exposed in the hills and mountains throughout the study area. Rocks of Paleozoic age include quartzite, limestone, and shale. Rocks of Mesozoic and Cenozoic age are mainly intrusive and include granite, granodiorite, diabase, and monzonite, all of which are Cretaceous or Tertiary in age. Rocks of Mesozoic and Cenozoic age are exposed in the hills and mountains north of Globe and Miami.

The igneous and metamorphic rocks include a major body of copper porphyry ore. Chalcocite, chalcopyrite, and pyrite predominate in the deeper parts of the ore body, while chrysocolla, malachite, and azurite predominate in its upper, oxidized zone.

The present basin configuration was created by high-angle block faulting associated with basin subsidence that began 19 to 15 million years ago and continued until about 8 million years ago. Basin fill, which is derived from rocks of the surrounding mountains, is Tertiary in age. Lithology ranges "from completely unsorted and unconsolidated rubble of angular blocks as much as 4.5 m in diameter, to well-stratified deposits of firmly cemented sand, silt, and gravel containing well-rounded pebbles and cobbles" (Peterson (1962). Carbonate content of the basin fill is about 1.5 percent (Eychaner, 1989, p 570).

Unconsolidated stream alluvium, which is quaternary in age, overlies the basin fill along Miami Wash, Pinal Creek, and other major drainages. The alluvium is from 300 to 800 m wide and is less than 50 m thick. The alluvium contains cobble- to clay-sized material (Hydro Geo Chem, 1989) although sand- to gravel-sized material is most abundant. Drill cuttings from USGS monitor wells generally contained greater than 90-percent sand and gravel by weight; auger samples indicated the presence of silt or clay beds several inches thick. Sand-sized particles contained mainly quartz, feldspar, and lesser amounts of mica and a variety of rock fragments. Gravel-sized material consisted mainly of rock fragments of granite, volcanic rocks, and schist. Alluvium contains interbedded clays and lenticular clay layers that were as much as 12 m thick at Nugget Wash (Hydro Geo Chem, Inc., 1989). Particle-size analyses of drill cuttings indicate that these lenticular clay layers thin toward the center of the basin and extend an indeterminate distance in length parallel to the axis of the basin.

A sample of alluvium collected in 1985 (Eychaner and Stollenwerk, 1985) contained 0.34 percent calcite by weight. This is equivalent to 0.18 moles of carbonate material per liter of water, using the bulk density of 1.65 g/cc and porosity of 0.316 determined for

alluvium used in a column experiment (Stollenwerk, 1994).

Estimates of the concentration of primary manganese oxide minerals were based on samples of alluvium not affected by acidic contamination. At well site 500, in the neutralized part of the plume, the depth-averaged content of manganese oxides was 0.079 mol/l, based on sequential extractions done by Ficklin and Others (1991). Stollenwerk (1994) estimated that 0.0449 mol/l of manganese could be available for reaction in a sample of alluvium obtained from a gravel quarry just east of well site 200.

Geohydrology

The geohydrology of the Pinal Creek basin is the result of past geologic events, the past and present climate, and human activities. Because the area climate is semiarid, most of the drainages in the basin are usually dry but convey large amounts of storm runoff during and after severe storms. Streams that drain the Pinal Mountains also flow during and following snowmelt in late winter and early spring. The amount and distribution of rainfall controls the size, frequency, and duration of streamflow, and the quantity and distribution of water that infiltrates permeable stream alluvium and recharges the regional aquifer.

Ground water in basin fill flows generally northward from the flanks of the Pinal Mountains and westward from the Apache Peak alluvial fan. Most ground water in the basin fill eventually flows upward into the alluvium and then moves generally north to the perennial reach of Pinal Creek. A greater quantity of water, however, recharges the alluvium directly and moves north, mixing with the water from the basin fill. In the northern part of the basin, the aquifer is constricted by impermeable rocks. This constriction forces ground water to the land surface, generating perennial flow from about 6 km above Inspiration Dam to the Salt River, which is a major source of drinking water for the Phoenix Metropolitan area.

INVERSE GEOCHEMICAL MODELING AT THE PINAL CREEK SITE

Like most sites of point-source ground-water contamination, the chemistry of ground waters in the Pinal Creek basin exhibits both spatial and temporal variations. The most heavily contaminated ground-waters are typically found near the base of the unconsolidated alluvial aquifer, where a zone of coarser (and possibly less carbonate-rich) material is suspected to be present. The wells with the most contaminated waters at each well site are 51, 101, 302, 402, 503, 601 and 702 in a down-gradient direction (Fig. 2). Although other wells at each site also show the presence of contaminated water, wells with the most contaminated waters (as measured by total dissolved solids, or chloride or any other relatively conservative constituent) present the most logical choice for inverse modeling. To further narrow the scope of the inverse-modeling study, we focus on the two wells which show the most significant change in the chemical characteristics of their waters, wells 402 and 503. The two water samples chosen represent an acidic contaminated water sampled from well 402 in January 1989 and a neutralized contaminated water sampled from well 503 in November 1991. The two wells are 5.6 kilometers apart. From the difference in sample times and from the distance, we calculate that a parcel of water leaving well 402 would have to travel at a linear ground-water velocity of about 5.2 m per day. This velocity is in the range of the 4.2 to 5.6 m/day velocities estimated by Brown (1995, 1996) using Darcy's law, assuming an effective porosity of 0.3 and a hydraulic conductivity of 200 m/d.

Inverse modeling with NETPATH

To start off our study, we will use the NETPATH inverse modeling code. Unlike the present version of PHREEQC, NETPATH has the advantage of being an interactive code and allows the user to quickly determine the primary issues of concern in an inverse geochemical modeling simulation. The NETPATH code will (1) help us identify some of the possible reaction mechanisms responsible for the chemical evolution of the ground waters between wells 402 and 503 and (2) will quantify some of the reaction mass-transfers involved.

Examination of end-member waters and their conservative constituents. The first step in an inverse modeling study is to examine the chemical composition and thermodynamic state of the waters that will be used in the model. The chemical analyses for the waters chosen for our study are given below in Table 1.

Table 1. Chemical composition of three ground waters from the Pinal Creek basin: an acidic contaminated water (well 402), a background uncontaminated water (well 504), and a neutralized contaminated water (well 503). Concentrations in mg/L. Concentration changes are expressed relative to well 402. ND: not determined. TDIC: total dissolved inorganic carbon. [1]Assumes chloride is conservative. The relative change expressed represents the relative difference in concentration between well 503 water and a mixture of waters from wells 402 and 504, determined on the basis of chloride concentrations. [2]Values were estimated by inspecting earlier and later analyses. [3]Average of two analyses.

	well 402 89/1/12	well 504 91/11/22	well 503 91/11/22	Change between wells 503 and 402	Change due to reaction only[1]
pH	4.13	7.05	5.59		
Eh (in mV)	420 est.[2]	350	410		
Temperature	18 °C	20.5 °C	18.2 °C	1.1 %	
Dissolved oxygen	0.3	6.64	< 0.1		
Calcium	502	44.6 [3]	634	26 %	57 %
Magnesium	161	15.6 [3]	200	24 %	54 %
Sodium	121	19.8 [3]	86	-29 %	-13 %
Potassium	7 est.[2]	2.1	5 est.[2]	-29 %	-16 %
Iron	591	0.004	< 0.1	-100 %	-100 %
Manganese	71.6	< 0.001	116	62 %	106 %
Aluminum	18.4	< 0.01	2.3 est.[2]	-88 %	-84 %
Strontium	2.29	0.335	2.7	18 %	44 %
Silica (as SiO_2)	85.6	27 [3]	91.8	7.2 %	26 %
Chloride	140	9.7 [3]	112	-20 %	0 %
TDIC (as C)	50	ND	ND	ND	ND
Alkalinity (as HCO_3)	ND	227	66	ND	ND
Sulfate	3260	14.2 [3]	2350	-28 %	-8 %
Fluoride	10 est.[2]	0.3	1.5 est.[2]	-85 %	-81 %

As can be seen, the most significant changes in the chemical evolution of the groundwater between wells 402 and 503 are: the increase in pH from 3.9 to 5.6, the 25% increase in calcium and magnesium, the complete removal of 590 mg/L of dissolved iron, the 90%

removal of 18.4 mg/L of dissolved aluminum, the 60% increase in manganese, the 30% decrease in sulfate, and the near-constant dissolved silica concentrations.

As is the case in any geochemical modeling analysis, however, conservative (i.e. non-reactive) constituents are perhaps the most important constituents to examine because they give some information on the physical flow and transport processes. Any ground-water sampling and analysis program should ensure the measurement of at least one, but preferably two or more, relatively non-reactive tracers, such as chloride, bromide, ^{18}O and ^{2}H contents. Sodium may also be relatively conservative although it may increase in solution due to ion exchange, feldspar dissolution, or evaporite dissolution processes. Sodium is rarely taken out of solution by reaction processes except in some instances by sorption and ion exchange processes. In the case of the Pinal Creek ground waters, the high Ca/Na ratio in the acidic waters (Ca/Na = 2.4 mol/mol in well 402) and the even higher ratio in the neutralized waters (Ca/Na = 4.2 mol/mol in well 503) suggests that removal of sodium by ion exchange is not a likely process.

The decrease in both Cl and Na between wells 402 and 503 suggests that a dilution process is occurring. This dilution may be caused either by longitudinal and transverse dispersion processes along the flow path or may be caused in part by the well-sampling process. It is also important to recognize that the ground water sample taken from well 503 in November 1991 was probably not exactly on the pathline originating from well 402 in January 1989. Well 503 may be further off the most contaminated pathline. In recognition of the difficulty in determining the causes and the exact proportions of the various ground waters responsible for the dilution of the well 503 water relative to the well 402 water, an uncontaminated water sampled in November 1991 from below the plume at well 504 was used as the source of diluting water in our inverse geochemical model.

Although chloride undergoes a 20% decrease between wells 402 and 503, sodium undergoes an even greater decrease of about 29%. If the decrease in chloride is used to calculate the fraction (0.2149) of water from well 504 diluting the water from well 402, the observed sodium concentration in well 503 is still 13% lower than the calculated diluted sodium concentration (Table 1, last column). This greater observed decrease in sodium may be at least partly due to a greater Cl/Na ratio in the average diluting water relative to that of the background water used (well 504) used in the calculation. Indeed, although the average Cl/Na ratio in the uncontaminated waters found below the plume (wells 404, 504) or upgradient (well 010) from the plume is 0.44 mg/mg ($\pm$ 0.10), the average Cl/Na ratio for the most contaminated waters along the flow path is close to three times higher (well 51: 1.48 $\pm$ 0.74, well 101: 1.35 $\pm$ 0.44, well 302: 1.32 $\pm$ 0.36, well 402: 1.29 $\pm$ 0.44, well 503: 1.17 $\pm$ 0.43; all ratios in mg/mg). [Note the decreasing Cl/Na ratio with distance downgradient, i.e. with increasing neutralization and dilution of the contaminated waters.] Dilute, only slightly contaminated, ground waters sampled from wells on the side of the plume (wells 201, 202) also have a much higher average Cl/Na ratio (0.91 $\pm$ 0.30) than that of the uncontaminated ground waters. An argument can therefore be made that these slightly contaminated waters should have been used as the source of the diluting waters in the NETPATH modeling, instead of the uncontaminated water chosen here. The discrepancy in the chloride and sodium dilution factors can be used, however, as a measure of the uncertainty inherent in trying to model the ground-water mixing process with a simple inverse geochemical model.

The thermodynamic state of the end-member waters. After examining the conservative constituent concentrations of the ground waters, the next step is to examine the aqueous-speciation results, in particular the mineral saturation indices (Table 2) calculated for the three end-member waters chosen in our model. The speciation

calculations were performed with the WATEQFP code incorporated in the database management code DB distributed with the NETPATH code. The thermodynamic database used in WATEQFP is a subset of the database described in Nordstrom et al. (1990) and is essentially similar to the thermodynamic databases used in all U.S. Geological Survey ion association codes.

Table 2. Saturation indices and carbon dioxide equilibrium partial pressures for an acidic ground water (well 402), an uncontaminated ground water (well 504) and a neutralized contaminated ground water (well 503) from the Pinal Creek alluvial and basin fill aquifers. NC: could not be calculated

Mineral	well 402 89/1/12	well 504 91/11/22	well 503 91/11/22
Calcite	-4.966	-0.448	-1.812
Dolomite	-10.170	-1.062	-3.867
Siderite	-2.602	-11.470	NC
Rhodochrosite	-3.253	NC	-0.003
Gypsum	0.010	-2.573	0.051
Fluorite	-3.200	-2.163	-2.511
SiO_2(am)	-0.063	-0.598	-0.038
Chalcedony	0.800	0.257	0.826
$Al(OH)_3$(am)	-4.032	NC	-0.849
Gibbsite	-1.277	NC	1.904
Kaolinite	0.745	NC	7.156
Alunite	1.817	NC	6.599
$Fe(OH)_3$(am)	-0.966	0.518	NC
Goethite	4.926	6.409	NC
K-Jarosite	0.033	-8.453	NC (< -3)
log pCO_2 (in atmospheres)	-0.992	-1.730	-0.921

The background water (well 504) is essentially a $Ca(Mg)HCO_3$ water typical of all the uncontaminated ground waters in the Pinal Creek basin. These waters are usually near saturation with calcite, dolomite and chalcedony, have near to slightly above neutral pH values and have equilibrium CO_2 partial pressures between $10^{-1.5}$ and $10^{-2.0}$. The uncontaminated ground waters are also typically rich in dissolved oxygen and other dissolved atmospheric gases (Glynn and Busenberg, 1994a, Robertson, 1991, Winograd and Robertson, 1982).

In comparison, the acidic water from well 402 is highly undersaturated with respect to calcite, dolomite, siderite ($FeCO_3$, SI: -2.60) and rhodochrosite ($MnCO_3$, SI: -3.25) and is near saturation with amorphous silica, kaolinite and gypsum. The water is also undersaturated with respect to amorphous $Fe(OH)_3$ but supersaturated with respect to goethite, and very highly undersaturated with respect to all manganese oxides (pyrolusite (MnO_2), hausmanite (Mn_3O_4), manganite (MnOOH) and pyrochroite ($Mn(OH)_2$)). These speciation results, based on the relatively high measured Eh (420 mV), are consistent with the high Fe and Mn contents of the water and the lack of any evidence of sulfate reduction. Surprisingly, the calculated equilibrium CO_2 partial pressure, $10^{-0.99}$ is very close to that of the neutralized water.

In comparison to the acidic water from well 402, the partially neutralized water from well 503 is not as highly undersaturated with respect to calcite and dolomite and remains close to saturation with respect to both gypsum and amorphous silica. Unlike its more acidic precursor, the water is highly supersaturated with respect to kaolinite and is instead near saturation with respect to an $Al(OH)_3$ phase. Although most of the dissolved iron has dropped out of the water, manganese has increased to near saturation with rhodochrosite. The water is still undersaturated with respect to several manganese oxides (pyrolusite SI: -9.14, hausmanite SI: -13.43, manganite SI: -4.67, pyrochroite SI: -7.22), although the uncertainty in these saturation indices is high, given the poor knowledge of manganese oxide thermodynamics and the dependence of the calculated saturation indices on the measured Eh. Indeed, lack of data on the vanishingly small dissolved Mn(IV) and Mn(III) concentrations makes any saturation index calculations for the Mn(IV) and Mn(III) minerals (pyrolusite, hausmanite, manganite) almost meaningless, because the calculations assume that the measured Eh values are representative of the Mn(IV)/Mn(II) and Mn(III)/Mn(II) aqueous activity ratios. Finally, the equilibrium CO_2 partial pressure ($10^{-0.94}$) is close to that of the acidic water from well 402, and is more than an order of magnitude higher than may be expected from equilibrium with unsaturated zone CO_2 partial pressures (Glynn and Busenberg, 1994b).

NETPATH inverse modeling: first simulation results. The first NETPATH simulation considered the following 11 mass balance constraints: Cl, Ca, Mg, Na, Al, Si, RS (redox state), Fe, Mn, C, S. The following 14 phases were considered (with additional limitations mentioned. Note: "forced inclusion" means that NETPATH was forced to consider only models that included the specific phase, or reaction):

calcite (forced inclusion dissolution only),
goethite (forced inclusion; precipitation only),
gypsum (forced inclusion; precipitation only),
kaolinite (precipitation only),
SiO_2,
dolomite (dissolution only),
MnO_2 (dissolution only),
rhodochrosite ($MnCO_3$),
anorthite ($CaAl_2Si_2O_8$; dissolution only),
gibbsite,
$Mn(OH)_3$ (precipitation only),
O_2 gas (dissolution only),
CO_2 gas (exsolution only),
a pure Na phase

This last phase was added simply to keep track of the Na imbalance. In this first simulation the mixing fractions of well 402 and well 504 waters were determined through the chloride concentrations, because no Cl phases were specified. As a result of the 11 element mass-balance constraints, and because of the mixing of the two initial waters (similar to having one forced phase mass-transfer), 10 out of 14 possible phases were present in each NETPATH model solution. Additional mass-transfer limitations were therefore necessary and were used to minimize the number of possible models found. NETPATH checked 330 models or possible solutions and actually found 12 that did not violate the limitations placed (whether a phase was forced to be included in all models, and whether it was allowed to dissolve only or to precipitate/exsolve only or both). Of the 12 models, 6 are given here (Table 3). They adequately represent the range of possible solutions given by the NETPATH code and will be further discussed. It should be remembered that linear combinations of any possible models also form possible solutions.

Table 3. NETPATH models. First simulation. Results in millimoles per kilogram of H_2O. Positive numbers indicate dissolution, negative numbers precipitation or degassing.

	Model 1 anorthite gibbsite	Model 2 gibbsite SiO_2	Model 3 kaolinite SiO_2	Model 4 e^- transfer	Model 5 O_2 gas	Model 6 O_2 gas rhodo. diss.
well 504 fraction	0.216	0.216	0.216	0.216	0.216	0.216
pure Na	-0.579	-0.579	-0.579	-0.579	-0.579	-0.579
dolomite +	2.899	2.899	2.899	2.899	2.899	2.899
gypsum - **F**	-2.219	-2.219	-2.219	-2.219	-2.219	-2.219
goethite - **F**	-8.339	-8.339	-8.339	-8.339	-8.339	-8.339
calcite + **F**	4.929	5.086	5.086	4.929	4.929	4.929
anorthite	0.157			0.157	0.157	0.157
kaolinite			-0.226			
gibbsite	-0.766	-0.452		-0.766	-0.766	-0.766
SiO_2		0.314	0.766			
rhodochrosite	-2.972	-2.972	-2.972			1.092
MnO_2 +	4.064	4.064	4.064	7.036	1.092	
$Mn(OH)_3$ -				-5.944		
O_2 gas +					1.486	2.032
CO_2 gas -	-6.033	-6.190	-6.190	-9.005	-9.005	-10.097
net protons consumed	5.707	5.707	5.707	5.707	5.707	5.707

The phases in the simulation were chosen based on our knowledge of the mineralogy of the basin fill and alluvial aquifer materials and also on our examination of the saturation indices of the well 402 and well 503 water. Although gypsum is not present in the uncontaminated aquifer, the acidic and especially the neutralized contaminated waters are consistently slightly supersaturated with respect to gypsum. In fact samples brought back from the field precipitate gypsum over the course of several months. Calcite and dolomite are known to be present in the aquifer materials and were therefore included in the model. Similarly, there is no lack of manganese oxides in the alluvial materials. Manganese oxides form at the contact between the Mn(II) rich-ground waters and oxygenated ground-waters, and are also widely disseminated in the uncontaminated sand and gravel (Ficklin et al., 1991). Lind and Stollenwerk (1994) conducted an elution experiment reacting acidic iron and manganese-rich ground water from well 101 with alluvial material from well 601, downgradient from the manganese-contaminated ground waters. Based on X-ray diffraction results, Lind and Stollenwerk (1994) found that pyrolusite (β-MnO_2) and a solid resembling kutnahorite ($CaMn(CO_3)_2$) were present before, but not after, the elution of the alluvial materials. Although goethite was the Fe(III) phase chosen (for precipitation only), choosing any other Fe(III) oxide would have resulted in the same Fe mass transfer values. Thermodynamic stability is numerically irrelevant in NETPATH calculations. Similarly, we could have picked amorphous $Al(OH)_3$ instead of gibbsite. In fact, Fe and Al are most likely precipitating as fairly amorphous precipitates, that may recrystallize to more

stable crystalline forms with time. The WATEQFP speciation results suggest that the waters near well 503 may be precipitating some $Al(OH)_3$ phase. The speciation results also suggest that kaolinite may be forming near well 402, but probably does not form very quickly near well 503 (as evidenced by the very high supersaturation with respect to kaolinite). The precipitation of amorphous forms of Al and Fe(III) minerals upon reaction of the alluvial sediments with acidic waters is also suggested by the elution experiments of Lind and Stollenwerk (1994) and by the selective extractions performed by Ficklin et al. (1991) on core materials from wells 107 (acidic), 451 (partially neutralized) and 505 (neutralized). Ficklin et al. (1991) also report no visible association between Al and SO_4 and argue therefore against the formation of an $AlOHSO_4$ phase. Stollenwerk and Eychaner (1987) had, however, earlier argued that this phase controlled aluminum concentrations in the acidic ground waters. Furthermore, in his column elution studies, Stollenwerk (1994) found that he could best simulate the behavior of dissolved aluminum by using amorphous $Al(OH)_3$ as the solubility-limiting phase at pH values above 4.7 and $AlOHSO_4$ at lower pH values. He did, however, change the solubility product of the $AlOHSO_4$ phase to best fit his experimental results (from log K = -3.23 to log K = -2.2). Considering the available evidence, we believe that the issue of $AlOHSO_4$ precipitation is not resolved and requires further research. The fact that the water from well 402 is close to saturation with kaolinite and the fact that kaolinite is known to form in acidic waters with high dissolved silica (Blair Jones, U.S. Geological Survey, pers. comm., 1996) leads us to prefer the hypothesis of Al control by kaolinite in the more acidic waters from the site. Nevertheless, we will also investigate the effect of using $AlOHSO_4$ in both our inverse and forward geochemical models.

Because well 503 water is close to saturation with respect to rhodochrosite, we chose this mineral as a possible Mn sink. We believe that reductive dissolution of MnO_2 is the primary process causing dissolved Fe(II) to oxidize and precipitate out of solution. The only problem with this reaction mechanism is that the increase in dissolved Mn(II) is too small relative to the decrease in Fe(II). Several other possible reactions could explain this fact. (1) Mn(II) may be precipitating out as rhodochrosite. (2) one mole of MnO_2 does not have to dissolve completely in order to oxidize two moles of Fe(II). An electron transfer process may be taking place during which the oxidation state of the Mn oxide simply decreases while only partially releasing Mn into the solution. (3) Mn(II) may be sorbing onto the freshly precipitated Fe-oxyhydroxides. (4) Oxygen is known to be diffusing through the unsaturated zone into the ground waters near the water table. Because of the depth of the well 402 and 503 waters below the water table, however, this last mechanism is not really considered to occur. Although O_2 ingassing was considered in our first NETPATH simulation, this reaction will be discarded in our second simulation.

For similar reasons, the possibility of CO_2 exsolution from a deep flow path can not be seriously entertained. Glynn and Busenberg (1994b) estimated, based on their measurements of dissolved gases in the Pinal Creek ground waters, that only waters down to ~2 m below the water table could possibly be exsolving dissolved gases and CO_2. Significant CO_2 exsolution would also cause exsolution of other dissolved gases such as N_2 and Ar. For example, exsolution of CH_4 and CO_2 from an hydrocarbon contaminant plume has been held responsible for the very low dissolved Ar and N_2 concentrations measured in ground waters from the U.S. Geological Survey Bemidji Toxics site (Revesz et al., 1995). Instead, ground waters from the Pinal Creek site show very high concentrations of both dissolved N_2 and Ar because of the large amounts (often above 20 mL/L) of excess air entrained during ground-water recharge at the site (Glynn and Busenberg, 1994b).

Interestingly enough the results of our first NETPATH simulation suggest that other

Ca and Mg sources (in addition to calcite and dolomite) are needed if CO_2 is disallowed as a sink for the excess carbon provided by the dissolution of the carbonates. We initially thought that rhodochrosite ($MnCO_3$) would provide an additional carbon sink but found out that given the Mn mass balance constraints, the rhodochrosite sink would not be a strong enough sink for the excess carbon. The presence of another Mn sink (such as Mn(II) sorption) instead or in addition to rhodochrosite precipitation would only exacerbate this problem. Therefore, because no other carbon sinks are likely to be present (the waters are undersaturated with respect to siderite), the next solution was to incorporate another Ca source, specifically a Ca silicate, so as to reduce the amount of carbon coming into solution. Although anorthite was chosen, it is likely that any silicate mineral dissolution accelerated by the acidic ground waters would also act as a source of Mg, Na and K (and probably Fe and Mn) to the solution. The dissolution of Ca-rich silicates and perhaps Mg-rich silicates, however, can be expected to be faster than that of the Na and K rich silicates. On the basis of their alluvium elution experiments, Lind and Stollenwerk (1994) suggest that tremolite ($Ca_2Mg_5Si_8O_{22}(OH)_2$) dissolution may be a source of both Ca and Mg to the Pinal Creek ground waters. Indeed, amphiboles, such as tremolite, and pyroxenes can be expected to have faster reaction rates than feldspar minerals, although their abundance in the alluvial materials is minor compared to that of the feldspar minerals. The presence of CO_2 degassing in all the models found by the the first NETPATH simulation suggests that some Mg-silicate phase (such as tremolite) must be included if models without CO_2 degassing are to be found.

The last row in Table 3 gives an estimate of the net number of millimoles of protons consumed by the various reaction models. Essentially, the number of protons consumed in each reaction model was calculated by estimating the number of protons consumed by the *dissolution* of one millimole of each solid or gaseous phase. The number of protons consumed is dependent on the degree of protonation or hydroxylation of the various aqueous species produced by the dissolution reactions. For example a calcite dissolution reaction will show consumption of two protons per mole of calcite dissolved if the reaction is written to produce $H_2CO_3^0$ (or equivalently aqueous CO_2; henceforth $H_2CO_3^0$ is meant to comprise the actual species and the much more dominant aqueous CO_2 species) but will show consumption of only one proton if the reaction is written to produce HCO_3^-. The proton consumption calculations shown here assume that the reaction byproducts are the dominant aqueous species determined from the speciation of the well 402 water, such as AlF^{2+}, AlF_2^+, $AlSO_4^+$, $Al(SO_4)_2^-$, Al^{+3} for Al, Mn^{2+}, $MnSO_4^0$ for Mn, Fe^{2+}, $FeSO_4^0$ for Fe, $H_2CO_3^0$ for TDIC (species listed are in order of decreasing predominance). Using this assumption, the number of moles of protons consumed per mole of phase dissolved are: 14 for tremolite, 8 for anorthite, 6 for kaolinite, 4 for dolomite, MnO_2 and O_2 gas, 3 for goethite (or $Fe(OH)_3$), gibbsite (or $Al(OH)_3$) and $Mn(OH)_3$, 2 for calcite and rhodochrosite, 1 for $AlOHSO_4$. All other phases mentioned in Tables 3 and 4 are assumed not to consume protons upon dissolution. The consumption of protons by the heterogeneous mass transfer reactions must necessarily be matched by an increase in solution pH and also by the release of protons from homogeneous deprotonation reactions (such as $H_2CO_3^0 \Rightarrow HCO_3^- + H^+$, and $HSO_4^- \Rightarrow SO_4^{2-} + H^+$). Given (1) that the increase in pH between wells 402 and 503 corresponds to approximately a 0.1 millimole decease in H^+ concentration, (2) that the difference in $H_2CO_3^0$ concentrations in well 402 and 503 waters, is less than 1 millimolal (and HCO_3^- is always at least 5 times lower than the $H_2CO_3^0$ concentration), (3) that the concentration of HSO_4^- in well 402 water is close to 0.1 millimolal, and (4) that there are no other major homogeneous deprotonation reactions, it appears that the 5.7 millimoles of proton consumption calculated for the various reaction models presented in Table 3 are at least 5 times too high. Unaccounted surface deprotonation or proton exchange reactions offer at least one possible reason for this

discrepancy. Erroneous reaction models and analytical uncertainty in the basic data collected are other possible reasons.

The most interesting results of the first NETPATH inverse modeling simulation are the following. Gas exsolution or dissolution were found to be necessary in all models, even though anorthite dissolution and rhodochrosite precipitation were included. Of all the models found by the first NETPATH simulation, we prefer the 3 models that considered MnO_2 dissolution and rhodochrosite precipitation, rather than an electron-transfer mechanism ($MnO_2 \Rightarrow Mn(OH)_3$) or O_2 ingassing (with or without acccompanying rhodochrosite dissolution). Out of those three models, we also prefer the two models (models 1 and 2 in Table 3) that did not involve kaolinite precipitation. Although possible, the very high supersaturation of well 503 water with respect to kaolinite suggests that the mineral does not undergo very fast precipitation, at least at pH values >4. Instead, we favor aluminum control by $Al(OH)_3$ precipitation (with possible recrystallization to gibbsite).

The second NETPATH simulation. A second attempt to run the same NETPATH simulation using Na as the conservative constituent, instead of chloride, resulted only in "invalid" models that required the dissolution, rather than the precipitation, of 2.22 millimoles of gypsum per kg of water. Because both the acidic and neutralized ground waters at Pinal Creek are supersaturated with respect to gypsum, slightly but consistently, a model with gypsum dissolution was not plausible. A pure chloride source (0.484 millimoles) was used in this second simulation. The calculated mixing fraction of background water from well 504 was 0.347 (instead of 0.216).

The third NETPATH simulation. A third attempt to run the initial NETPATH simulation described above, using an intermediate mixing fraction of 0.281 (instead of 0.216 or 0.347) resulted in 12 models that were similar to those of the first NETPATH simulation, but had different mass-transfer amounts. Gypsum precipitation was very small (-0.003 millimoles). All models found required CO_2 mass transfer, but in somewhat smaller amounts (e.g. -5.4 instead of -6.0 millimoles for Model 1, Table 3).

The fourth NETPATH simulation. A fourth NETPATH simulation was used to explore the effects of including tremolite [$Ca_2Mg_5Si_8O_{22}(OH)_2$], biotite [$KMg_{1.5}Fe_{1.5}AlSi_3O_{10}(OH)_2$], forsterite [$Mg_2SiO_4$], a pure Mn sink (to simulate Mn II sorption) and $AlOHSO_4$, while excluding some of the reactions considered unrealistic in the previous simulations, namely CO_2 exsolution, O_2 dissolution and kaolinite precipitation. Forsterite was included for numerical reasons because it is a pure Mg-silicate with a high Mg/Si ratio. Tremolite and biotite were included because those minerals are commonly found in the Pinal Creek sediments. Although K is present in biotite no mass-balance for K was included in the NETPATH simulations because of the large uncertainties in our estimated K data. The NETPATH simulation resulted in 19 possible models. Of the 19 models, 6 included more than 1 Mg-silicate phase and are therefore not presented here (Table 4) for reasons of space and simplicity. Five models included tremolite as the only Mg-silicate phase, and differed from each other in their treatment of the Mn and Al mass-balances (Models 7, 10-13 in Table 4). Five other similar models included biotite instead of tremolite (Model 8 in Table 4) and 3 remaining models considered forsterite but did not include $AlOHSO_4$.

None of the models found included dolomite, a mineral that we definitely know is present in alluvium (we have seen dolomite rock fragments in the alluvium; dolomite formations are also present in the surrounding hills). Dolomite should certainly be as reactive with the acidic waters as some of the silicate minerals. The problem appears to be that to include dolomite dissolution as a primary contributor of dissolved magnesium a

carbon sink must be found, in addition to rhodochrosite. This carbon sink remains enigmatic so far. In the meantime, of all the models presented in Table 4, we prefer the models (Models 7-9) that considered MnO_2 dissolution and rhodochrosite precipitation and did not include $AlOHSO_4$. The electron transfer models with any Mg-silicate phase are also believable. In reality, the reactions occurring and responsible for the evolution of well 402 water to well 503 water are likely to be some linear combination that may include, but will not be restricted to, the mass transfer models that we found using the NETPATH code. Many more models could have been found had we included other phases (silicates in particular), but their description and classification would have been pointless for the purposes of this manuscript.

Table 4 also gives the millimoles of protons consumed for each reaction, using the assumptions discussed earlier (see discussion of Table 3). Once again it appears that the millimoles of proton consumption calculated for the various reaction models presented in Table 4 are about 3 to 10 times too high. Unaccounted surface deprotonation and proton

Table 4. Fourth NETPATH simulation. Same phases included as in first three simulations, except for the following changes: (1) tremolite, biotite, forsterite, $AlOHSO_4$, a pure Mn sink included as possible phases; (2) kaolinite and gas mass transfers excluded. e^- trans.: electron transfer mechanism.

	Model 7 tremolite	Model 8 biotite	Model 9 forsterite	Model 10 tremolite e^- trans.	Model 11 tremolite Mn sink	Model 12 tremolite $AlOHSO_4$	Model 13 tremolite no anorthite $AlOHSO_4$
well 504 fraction	0.216	0.216	0.216	0.216	0.216	0.216	0.216
pure Na	-0.579	-0.579	-0.579	-0.579	-0.579	-0.579	-0.579
dolomite +							
gypsum - **F**	-2.219	-2.219	-2.219	-2.219	-2.219	-0.648	-0.089
goethite - **F**	-8.339	-11.238	-8.339	-8.339	-8.339	-8.339	-8.339
calcite + **F**	4.696	6.146	4.696	1.724	1.724	4.696	4.696
anorthite	2.130	1.840	3.290	5.102	5.102	0.559	
$AlOHSO_4$ -						-1.571	-2.130
gibbsite	-4.712	-6.066	-7.032	-10.656	-10.656		1.678
SiO_2	-8.587	-9.166	-7.717	-14.530	-14.530	-5.445	-4.326
rhodochrosite	-2.972	-4.422	-2.972			-2.972	-2.972
MnO_2 +	4.064	5.514	4.064	7.036	4.064	4.064	4.064
$Mn(OH)_3$ -				-5.944			
Mn sink -					-2.972		
tremolite	0.580			0.580	0.580	0.580	0.580
biotite		1.933					
forsterite			1.450				
net protons consumed	5.711	7.642	5.711	5.711	11.655	5.708	5.711

exchange reactions and analytical data uncertainty offer possible reasons for the discrepancy. This problem will be circumvented in the PHREEQC inverse modeling demonstration discussed later on, because PHREEQC always includes alkalinity mass-

balance and charge balance equations and also considers possible uncertainties in the analytical data.

The fifth and sixth NETPATH simulations. A fifth NETPATH simulation was conducted using Na, instead of Cl, as the conservative element dictating the mixing fractions of the waters from wells 402 and 504. Fifty-one models were found, but all dissolved more than 2 millimoles of gypsum. Similarly to the third NETPATH simulation conducted above, a sixth simulation was also conducted using an average mixing fraction of well 504 water (0.2814) midway between those of simulations 4 and 5. The 13 models found were similar to those of the fourth NETPATH simulation, but had different mass-transfer amounts. Gypsum precipitation was very small (-0.003 millimoles). None of the models found included $AlOHSO_4$ precipitation or dolomite dissolution. It is likely, however, that the dissolution of Ca- and Mg-silicates would also provide a source of Na. If that is the case, and if we assume that well 503 water (Nov. 1991) is indeed derived from well 402 water (Jan. 1989), then a Na sink remains to be found. Alternatively, we may consider that (1) the background water chosen does not have a Na composition representative of the diluting waters mixing with well 402 type water, or (2) analytical errors are present in the reported Na concentrations, which prevent the use of this element as a conservative constituent. Although the increase in Ca/Na ratios would normally argue against removal of dissolved Na by ion exchange, dissolution and accelerated weathering of silicate minerals by the acidic waters may be causing a significant increase in the cation exchange capacity of minerals exposed to the ground waters and may thus be responsible for a net removal of Na (and other cations) from solution (Blair Jones, U.S. Geological Survey, verbal communication).

Conclusions from the NETPATH simulations. Perhaps the most important conclusion provided by the NETPATH simulations above is that Ca- and Mg-silicate mineral dissolution must be a significant process. Many researchers at the Pinal Creek site originally believed that calcite and dolomite dissolution was responsible for the most of the acid neutralization. However, Glynn (1991) demonstrated that the increase in Sr concentrations between wells 51 and 402 must have been caused by silicate mineral dissolution, because the amount of Sr present in limestone and dolomite formations contributing to the carbonate content of the alluvial materials is too small relative to the amount of Sr that precipitates out as an impurity in gypsum. Sr is a significant impurity in Ca-silicate minerals and is released to the solution during their dissolution and weathering. Similarly, dissolved inorganic carbon $\delta^{13}C$ data (Glynn, Busenberg and Brown, unpublished data collected in June 1993) ranges from -9.15 to -12.90 per mil for the acidic or neutralized contaminated ground waters, and from -10.95 to -14.00 per mil for the uncontaminated waters, suggesting that neutralization of the acidic plume by silicate minerals must indeed be very important. [All $\delta^{13}C$ values are expressed relative to the Vienna PDB standard.] If the calcite and dolomite $\delta^{13}C$ values are near 0 per mil, as is reasonable for most marine carbonates, closed system dissolution of those carbonates, as may be caused by acid neutralization reactions deep within the aquifer, should have resulted in significantly higher $\delta^{13}C$ values. This theory awaits confirmation (or denial) from a determination of the actual solid carbonate $\delta^{13}C$ values.

Inverse geochemical modeling with PHREEQC. PHREEQC provides additional capabilities for modeling of the chemical evolution between the well 402 and well 503 waters, because it considers uncertainties associated with individual element analyses and also solves alkalinity-balance, water mass-balance and charge-balance equations. PHREEQC allows each analytical datum for each aqueous solution to be adjusted within an uncertainty range that is specified by the user. PHREEQC will determine sets of phase mass-transfers, solution mixing fractions, and adjustments to the analytical data that satisfy

mass-balance constraints and are consistent with the specified uncertainties. As an option, PHREEQC will also determine mass-transfer models (later referred to as "minimal" models) that minimize the number of phases involved. The constraints used by PHREEQC inverse modeling are automatically specified by providing a list of the potentially reactive phases. For example, if tremolite is identified as a potential reactant, PHREEQC will automatically use mass-balance constraints on Ca, Mg, and Si (NETPATH does not do this). In addition to the mass-balance constraints defined by specifying a list of potential reactants, PHREEQC also lets the user specify additional mass-balance constraints that may be used in determining the mixing fractions for two or more solutions that mix to form a final solution. Unlike NETPATH, PHREEQC includes a charge-balance constraint, which specifies that the sum of the deviations from the analytical data for a given solution must equal the charge imbalance present in that solution. PHREEQC also uses a water mass-balance constraint to account for mixing, water derived from mineral reactions, and water evaporation or dilution (PHREEQC and NETPATH are not limited to ground-water problems). The charge-balance and water mass-balance constraints used by PHREEQC are equivalent to including a mass balance on hydrogen or oxygen. During the inverse modeling simulation, PHREEQC will adjust not only the analytical element concentrations, it will also adjust the pH of the waters. The adjustment to total dissolved inorganic carbon is constrained to be consistent with the adjustments to pH and alkalinity.

A PHREEQC simulation was constructed using all the phases used in the NETPATH simulations described above, except for kaolinite and CO_2 and O_2 gases which were excluded. Including biotite [$KMg_{1.5}Fe_{1.5}AlSi_3O_{10}(OH)_2$] in PHREEQC forced the code to account for K mass-balance. K, however, can not be expected to accumulate in the Pinal Creek ground waters and should also not be used to determine the mixing fractions of well 402 and well 504 waters. Therefore, a pure potassium-montmorillonite [$K_{0.33}Al_{2.33}Si_{3.67}O_{10}(OH)_2$] was also included in the simulations with biotite and only allowed to precipitate. Both sodium and chloride were also specified as mass balance constraints. Pure Na, pure Cl or pure Mn sinks were not specified, because PHREEQC does not allow the specification of charge-imbalanced phases. Adding charge imbalance would prevent PHREEQC from correctly adjusting the analytical data within the user-specified uncertainties. Adding Na as NaOH would also interfere with the PHREEQC results, because it would affect the alkalinity balance by causing a change in pH. A ±5% relative uncertainty was chosen for all elements, except for K (±20%) and for Cl for which an uncertainty of ±10% was initially chosen but later was reduced to ±5%. The lower uncertainty for Cl did not affect the number of possible mass-transfer models calculated by PHREEQC, minimal or otherwise, did not significantly affect the calculated mixing fractions of well 504 water, and did not result in any changes in the phases included in the mass-transfer models. The uncertainty in the pH of the three waters from wells 402, 504 and 503 was ±0.05 pH units. The "minimal" option was initially chosen to reduce the number of possible models to those minimizing the number of phases involved. Some additional precipitation-only and dissolution-only constraints were added on the phases chosen. The models shown in Table 5 represent a representative selection of all the models found by PHREEQC. Table 5 shows most of the tremolite-containing models, but all other models found (with biotite/K-montmorillonite, forsterite or tremolite) were essentially variations on the combination of reactions shown in Table 5. It should also be remembered that, similarly to the NETPATH models, linear combinations of PHREEQC inverse models also represent possible models. With the exception of Model 1 (compare with Model 2!), all models reported in Table 5 are "minimal" models, i.e. had the minimum number of phases.

PHREEQC also calculates, as an option, the minimum and maximum mass transfers associated with any given phase in any given model. These minimum and maximum mass-

transfers are calculated from the minimum and maximum values associated with the various element and pH analyses. Due to space considerations, only the minimum and maximum mixing fractions of well 504 water are given in Table 5. The optimal mixing fractions of well 504 water reported by PHREEQC are very close to the minimum possible values and do not change significantly between the various models found. The mixing fraction of 0.258 reported in Table 5 is in between the values of 0.216 and 0.347 determined by NETPATH respectively assuming either conservative dissolved Cl or conservative dissolved Na.

The fact that gypsum precipitation is not present in any of the minimal or non-minimal models found is one of the most important results of the PHREEQC inverse modeling on the well 402 + well 504 $\Rightarrow$ well 503 chemical evolution problem. PHREEQC revealed the fact that SO_4 could essentially be considered a conservative entity given the ±5% uncertainty associated with its analysis. Although most of the reasonable NETPATH mass-transfer models based on chloride conservation showed that 2 millimoles of gypsum should precipitate, this mass-transfer was essentially insignificant given the ±5% relative uncertainty on the SO_4 concentrations and the very high SO_4 concentrations in the well 402 and 503 waters. In contrast to the PHREEQC results, the mass-transfer models reported by NETPATH all included 10 phases. Given the uncertainties in the analytical data, PHREEQC shows that only 7 or 8 phases were really required.

The second major conclusion confirmed the earlier NETPATH simulation result that Ca- and Mg-silicate phases are definitely needed in addition to calcite and dolomite to explain the Ca, Mg and C mass balances. Another conclusion, not revealed by the previous NETPATH simulations, was the inclusion of dolomite in some of the minimal phase models. This conclusion was satisfying, because we do believe that dolomite is indeed reacting and it is definitely present in the aquifer.

The PHREEQC results presented in Table 5 appear to show a net production of close to 0.3 millimoles of protons. This was calculated, as previously done for the NETPATH model results (see discussion of Table 3), from the mass-transfer amounts given in the PHREEQC models. The amount of net proton consumption calculated for the PHREEQC models is an order of magnitude smaller than the amounts calculated for the NETPATH models presented earlier. Because of its solution of the alkalinity-balance and charge-balance equations, PHREEQC actually ensures that the net amount of protons released and consumed by heterogeneous and homogeneous reactions is consistent with the pH values of the initial and final waters, and with the uncertainties specified by the user. The proton consumption numbers can be checked against the change in alkalinity between the final well 503 water and the mixture of the well 402 and 504 waters. The alkalinity changes reported in Table 5 use the adjusted alkalinities used by PHREEQC in each calculated inverse model. The difference between the net proton consumption numbers and the net alkalinity changes is caused by the fact that the consumption of dissolved oxygen (6.64 mg/L in well 504) was not accounted for in our proton consumption calculations (David Parkhurst, pers. comm.). The difference of 0.49 millimoles is close to 4 times the difference between the oxygen content of the well 503 water and a mixture of the well 504 and well 402 waters (4 $\times$ 0.121 = 0.484 millimoles). Essentially, the presence of dissolved O_2 in the well 504 water reduces the amount of MnO_2 which undergoes reductive dissolution. The fact that 4 protons are consumed rather than 2 for each mole of oxygen consumed appears to be an error in the PHREEQC code (David Parkhurst, pers. comm.). Because the MnO_2 mass transfer is 30 times greater than the oxygen mass-transfer, this error should not significantly affect our results.

Out of the 6 minimal models presented in Table 5, our favorite models are Models 7,

2, 4 and 3. These models do not involve $AlOHSO_4$ precipitation. The evidence for possible Al control by $AlOHSO_4$ precipitation during the evolution from well 402 water to well 503 water is weak, although the possibility cannot yet be rejected. Until proven wrong, we prefer to believe that amorphous $Al(OH)_3$ is the controlling Al phase. Tremolite is present in the alluvial materials and its reaction with acidic water from the Pinal Creek site has been documented by Lind and Stollenwerk (1994). Nevertheless, it probably contributes much less Ca, compared to Ca-rich plagioclase feldspars (such as anorthite and labradorite), during the neutralization of the acidic ground waters. The accompanying release of Na during feldspar dissolution could still remain a problem, however, because the above PHREEQC models consider Na as a conservative constituent, within the uncertainty of the analytical data. Too much Na dissolution would require finding a Na sink which remains elusive. As mentioned earlier, additional cation exchange capacity resulting from the trans-

Table 5. PHREEQC inverse-modeling simulation results. Amounts of mass transfer and net proton consumption are reported in millimoles per kilogram of H_2O. Only mass-transfer sets (models) with the minimum significant number of phases are shown. The sum of residuals gives an indication of the sum of the analytical data adjustments made by PHREEQC.

Abbreviations: 504 mf., well 504 mixing fraction; +, dissolution only; -, precipitation only; Alk., alkalinity change; non-min., not a "minimal" model; K-mont., K-montmorillonite.

	Model 1 tremolite non-min.	Model 2 tremolite	Model 3 tremolite no calcite	Model 4 tremolite e⁻ trans.	Model 5 tremolite $AlOHSO_4$	Model 6 tremolite $AlOHSO_4$ e⁻ trans.	Model 7 biotite
504 mf.	0.258	0.258	0.258	0.258	0.258	0.258	0.258
504 mf. min.	0.258	0.258	0.258	0.258	0.258	0.258	0.258
504 mf. max.	0.277	0.277	0.277	0.277	0.264	0.264	0.263
dolomite +	0.398		2.191		0.290		2.291
gypsum -							
goethite -	-8.292	-8.292	-8.292	-8.291	-8.292	-8.292	-9.074
calcite +	3.588	4.383		1.626	3.817	3.991	
anorthite +			2.512	2.202			2.691
$AlOHSO_4$ -					-0.423	-0.423	
gibbsite -	-0.423	-0.423	-5.448	-4.827			-2.167
SiO_2 -	-3.649	-3.649	-5.803	-8.687	-3.165	-3.629	
rhodochrosite	-2.757	-2.757	-2.756		-2.769	-2.364	-3.253
MnO_2 +	3.903	3.903	3.903	6.659	3.903	4.309	4.294
$Mn(OH)_3$ -				-5.512		-0.811	
tremolite +	0.500	0.500	0.142	0.580	0.440	0.498	
biotite +							0.521
K-mont. -							-1.796
Sum of resid.	6.180	6.611	6.182	6.184	7.226	7.227	10.830
Net protons consumed	-0.279	-0.281	-0.272	-0.266	-0.271	-0.270	-0.298
Alk. change	0.214	0.213	0.213	0.213	0.213	0.213	0.190
Difference	0.493	0.494	0.485	0.479	0.484	0.483	0.487

formation of the feldspars and other aluminosilicates into secondary clays minerals is the only Na sink that we can think of. Sorption on freshly precipitated iron oxyhydroxides could also represent a possible Na sink, although the affinity of Na for these precipitates is considerably weaker than the affinity of the other metals and cations present in the solution.

Two additional PHREEQC simulations were conducted allowing ion exchange of Na for Ca in one simulation and exchange of Na for H in another. The ion exchange reactions were simulated by adding phases NaX and CaX_2 or HX to the list of postulated phases (X is an ion exchange site in the PHREEQC database). Because element "X" is not specified in either the initial or final solutions, PHREEQC automatically sets its concentration (and its associated uncertainty) to 0 in all three solutions, and thereby ensures that any loss of Na by ion exchange is automatically matched by an equivalent release of Ca or H from CaX_2 or HX. For the sake of brevity, only a representative selection of the models found with the proton exchange reaction are presented here (Table 6). The mixing fraction of well 504 water determined in all the ion-exchange models found was close to, or significantly lower than 0.216, the fraction determined on the basis of conservative dissolved chloride in the NETPATH simulations. Interestingly, gypsum dissolution was included in three of the proton exchange models found that included biotite/K-montmorillonite. All three had unrealistically low mixing fractions of uncontaminated water from well 504 (2.6%). All models found that included tremolite, in either the Na/Ca exchange or the Na/H exchange simulations, also included $AlOHSO_4$ precipitation. The lower mixing fractions of uncontaminated water invariably resulted in lower dissolved-oxygen transfers. As discussed earlier and shown in Table 6, if the oxygen transfer (in millimoles of O) is multiplied by 4 and added to the calculated net proton consumption for the dissolution of the mineral phases, a very close match is obtained with the PHREEQC-calculated alkalinity change. We do not favor the ion-exchange models because we estimate that the cation exchange capacity of the Pinal Creek alluvial sediments is very low, probably lower than 1 meq/100 g, given the coarseness of the sediment and the less than 1% organic carbon content. Until more information becomes available concerning the possible ion-exchange reactions at the Pinal Creek site, Models 7, 4, 2 and 3 from the earlier PHREEQC simulation without ion exchange (Table 5) remain our preferred models. Simulating ion exchange in an inverse geochemical model presumes that the user has some knowledge of the thermodynamically preferred directions of exchange. Although we feel that Na replacement for Ca on exchange sites should generally not occur given the preferential dissolution of Ca over Na resulting from other mineral dissolution reactions, determining the direction of exchange for some other ion-exchange reactions is fraught with much greater uncertainty. Proton release from exchange sites during the neutralization of well 402 water is certainly conceivable, however. Our inverse geochemical modeling simulations point out the need for further experiments to determine more exactly actual cation exchange capacities and directions of exchange. The ability of inverse modeling to highlight knowledge gaps is perhaps one of its greatest benefits. As will be demonstrated in the next section, forward geochemical modeling may be able to provide greater insight into ion exchange reactions.

Although some mass transfer processes are likely to be occurring continuously throughout the flow path section used in inverse modeling, some mass transfer processes (such as ion exchange reactions) will be affecting the ground-water chemistry only in narrow portions of the flow system. In the case of continuous processes, an overall rate of reaction (expressed for example in moles per kg of H_2O per travel time and per traveled volume of aquifer) may be provided by the inverse modeling results. In the case of a non-continuous process, however, such rates will have little meaning. Unfortunately, inverse geochemical modeling can not provide information on the heterogeneous mass-transfer reactions occurring at specific points along a flow-path, but provides, instead, only the net

Table 6. PHREEQC inverse-modeling simulation with Na/H exchange. Amounts of mass transfer and net proton consumption reported in millimoles per kilogram of H_2O. Only mass-transfer sets (models) with the minimum significant number of phases are shown.
504 mf.: well 504 mixing fraction; + : dissolution only; – : precipitation only

	Model 1	Model 2	Model 3	Model 4	Model 5
504 mf.	0.205	0.219	0.026	0.135	0.142
504 mf. min.	0.190	0.206	0.026	0.259	0.103
504 mf. max.	0.274	0.254	0.091	0.195	0.220
dolomite +		2.242			0.825
gypsum -			-6.818		
goethite -	-8.457	-8.312	-11.640	-9.208	-10.480
calcite +	4.590		6.602	1.657	
anorthite +		3.872	3.798	1.420	3.958
$AlOHSO_4$ -	-0.459			-3.349	-2.733
gibbsite -		-8.194	-2.664		
SiO_2	-3.744	-7.428		-6.461	
rhodochrosite	-2.950	-2.848	-4.920		
MnO_2 +	4.028	3.944	5.763	7.932	9.183
$Mn(OH)_3$ -				-6.947	-8.188
tremolite	0.506			0.482	
NaX	-0.628	-0.568	-1.423	-0.941	-0.909
HX	0.628	0.568	1.423	0.941	0.909
Biotite			0.854		0.899
K-montmorillonite			-2.733		-2.826
Sum of residuals	2.580	3.996	4.531	3.003	3.179
Net protons consumed	0.018	-0.062	0.994	0.395	0.354
Alkalinity change	0.417	0.363	1.102	0.685	0.655
O-transfer	0.1	0.106	0.029	0.072	0.075
O-adjusted Difference	-0.002	0.002	-0.009	0.001	0.001

amounts of mass transfer between an initial and a final endpoint. Forward geochemical modeling can, however, provide insight on the possible evolution through time of chemical compositions at specific points along a postulated flow path. *Verification* of the forward modeling simulations may nevertheless also necessitate more spatial information than may be available.

REACTIVE TRANSPORT MODELING AT THE PINAL CREEK SITE

Inverse modeling is a valuable tool that can be used to gain an improved understanding of the geochemical processes that may be occurring, or have previously occurred, in an aquifer. By itself however, inverse modeling can not be used to make predictions on the future chemical evolution of a ground-water system, or in the case of a contaminated ground-water, on the movement of contaminants. Forward reactive transport modeling is needed to make any such predictions. Inverse modeling results, nevertheless, can be used to suggest the possible reactions that should be considered by a reactive transport model.

In metal-contaminated acidic ground waters such as those present at the Pinal Creek site, pH and Eh conditions are the primary chemical variables controlling the transport of metals and determining the quality of the ground waters. The partially-neutralized, Fe(II)-poor ground waters (such as the well 503 water used in our inverse modeling exercise) have significantly lower metal concentrations than the more acidic Fe(II)-rich waters (such as the well 402 water used above). The partially neutralized waters are still contaminated and have high SO_4, Ca, and Mn concentrations that make them unsuitable for normal human or domestic use, but nevertheless offer a significant improvement in water quality. Therefore, being able to predict the movement of the low-pH and Fe(II)-rich ground-water zones or at least their movement relative to that of unreactive conservative constituents, would be very desirable.

Inverse modeling can help identify the possible reactions affecting the neutralization and oxidation of the low-pH and Fe(II)-rich ground waters. Generally however, the movement of the low-pH and Fe(II)-rich waters will be controlled by the following factors: (1) the ground-water velocity field, (2) the dilution of the contaminated ground-waters by longitudinal and transverse dispersion, (3) the amounts of heterogeneous mass-transfer reactions affecting the pH and Fe(II) concentrations in the ground waters (causing the low-pH Fe(II)-rich waters to evolve into higher-pH Fe(II)-poor waters) and (4) the initial concentration and composition of phases present in the background or fully neutralized aquifer and responsible for the chemical evolution of the contaminated waters. The following sections briefly discuss ongoing research efforts aimed at a better understanding of the movement of acidic metal-rich ground waters at the Pinal Creek site. The research findings from the Pinal Creek site will hopefully provide information, not only on the processes controlling the spread of acidic metal-laden ground waters in semi-arid alluvial basins, but also on the most efficient techniques that can be used to characterize and model the spread of contaminated waters at similar sites with sparse spatial information.

The ground-water velocity field

Gound-water velocities can be determined through the construction of a ground-water flow model. Although calculations using Darcy's law on observed heads and estimated hydraulic conductivities have provided some estimates of ground-water velocities in the Pinal Creek basin (Brown, 1996; Neaville and Brown, 1993), efforts are currently under way to construct a general flow model for the alluvial and basin-fill aquifers, using not only observed heads and other hydrologic properties and characteristics, but also chemical and isotopic tracers (Glynn and Busenberg, 1994a) as evidence of ground-water provenance (O^{18}, H^2, dissolved Ar and N_2, Cl and conductivity) and ground-water residence times (chlorofluorocarbon, SF_6 and H^3/He^3 age-dating techniques). Because of the paucity of available hydrologic data, alternative sources of information, such as geochemical and isotopic information, are proving themselves invaluable at the Pinal Creek site. Inverse flow modeling with the MODFLOWP code (Hill, 1992) in conjunction with the MODPATH particle-tracking code (Pollock, 1989) will be used to estimate hydraulic conductivities and appropriate boundary conditions from observed hydraulic heads and from chemically and isotopically-estimated ground-water recharge dates and provenance. Having an adequate ground-water flow model is an essential prerequisite to understanding the movement of contaminated waters at the Pinal Creek site and the impact of anthropogenic or natural remediation processes.

Transport processes and contaminant dilution

The dilution of the acidic metal-contaminated ground waters is certainly one of the most important processes responsible for the downgradient decrease in dissolved-metal concentrations in the Pinal Creek basin. Although this dilution process was already evident

in the dry to normal recharge years of the period 1984-1991, further dilution occurred as a result of the greater than normal recharge events that started in the spring of 1991, continued in 1992 and culminated in a 100-year-magnitude flooding event in spring 1993 (ground-water levels rose as much as 16 meters). Advanced modeling techniques are not needed to determine that such a dilution process exists; plots of metal concentrations as a function of chloride, or of other non-reactive constituents associated with the contaminated waters, clearly illustrate the process (Figs. 3 and 4). However, a 2- or 3-dimensional transient transport model of the site would clearly be of use in determining the effects and contributions of transverse dispersion, longitudinal dispersion, flow convergence and transient high-intensity recharge events in the dilution process. An appropriate ground-water flow model is required before such a useful transport model can be built; the construction of this transport model therefore also depends on the results of chemical and isotopic tracer and age-dating investigations currently being conducted at the site.

First simulation example:

The Brown (1996) 1-D reactive transport model for the Pinal Creek basin

Brown (1996) used the ground-water chemical data collected by the U.S. Geological Survey since 1984, to construct a 1-D reactive transport model of the site using the PHREEQC computer code. The author used measured chloride concentrations to back-fit the observed dilution of the most contaminated ground waters in the Pinal Creek basin as a function of time (from 1984 until 1994) and distance along a flow-path that extended from well 51, through wells 302, 402, 451, 503, 601, all the way to well 702 (Fig. 5). Only a few adjustments were made to the external dilution of the 1-D column after the initial fit of the 1984 chloride profile. Adjustments were made in March 1985 and in January 1988 just downgradient of well 101 (near km 1 in the profile), and more importantly in February 1993 in the profile section between wells 402 (km 5.8) and 503 (km 11.4). This later adjustment was necessitated by the very large flooding events that occurred during the spring of 1993. The PHREEQC code was used, because it allows simulation of advective transport, simulation of mixing processes and simulation of equilibrium geochemical reactions, including heterogeneous redox reactions and sorption with a diffuse double-layer surface-complexation model. The results of the modeling investigation showed that dilution, rather than sorption or other reaction processes, could account for the decrease of Cu, Zn, Ni and Co in the acidic ground-water upgradient from well 451. The results also suggested that reductive dissolution of Mn oxides by Fe(II) was taking place not only between wells 402 and 503 (where Fe(II) has completely disappeared), but also between wells 302 and 402, perhaps because of slow reaction kinetics. Indeed, the simulated Fe(II) concentrations are higher than the observed concentrations, and simulated Mn(II) concentrations are lower than the concentrations observed in this part of the flow path (Figs. 6 and 7). In the neutralized Fe(II)-poor ground-waters, dilution is a much less significant process and Brown (1996) suggested that sorption was an important removal process for Cu, Ni, Zn and Co. Brown (1996) also proposed that O_2 ingassing might be important in removing dissolved Mn(II) from the ground waters between wells 503 and 601. Rhodochrosite precipitation was not allowed in the Brown (1996) model (unlike most of the reactive transport simulations presented later in this paper). To better match the observed or calculated TDIC values (Fig. 8), the model also allowed CO_2 exsolution between wells 451 and 702 in equilibrium with a specified CO_2 partial pressure of $10^{-1.33}$. This pCO_2 value was determined from dissolved CO_2 measurements and considered appropriate for well 503 (Glynn and Busenberg, 1994a,b). The results of our inverse modeling work show, however, that CO_2 exsolution, between wells 402 and 503, does not need to be considered if Ca- and Mg-silicate mineral dissolution occurs.

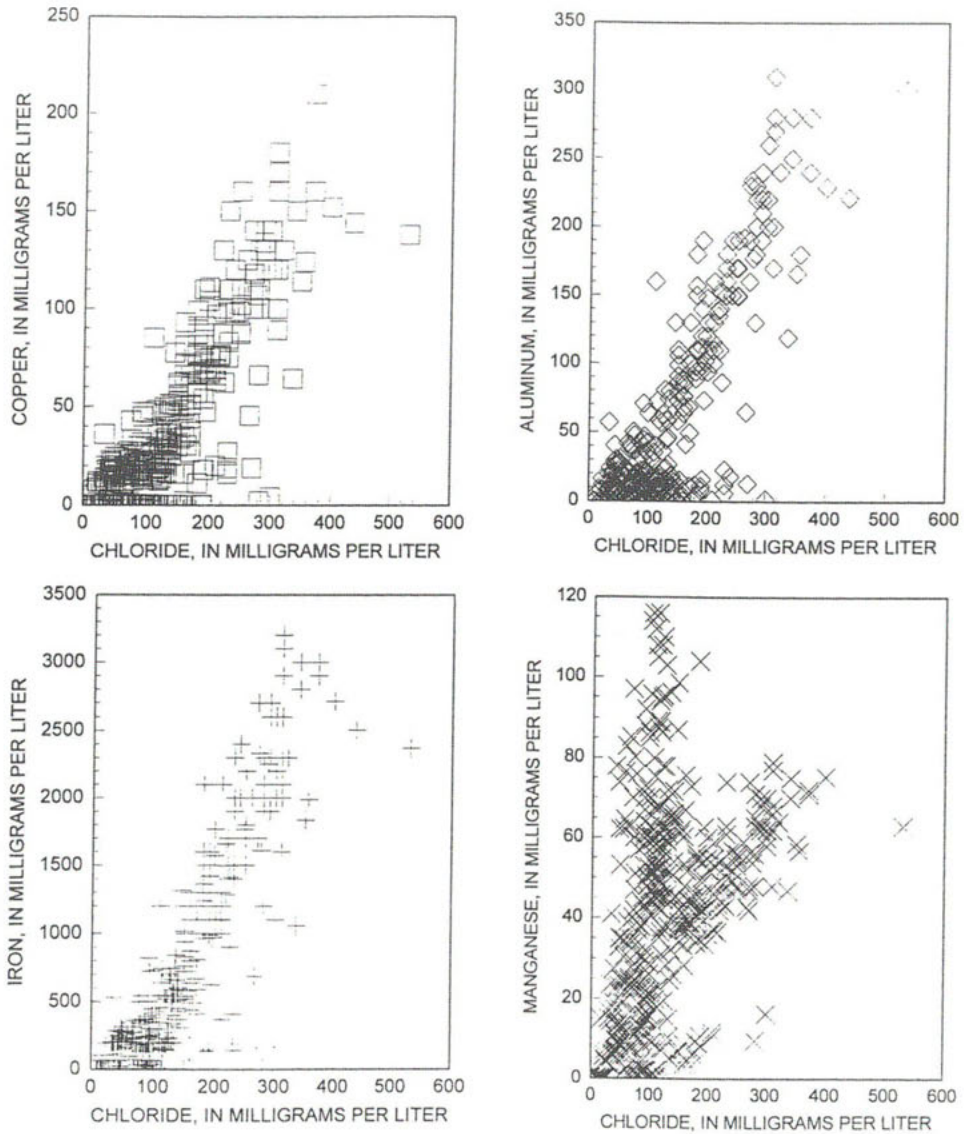

Figure 3. Copper, aluminum, iron and manganese concentrations in Pinal Creek ground waters as function of dissolved chloride. The linear decrease in metal concentrations as a function of chloride indicates the effects of dilution. Relatively low metal concentrations in waters with high chloride concentrations are the result of precipitation reactions. Waters with high manganese and relatively low chloride concentrations are typical of dilute partially-neutralized Fe(II)-poor contaminated ground waters.

Second simulation example:
The Glynn, Engesgaard and Kipp (1991) 1-D reactive transport model

In a comparison of the PHREEQM and MST1D (Engesgaard and Kipp, 1992) reactive transport codes, Glynn et al. (1991) simulated the movement of acidic water from well 51

(August 1987 sample) into a 1-dimensional column with the following minerals assumed to be initially present and distributed homogeneously throughout the column (contents expressed in mol/kg H_2O): calcite (4.2×10^{-2}), dolomite (2.1×10^{-2}), microcline (1.75×10^{-2}), birnessite (2.0×10^{-2}). Amorphous $Fe(OH)_3$, gypsum, silica gel and gibbsite were allowed to precipitate. Unlike most of the transport simulations presented later in this paper, the column was also left open to an equilibrium pCO_2 of 10^{-2} and rhodochrosite was not allowed to precipitate. The local equilibrium assumption was used for all simulated reactions.

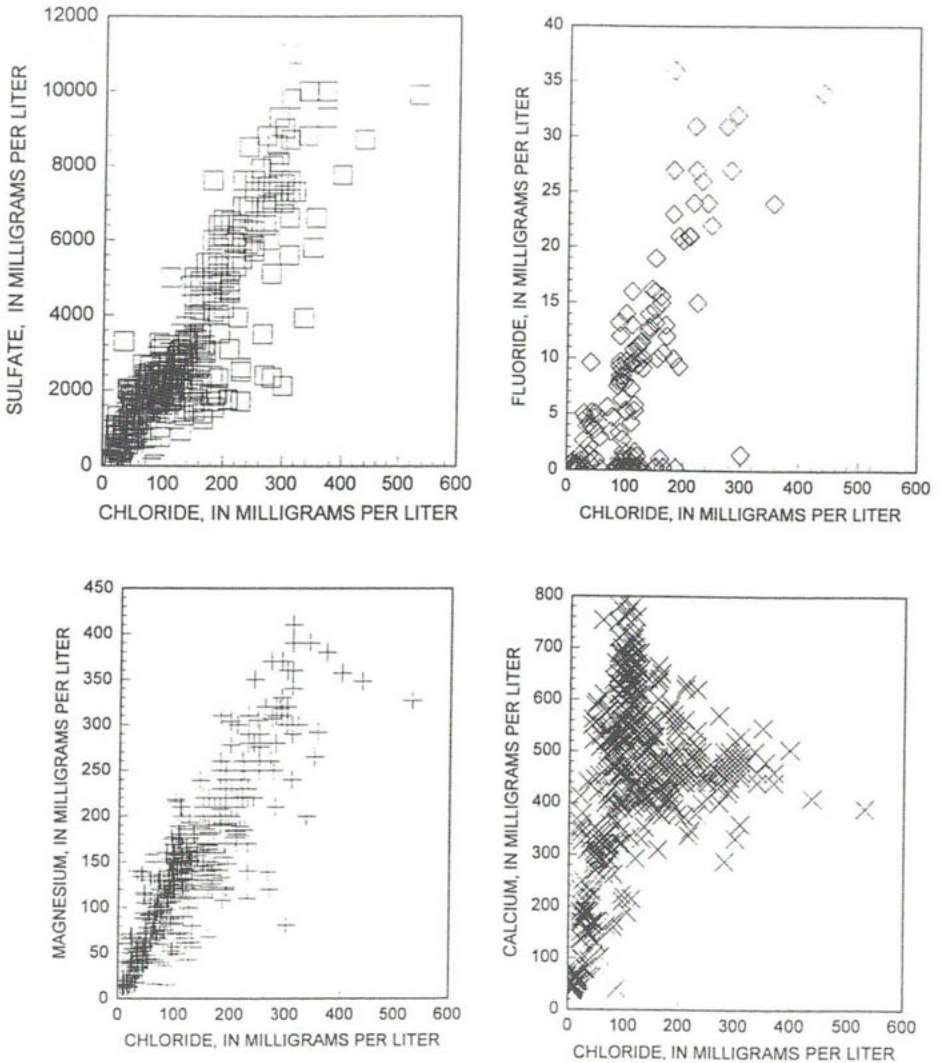

Figure 4. Sulfate, fluoride, magnesium and calcium concentrations in Pinal Creek ground waters as function of dissolved chloride. The chloride versus calcium plot indicates the effect of calcium mineral dissolution reactions in addition to dilution processes.

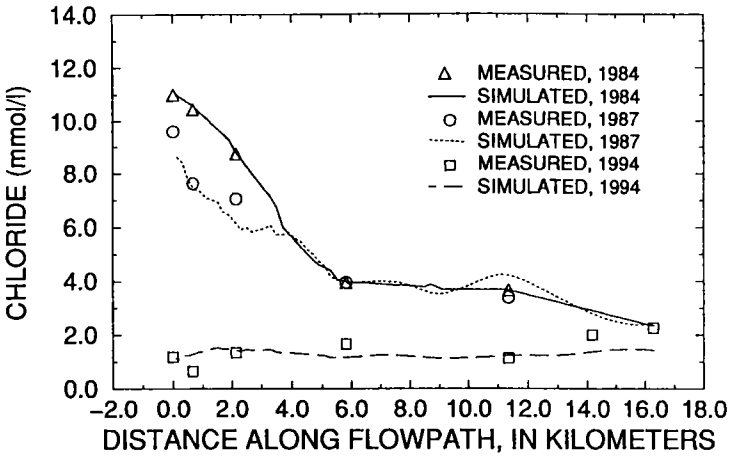

Figure 5. Measured and simulated chloride concentrations in Pinal Creek ground waters along an aquifer flowpath (modified from Brown, 1996). Observed data are for the following wells: 51 (km 0), 101 (km 0.7), 302 (km 2.1), 402 (km 5.8), 503 (km 11.4), 601 (km 14.2) and 702 (km 16.3).

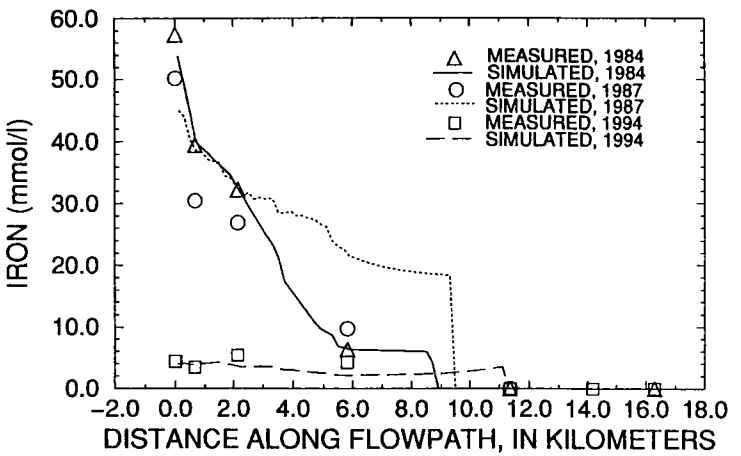

Figure 6. Measured and simulated iron concentrations in Pinal Creek ground waters along an aquifer flowpath (modified from Brown, 1996). See Figure 5 caption for well locations. Note the large decrease in dissolved iron concentrations between 1984 and 1994. This decrease (also seen in the Cl concentrations, Fig. 5) is attributable to the very large recharge events during 1992-1993 (and especially during the spring of 1993), to pumping of some of the more contaminated waters for remediation purposes and to the removal of one of the major sources of contamination (Webster Lake) during 1987.

The water from well 51 used in the simulation was significantly more contaminated than the well 402 water used in the inverse modeling example presented in this paper and used in reactive transport simulations presented later on. The concentration factors relative to the well 402 water used in this paper (Table 7) show that the well 51 water was approximately 2.4 times more concentrated in conservative consituents (Cl, SO_4 and Mg!), only 1.7 times more concentrated in Na (suggesting the existence of a Na source between wells 51 and 402), was significantly more concentrated in Fe and Al, and less concentrated

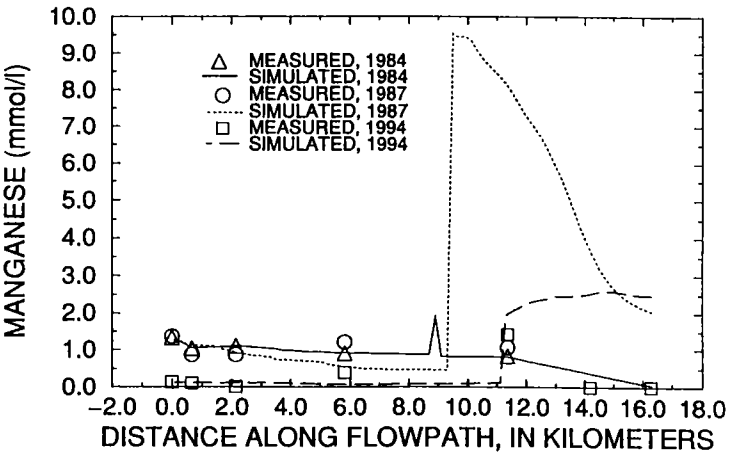

Figure 7. Measured and simulated manganese concentrations in Pinal Creek ground waters along an aquifer flowpath (modified from Brown, 1996). See Figure 5 caption for well locations.

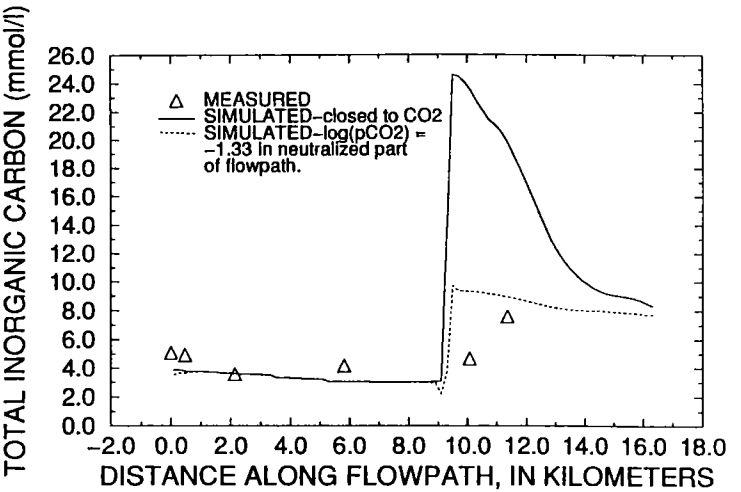

Figure 8. Measured and simulated dissolved inorganic carbon concentrations in Pinal Creek ground waters along an aquifer flowpath (modified from Brown, 1996). See Figure 5 caption for well locations.

ed in Ca and Sr, but had similar SiO_2, TDIC and Mn concentrations. The acidity represented by the potential oxidation and precipitation of the dissolved Fe(II), Mn(II) and Al in the water from well 51 was 1.31×10^{-1} moles of protons instead of 2.60×10^{-2} for the well 402 water, or about 5 times greater. Adding the acidity represented by TDIC does not significantly change the potential acidity of well 51 water, but does increase the potential acidity of well 402 water to a proton molality of 3.01×10^{-2}, a value still 4.5 times lower than that of well 51 water. [The potential acidity is calculated by assuming: (1) each mole of Fe^{2+} oxidation and precipitation (by reductive dissolution of MnO_2 or by reduction of dissolved O_2) can produce 2 moles of H^+, (2) oxidation of dissolved Mn^{2+} and precipitation as MnO_2 (or simply precipitation of $MnCO_3$) can produce 2 moles of H^+, (3) precipitation of Al^{3+} can produce 3 moles of protons, and (4) each mole of H_2CO_3 can produce one mole of H^+.]

Despite the difference in their algorithms, the PHREEQM and MST1D simulations gave very similar results (Figs. 9 and 10). [The MSTID code used a sequential iteration algorithm that iterated at each time step between the solution of the PHREEQE chemical equilibrium code and a solution of the advective-dispersive transport equations solved by an implicit finite difference approximation (based on the HST solute transport code).] The slight observed differences were most likely the result of numerical dispersion in the MST1D simulation. Both simulations showed that, given the mineral and aqueous concentrations used in the simulation, the velocity of the low-pH front would be retarded by a factor of 5 relative to that of the conservative constituents; the velocity of the Fe(II) front would be 1.8 times less than that of the conservative constituents.

Table 7. Chemical composition of the highly acidic ground water used as the infilling solution in the reactive transport simulation of Glynn et al. (1991). Concentrations are expressed as molalities. The 'concentration factors' represent the concentration of a constituent in well 51 water (87/8/18) divided by its concentration in well 402 water (89/1/12).

	Well 51 (87/8/18)	Concentration factors relative to well 402
pH	3.74	2.45 times H^+ activity
Calcium	1.10×10^{-2}	0.87
Magnesium	1.60×10^{-2}	2.40
Sodium	9.13×10^{-3}	1.73
Strontium	1.48×10^{-5}	0.56
Iron	5.01×10^{-2}	4.73
Manganese	1.37×10^{-3}	1.05
Aluminum	9.27×10^{-3}	13.5
Sulfate	9.16×10^{-2}	2.69
Chloride	9.59×10^{-3}	2.42
Silica	1.66×10^{-3}	1.16
TDIC	4.16×10^{-3}	0.99
potential Fe, Al, Mn and TDIC acidity (as proton molality)	1.35×10^{-1}	4.48

The Glynn et al. (1991) simulation of the reactive transport of the most acidic ground water (from well 51) found at the Pinal Creek site serves as a useful comparison for the reactive transport simulations discussed in the next section. These simulations will simulate the evolution of a less acidic water, water from well 402, and will be based on some of the inverse geochemical modeling results discussed earlier in this paper.

A 1-D reactive-transport sensitivity analysis on the movement of pH- and pe-controlling mineral fronts

Some of the reactions identified by inverse modeling of the chemical evolution of ground waters between wells 402 and 503 were used in 1-D PHREEQM and PHREEQC reactive-transport simulations to determine their effect on the movement of the low-pH and high-Fe(II) ground waters in the Pinal Creek basin. Many of results of this study will also be applicable at other ground-water contamination sites by sulfuric acid and heavy metals.

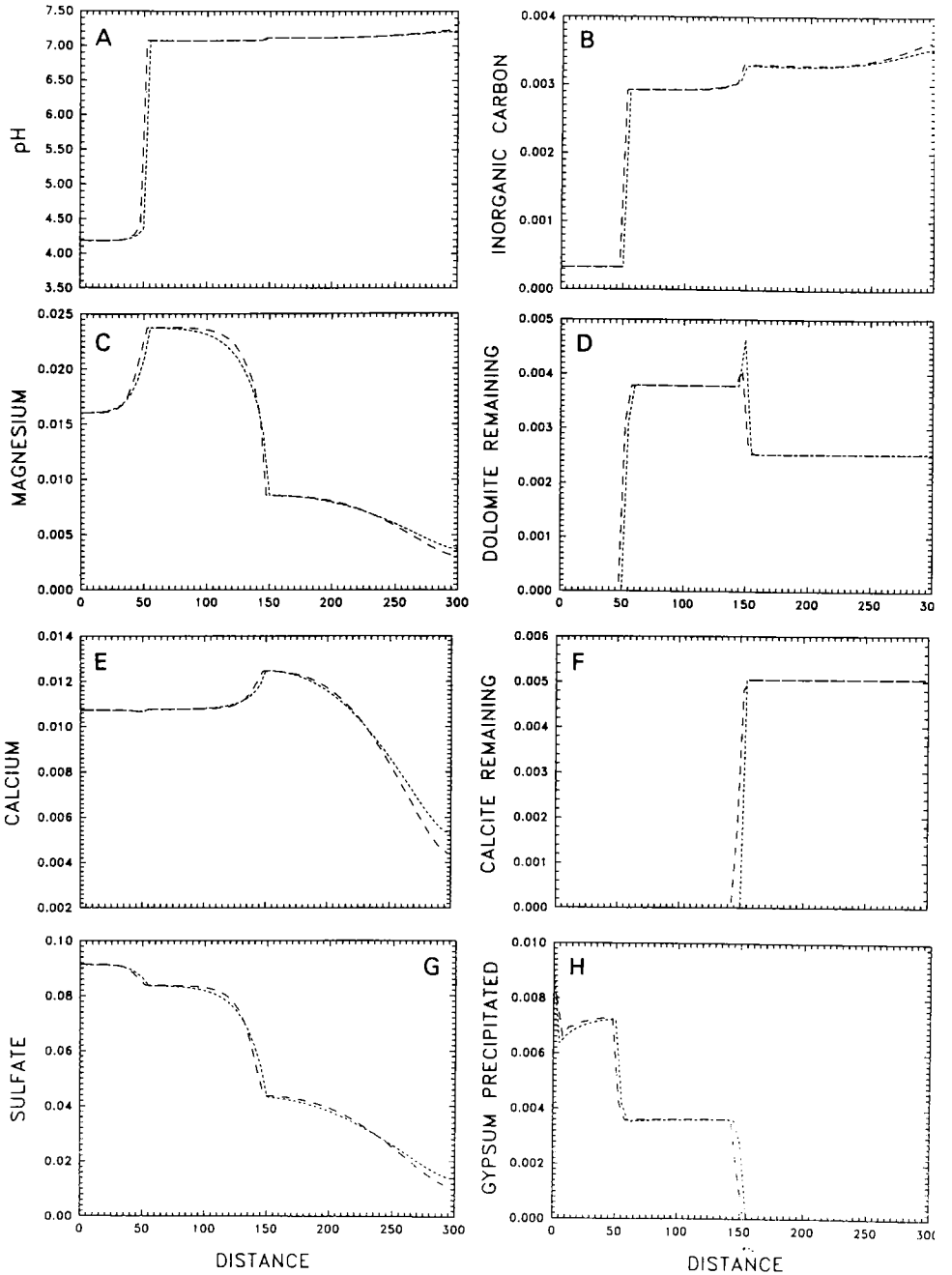

Figure 9. Profiles at 50 days of various pH-dependent aqueous and mineral constituents resulting from the PHREEQM (dashed lines) and MST1D (dotted lines) simulations of an acidic water (from well 51) from the Pinal Creek site intruding into a 1-dimensional model aquifer column with calcite, dolomite and MnO_2 initially present. The column is in equilibrium with a fixed pCO_2 of 10^{-2}. Rhodochrosite is not allowed to precipitate (Glynn et al., 1991).

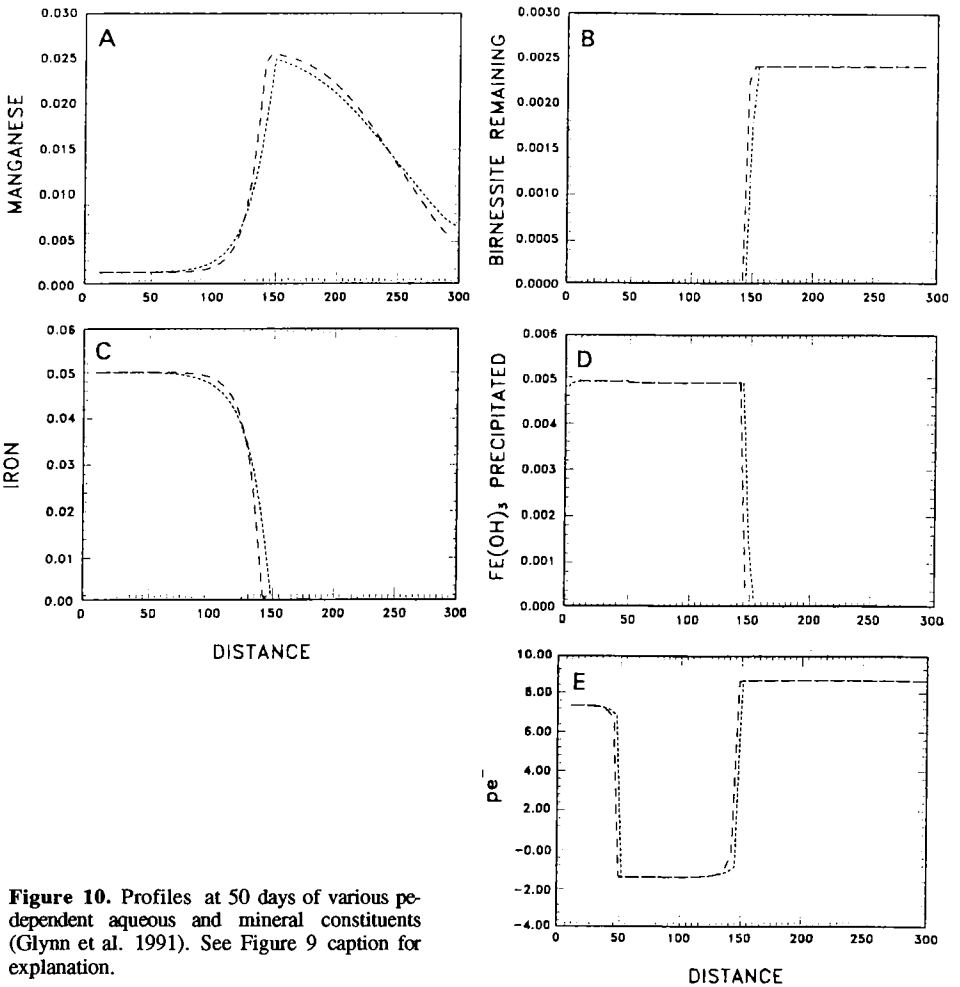

Figure 10. Profiles at 50 days of various pe-dependent aqueous and mineral constituents (Glynn et al. 1991). See Figure 9 caption for explanation.

Before discussing the results of the PHREEQM and PHREEQC transport simulations, however, we will show how the movement of a single mineral dissolution front, critical in controlling the redox state of the Pinal Creek ground waters, can be modeled without the use of a computer code.

A simple model for advective reactive transport of a dissolution front: The MnO_2 dissolution front. If O_2 ingassing is assumed not to affect the concentrations of Fe(II) at significant depths below the water table (11 m for well 402, 21 m for well 503), the movement of dissolved Fe(II) will probably be entirely determined by the reduction of manganese oxides such as exemplified by the following reaction:

$$2\ Fe^{2+} + MnO_{2,s} + 4\ H_2O \Leftrightarrow 2\ Fe(OH)_{3,am} + Mn^{2+} + 2\ H^+$$

The free energy change associated with the above reaction is so highly negative that for all practical purposes the reaction can be considered an irreversible reaction, regardless of which crystal structure is used for $MnO_{2,s}$ (birnessite, pyrolusite) or for the precipitated iron oxyhydroxide. As a result, if the kinetics of the reductive dissolution

reaction are fast relative to the movement of the water (5 m/day), the velocity of the dissolved Fe(II) front, V_{Fe}, can be related to the velocity, V_{H_2O}, of the water through an apparent retardation factor R

$$V_{Fe} = V_{H_2O}/R \tag{14}$$

where R is simply related to the amount, M_{ini}, of MnO_2 initially present in the aquifer (expressed in moles/kg H_2O) and to the amount, ΔM, of MnO_2 dissolved by a unit mass (1 kg of H_2O) of Fe(II)-rich water:

$$R = 1 + \frac{M_{ini}}{\Delta M} \tag{15}$$

Equation (15) can be related to the more general equation describing the retardation of sharp reaction fronts in systems with advective transport but no dispersive transport (Dria et al., 1987; similar expressions for the "traveling wave" approximation can also be found in Lichtner, 1988, 1985; Ortoleva et al., 1986):

$$R = 1 + \frac{\sum_{k=1}^{K} g_{ik}\left(m_k^D - m_k^U\right)}{\sum_{j=1}^{J} h_{ij}\left(c_j^D - c_j^U\right)} \tag{16}$$

where g_{ik} and h_{ij} are the stoichiometric coefficients of element i in minerals k and aqueous-species j. m_k and c_j are the mineral and aqueous-species concentrations, respectively. Superscripts D and U indicate downstream and upstream concentrations, respectively.

Determination of the initial MnO_2 and carbonate mineral concentrations. Although inverse modeling can be used to determine the mass-transfer amounts (ΔM) for various heterogeneous reactions, inverse modeling can not usually reveal the initial amounts (M_{ini}) of minerals present in an aquifer. Estimates of the average initial mineral contents must be made, either by using batch or column experiments on unaffected aquifer materials, or by judging what a reasonable amount may be on the basis of X-ray evidence or on some knowledge of the retardation observed in the field.

By determining the net mineral mass transfer (ΔM) experienced by a fluid packet between two points along a flow path, an inverse model may be used to set a lower bound on the initial concentration of that mineral ($M_{ini} \geq \Delta M$), but only if the mineral mass transfer occurs in a unique and localized part of the flow path, such as a single reaction front. Indeed, although commonly expressed in mol/kg of H_2O, the mineral mass-transfer determined by an inverse model really applies to the entire volume of aquifer traveled through by a unit packet of water between an initial and a final endpoint. In the case of a slow mass transfer reaction (relative to the movement of the water), the value of ΔM determined by an inverse model will change with increasing flow path length until some equilibrium or steady state is reached. The initial mineral concentration, M_{ini}, in Equation (15) is also expressed in terms of mol/kg H_2O, but really refers to a static mass of water and therefore a localized aquifer volume. In contrast, the value of ΔM determined by inverse modeling has a Lagrangian frame of reference and its units refer to a dynamic mass of H_2O that has traveled along a specific flow path length. In the case of a sharp reaction front responsible for the entire mass transfer, the difference in units may be moot, at least if the mineral concentration M_{ini} was initially uniform between the initial and final end points of the flow path. In any case, Equations (15) and (16) will be of limited use in describing the progression of a slow reaction, one that does not result in the development of a sharp reaction front*.

---

* Lichtner (1988) and Ortoleva et al. (1986) have shown that reaction kinetics will not affect the rate of front propagation *given enough time and distance*. The front may not be as sharp but it will still propagate at the same rate as a front resulting from a simulation that uses the Local Equilibrium Assumption.

We decided to use a value of 2×10^{-2} mol MnO_2 per kg H_2O in our PHREEQC and PHREEQM transport simulations, primarily to stay consistent with the simulations conducted by Glynn et al. (1991). A higher value would perhaps have been more appropriate. Indeed, on the basis of his column elution experiments, Stollenwerk (1994) suggests a value of 7.1 millimoles of MnO_2 per kg of sediment. Depending on the values of porosity and bulk density used, this is equivalent to a value between 3.2×10^{-2} (our estimate) to 4.49×10^{-2} mol/kg of H_2O (value calculated by Brown, 1996). Based on the selective extraction results of Ficklin et al. (1991), Brown (1996) used a value of 7.9×10^{-2} mol/kg H_2O in his 1-D simulation. The maximum and minimum amounts of MnO_2 dissolved between wells 402 and 503 in our inverse modeling simulations were 9.2×10^{-3} (Table 6) and 3.9×10^{-3} mol/kg H_2O (Table 5), respectively. These values may be considered lower bounds for the initial amount of MnO_2 present in the aquifer, if it is assumed that the reductive dissolution of MnO_2 is fast relative to the movement of the water, an assumption made in all the forward PHREEQM and PHREEQC simulations presented in this paper. The lack of accurate ground-water flow and transport models, the large distances between the well sites, and the suggestion that the reductive dissolution of MnO_2 may be slow compared to the ground-water velocities make it difficult to calculate with any accuracy what the exact Fe(II) retardation factor may be, and therefore what the appropriate initial MnO_2 content may be. In any case, the results of our simulations, and in particular the MnO_2 dissolution front retardation factors that we determine, can easily be extrapolated to other initial MnO_2 concentrations.

Determining appropriate initial carbonate (calcite and dolomite) concentrations to use in the reactive transport simulations was also a problem. Brown (1996) used a concentration of 0.18 mol/kg H_2O in his simulation, a value consistent with the carbonate content determined by Eychaner and Stollenwerk (1985) for a sample of alluvium collected in 1985. Brown (1996) noted that the buffering capacity measurements conducted by Hydro Geo Chem (1991) on alluvial samples collected from three different locations in the Pinal Creek basin could be translated into equivalent carbonate concentrations of between 0.12 mol/L for sand and gravel and 0.76 mol/L for calcareous clay. These measurements, however, did not correct for possible proton adsorption and silicate dissolution reactions. Based on a description of the Pinal Creek site by Eychaner (1989, and pers. comm.), Glynn et al. (1991) used an initial carbonate concentration of 0.084 mol/kg H_2O (0.048 mol/kg H_2O calcite and 0.021 mol/kg H_2O dolomite). The resulting pH front retardation factor of 5, for the acidic well 51 water used in the simulation, approximately matched the relative rate of advance of the low-pH waters at the Pinal Creek site over the last 50 years. The inverse modeling results discussed in the present paper show a net dissolution of usually 1.5×10^{-3} to 4.6×10^{-3} mol/kg H_2O of primary carbonate minerals (Table 5) between wells 402 and 503. If the questionable assumption is made that the carbonate mineral dissolution rates are relatively fast, resulting in localized dissolution, a value of 5×10^{-3} mol/kg H_2O may be considered a reasonable lower bound on the possible initial carbonate concentration representative for the Pinal Creek alluvial sediments. In any case, because the initial carbonate mineral concentration chosen for the simulations proved to be the most important adjustable parameter determining movement of the low-pH waters in our simulations (and is also probably the most important determining factor in Pinal Creek ground waters), a set of 8 different initial carbonate concentrations ranging from 5.25×10^{-3} to 3.32×10^{-1} mol/kg H_2O were used in different simulations to test other reaction-model modifications.

Setup of the 1-D reactive transport simulations. Unless specified otherwise, most of our simulations were conducted with the local equilibrium advective transport code PHREEQC. Dispersion was not usually simulated. The reactive transport simulations investigated the effect of the following model variations on the retardation of

the low-pH and high Fe(II) fronts:

(1) changing solid-carbonate concentrations. The initial concentrations chosen were: 5.25×10^{-3}, 1.05×10^{-2}, 2.1×10^{-2}, 3.05×10^{-2}, 4.2×10^{-2}, 8.4×10^{-2}, 1.68×10^{-1}, and 3.32×10^{-1} mol/kg H_2O.

(2) using a longitudinal dispersivity of 560 m. This dispersivity represented 10% of the total simulation length, a rule of thumb often applied in ground-water transport modeling. Most simulations used a dispersivity of 0 m, primarily because of shorter execution times. The PHREEQM and PHREEQC v. 2 (unpublished) geochemical transport codes were used for all simulations with a dispersivity of 560 m.

(3) including or excluding dolomite. Most simulations did not include dolomite.

(4) allowing or disallowing rhodochrosite precipitation.

(5) allowing either $Al(OH)_3$, kaolinite, or $AlOHSO_4$ precipitation. Two different solubility products were used for $AlOHSO_4$ ($10^{-3.2}$ and $10^{-2.2}$). The higher solubility product is the value adopted by Stollenwerk (1994) in fitting the results of his laboratory column experiments, investigating the reaction of Pinal Creek acidic ground water with Pinal Creek sediments.

(6) allowing or disallowing equilibrium with an infinite reservoir of CO_2 at partial pressures of either $10^{-0.9865}$, a value based on unsaturated zone CO_2 gas measurements at the Pinal Creek site (Glynn and Busenberg, 1994b), or $10^{-1.33}$, the value used in Brown's (1996) simulation. This latter value was based on the dissolved CO_2 concentration at well 503 (91/11) reported by Glynn and Busenberg (1994a).

(7) allowing or disallowing cation exchange. Two different cation exchange capacities, 1 meq/100g and 10 meq/100g, were tested.

(8) allowing or disallowing sorption, using a diffuse double-layer surface-complexation model, based on Dzombak and Morel's (1990) thermodynamic data compilation for sorption onto hydrous ferric oxide.

(9) including or excluding the irreversible dissolution of Ca and Mg silicates to match the amounts calculated by two of our inverse modeling simulations (PHREEQC Models 2 and 7 in Table 5). These simulations all assumed a zero-order kinetic dissolution process for the silicate minerals with an inexhaustible supply of silicate minerals. Two of the simulations were also conducted assuming a zero-order kinetic dissolution process for MnO_2. In all cases, the zero-order kinetic dissolution processes were specified so that the acidic contaminated water would receive, during the course of its evolution through the transport column, exactly the silicate mineral mass-transfers (and possibly the MnO_2 mass-transfer) determined by inverse Models 2 and 7 in Table 5. The dissolution/precipitation of all other minerals was allowed to proceed to thermodynamic equilibrium at each time step and in each cell.

More than 160 reactive-transport simulations were conducted. All simulations used the water from well 402 (89/1/12) as the infilling solution. The water from well 504 (91/11/22) was used as the background water initially present in the 1-dimensional column. The 5.6 km-long column was subdivided into 10 cells of equal length and with initially homogenous mineral, surface, and aqueous concentrations. (Because mineral concentrations in PHREEQC and PHREEQM are expressed in terms of mol/kg H_2O, the porosity and bulk density of the sediments is implicitely ignored by the programs). A timestep of 112 days was used, thereby simulating an average linear ground-water velocity of 5 m/day (representative of the average ground-water velocity between wells 402 and 503). Up to a maximum of 5000 timesteps (1534 years) were simulated.

Amorphous $Fe(OH)_3$, and an aluminum phase (either amorphous $Al(OH)_3$, kaolinite or $AlOHSO_4$) were allowed to precipitate in all the simulations. The aluminum phase allowed was usually either amorphous $Al(OH)_3$ or $AlOHSO_4$ (with a solubility product of $10^{-2.2}$; Stollenwerk, 1994). Gypsum was allowed to precipitate in all the simulations except in some of the simulations that allowed irreversible, zero-order kinetic dissolution of Ca- and Mg-silicate minerals (according to Models 2 and 7 in Table 5). Rhodochrosite was allowed to precipitate in all except one set of simulations. An essentially infinite amount of chalcedony was present in all cells. An initial concentration of 2×10^{-2} mol/kg H_2O of MnO_2 was specified in all the simulations (except a few of the simulations that allowed irreversible dissolution of Ca and Mg silicates). Initial concentrations of carbonate minerals (calcite and dolomite) were specified in all the simulations and 8 different initial concentrations were specified within each set of simulations. Dolomite was included with calcite in only a few simulations (they all had an initial mineral carbonate concentration of 8.4×10^{-2} mol/kg H_2O), and was also the only carbonate mineral present in simulations that attempted to emulate Model 7 in Table 5. Although impossible to graphically present the results of all the simulations, a few representative pH-breakthrough curves are shown in Figures 11, 12 and 13 for the midpoint of the last cell (cell 10). We will attempt to summarize the essential findings of our study.

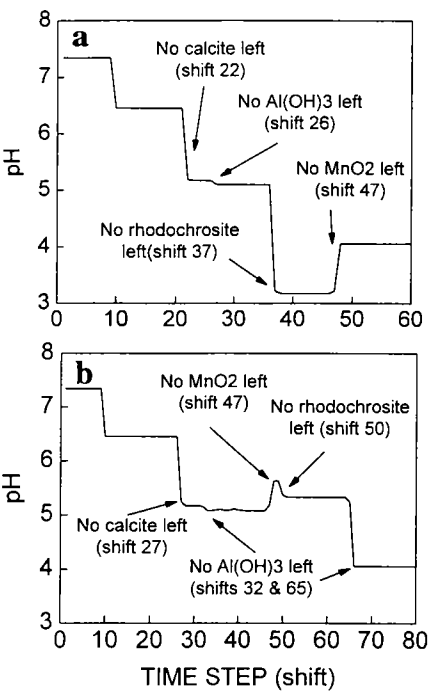

Figure 11. pH breakthrough curves for two PHREEQC advection/reaction simulations following our "basic reaction model" (BRM) with amorphous $Al(OH)_3$ as the Al-bearing phase allowed to precipitate. The BRM specifies fixed initial concentrations of calcite and of MnO_2, and an essentially infinite amount of chalcedony. In addition, the BRM allows secondary precipitation of the following minerals: gypsum, amorphous $Fe(OH)_3$, and an Al-bearing phase. An initial MnO_2 concentration of 2×10^{-2} mol/kg H_2O was used in both simulations shown, but the initial calcite concentrations differed. (a) *Initial carbonate concentration: 2.1 x 10^{-2} mol/kg H_2O.* (b) *Initial carbonate concentration: 3.0 x 10^{-2} mol/kg H_2O.*

Simulation results: movement of the Fe(II)-rich waters and of the MnO_2 dissolution front. The movement of the low-pe Fe(II)-rich ground-water zone was found to be primarily dependent on the amount of initial MnO_2 chosen for each simulation and was usually little affected by any other factors. A retardation factor (R) of 4.74 was determined for the simulations containing 2×10^{-2} mol MnO_2 per kg of H_2O. As mentioned earlier the movement of the MnO_2 dissolution front, and of the attendant Fe(II) and low-pe fronts, can easily be calculated by hand using Equation (15). Indeed, in that the

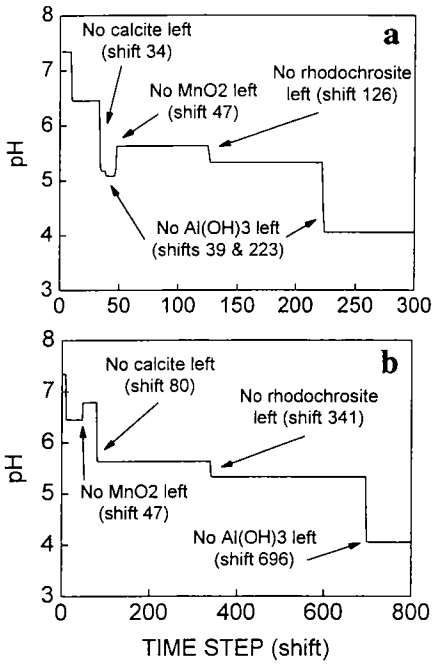

Figure 12. The pH breakthrough curves for two PHREEQC advection/reaction simulations following our "basic reaction model" with amorphous $Al(OH)_3$ as the Al-bearing phase allowed to precipitate. An initial MnO_2 concentration of 2×10^{-2} mol/kg H_2O was used in both simulations, but the initial calcite concentrations differed. (a) *Initial carbonate concentration: 4.2 × 10^{-2} mol/kg H_2O.* (b) *Initial carbonate concentration: 8.4 × 10^{-2} mol/kg H_2O.*

Fe(II) concentration of the infilling solution is 591 mg/L (Table 1), or 10.58 millimolar, and that it takes two moles of Fe(II) to dissolve one mole of MnO_2, the applicable ΔM will be close to 5.29×10^{-3} mol/L and if M_{ini} is 2×10^{-2} mol/kg H_2O, the calculated R is 4.78. The slight difference between our calculated result and the retardation factor determined from the PHREEQM simulations comes from the fact that we used molar concentration units for ΔM in our calculation instead of the correct molal units. The only processes that could conceivably affect the retardation of the MnO_2 dissolution front would be processes affecting the concentration of the reductant (dissolved Fe(II)) in the infilling water. Dispersion and cation exchange were the only two processes simulated that could potentially affect dissolved Fe(II) concentrations in the infilling water. And indeed, although the simulations that included a dispersivity of 560 m showed only a slight decrease on the retardation of the MnO_2 dissolution front (an R value of 4.6 for an MnO_2 concentration of 2×10^{-2}), the simulations that included cation exchange resulted in significantly greater MnO_2 retardation factors: 5.2 for the simulations with a cation exchange capacity (CEC) of 1 meq/100g and 9.2 for the simulations with a 10 meq/100g CEC (The lower CEC is more realistic for the Pinal Creek alluvial sediments). This effect is due to the retardation and lowering of the dissolved Fe(II) concentrations in the infilling water by cation exchange reactions, such as for example Fe/Ca exchange:

$$Fe^{2+} + CaX_2 \Leftrightarrow Ca^{2+} + FeX_2$$

Because Fe(II) sorption and Fe(II) surface complexation on hydrous ferric oxide was never simulated, the simulations that included surface-complexation sorption reactions did not result in increased retardation factors for the MnO_2 dissolution front.

Simulation results: evolution of the low-pH waters. Unlike the movement of the low-pe Fe(II)-rich front, the movement of the low-pH ground-waters is much more difficult to predict and it is not controlled by a unique mineral dissolution/precipitation

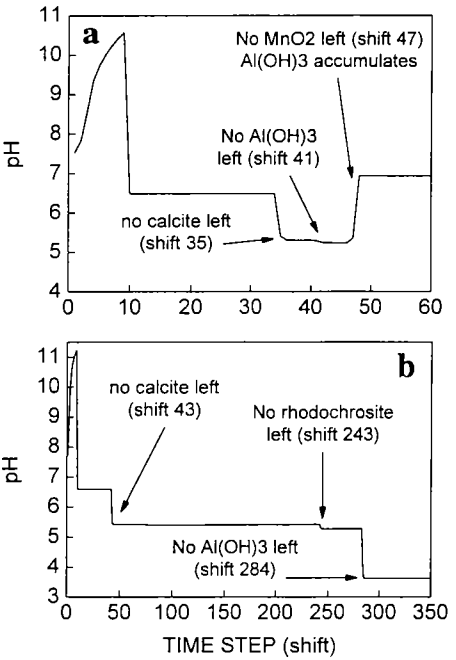

Figure 13. The pH breakthrough curves for two PHREEQC advection/reaction simulations allowing some of the reactions determined by inverse Model 2 in Table 5. The reactions allowed in the two simulations differ from our "basic reaction model" in two respects. First, the irreversible dissolution of tremolite (5.00 x 10^{-5} moles per cell per time step) was simulated as a continuous zero-order reaction process matching over the length of the simulation column the amount of tremolite mass-transfer specified in inverse Model 2. Secondly, gypsum was not allowed to precipitate. An initial concentration of 3.0 x 10^{-2} mol/kg H_2O of calcite was specified in both simulations shown. The two simulations shown differed in their consideration of MnO_2. (a) *an initial concentration of MnO_2 of 2 x 10^{-2} mol/kg H_2O was specified and allowed to react to equilibrium at each time step.* (b) *MnO_2 was added as a continuous irreversible dissolution process at the rate of 3.903 x 10^{-4} moles per cell per time step so as to match over the length of the simulation column the amount of tremolite mass-transfer specified in inverse Model 2.*

reaction. Indeed, the PHREEQM and PHREEQC simulation results show the development of several pH fronts, all controlled by mineral dissolution and precipitation fronts. The consumption of all the initial calcite present in the column (and of dolomite if initially present), is typically followed by the complete dissolution of secondary rhodochrosite and usually much later, if at all, by the dissolution of the secondary Al-bearing phase ($Al(OH)_3$, $AlOHSO_4$ or kaolinite) allowed to precipitate in the simulation. The complete dissolution of these minerals and the loss of their proton-consuming capacity leads to abrupt pH decreases. In contrast, the disappearance of MnO_2, and the ensuing halt of Fe(II) oxidation and $Fe(OH)_3$ precipitation results in a sharp pH increase.

The pH breakthrough curves shown in Figures 11 and 12 for the last of the 10 cells in the column are typical of the pH breakthrough curves seen for most of the simulations without silicate dissolution. pH remains high at 7.34, until the first pore volume (at shift 10) flushes through and neutralized infilling water with a pH of about 6.5 comes in. If MnO_2 is the first mineral consumed and $Al(OH)_3$ is allowed to precipitate, the pH will increase upon its disappearance from 6.5 to 6.8. The complete consumption of calcite will then result in a pH decrease from about 6.8 to about 5.6, and the ensuing consumption of rhodochrosite will result in another pH drop to near 5.3. Finally, the disappearance (with a long enough simulation time) of the secondary aluminum phase will eventually finally result in yet another pH drop to about 4.06, close to the initial infilling water pH of 4.13. Although the pH values reached during the simulations with silicate mineral dissolution differ somewhat from the pH values mentioned above, the general pattern of pH evolution in those simulations is also strongly dependent on the disappearance of calcite (or dolomite), MnO_2, secondary rhodochrosite, and the secondary aluminum phase (Fig. 13).

Many of the pH values obtained during the transport simulations can be simulated by equilibrating the infilling solution (well 402 water) with the various possible assemblages

of coexisting mineral phases found during the transport simulations (Table 8). The resulting pH values usually closely agree with the pH values obtained during most of the simulations (and are even within half a pH unit of the values reached in the simulations that incorporated CO_2 exsolution and surface-complexation). The PHREEQC equilibration results clearly indicate that although the loss of calcite results in a pH decrease down to 5.1 to 5.7, the subsequent loss of rhodochrosite results in a further pH decrease, to values well below 5 if $Al(OH)_3$ is not present. Table 8 indicates the importance of the aluminum phase chosen for equilibration in determining the lowest pH values reached during the simulations, after the complete dissolution of rhodochrosite. Invariably, the simulations that allowed amorphous $Al(OH)_3$ precipitation resulted in higher pH values than those found in the simulations allowing kaolinite, or especially, $AlOHSO_4$ precipitation. In the presence of rhodochrosite (and possibly calcite), however, the choice of aluminum phase allowed to precipitate had little effect on the resulting pH values. Finally, Table 8 confirms our finding that the lowest pH values (near 3.1) were invariably attained when MnO_2 was still present but all other carbonate and Al-phases had dissolved away.

Table 8. pH values computed with the PHREEQC geochemical code by equilibrating well 402 water with various mineral phases, including chalcedony, gypsum and amorphous $Fe(OH)_3$ and one of four possible Al bearing phases (see table note). The last pH column indicates the pH value in the absence of any aluminum phase.

Presence of additional minerals?			Computed pH				
			Identity of Al bearing phase				
MnO_2	Calcite	Rhodochrosite	1	2	3	4	no Al phase
Yes	Yes	Yes	6.453	6.442	6.462	6.467	
Yes	**No**	Yes	5.174	5.071	5.095	5.090	
Yes	No	**No**	**5.011**	**3.810**	**3.364**	**3.186**	**3.175**
No	Yes	Yes	6.788	6.772	6.748	6.818	
No	**No**	Yes	5.633	5.576	5.666	5.659	
No	No	**No**	**5.330**	**4.190**	**4.554**	**3.946**	4.056

Note: the identity of the Al bearing phase is indexed as follows. (1) $Al(OH)_3$, (2) kaolinite, (3) $AlOHSO_4$ with log K_{sp} = -2.2, (4) $AlOHSO_4$ with log K_{sp} = -3.23).

The effect of the initial carbonate to initial MnO_2 ratio on the evolution of the low-pH waters. The set of simulations that allowed irreversible dissolution of Ca- and Mg-silicate minerals gave very different results from the set of simulations that did not incorporate Ca- and Mg-silicate dissolution. Unless mentioned otherwise, the following discussions apply only to the set of simulations that did not incorporate silicate mineral dissolution, although many of our conclusions will also be relevant to the simulations with Ca- and Mg-silicate dissolution.

The initial carbonate mineral concentration specified in each simulation offered the most important control on the movement of the calcite, rhodochrosite and Al-phase dissolution fronts (Tables 9, 10 and 11). The ratio of initial carbonate to MnO_2 (CMR) was the second most important determining factor affecting the retardation of the dissolution fronts for rhodochrosite and the Al-bearing phase (the rhodochrosite dissolution front is important because of the decrease in pH associated with the front, particularly in the absence of an $Al(OH)_3$ phase). Indeed, the timing of the complete dissolution of MnO_2 in

relation to the disappearance of the carbonate phases, and therefore the CMR ratio specified in a given simulation, is important because the presence or absence of MnO_2 affects the pH values reached upon disappearance of the various carbonate phases. The lowest pH values reached in the transport simulations usually occurred when MnO_2 remained in a cell, but all the initial and secondary carbonate (rhodochrosite) phases had completely dissolved. (If additionally the Al-bearing phase had been completely dissolved, the pH was even lower). This transient situation (third row in Table 8) occurred in all simulations with a CMR ratio of less than 3/2 (5.25×10^{-3}, 1.05×10^{-2} and 2.1×10^{-2} initial carbonate concentrations and 2×10^{-2} initial MnO_2 concentration). The lower pH values generally reached in the presence of MnO_2 resulted in more aggressive waters and therefore in relatively lower retardation factors for the rhodochrosite and Al-phase dissolution fronts in simulations with an initial carbonate to MnO_2 ratio of less than 3/2 (Tables 10 and 11; Fig. 11a).

In simulations with CMR ratios near 3/2, the complete dissolution of MnO_2 was usually accompanied by the nearly simultaneous disappearance of precipitated rhodochrosite, but was preceded by the complete dissolution of calcite (Fig. 11b). For most of these simulations, therefore, the rhodochrosite dissolution front had a retardation factor (R) close to 4.7, that of the MnO_2 front. Disregarding the Ca and Mg silicate dissolution simulations, the highest rhodochrosite R values were obtained for the simulations that specified a high ion exchange capacity (CEC) or a surface complexation model or equilibrium with a low fixed pCO_2 value ($10^{-1.33}$). In the high CEC simulations, however, the R value of the rhodochrosite front was still lower than that of the MnO_2 dissolution front (R = 9.2), i.e. the rhodochrosite dissolution front preceded the MnO_2 dissolution front.

Finally, in the simulations with a CMR ratio greater than 3/2 (4.2×10^{-2}, 8.4×10^{-2}, 1.68×10^{-1} and 3.32×10^{-1} initial carbonate concentrations and 2×10^{-2} initial MnO_2 concentration), exhaustion of the initial MnO_2 generally proceeded faster than that of the secondary rhodochrosite (with the exception of the 2 high CEC simulations). In simulations with an initial carbonate concentration of 8.4×10^{-2} or greater, exhaustion of the initial MnO_2 also proceeded faster than that of the initial carbonate minerals. The faster movement of the MnO_2 dissolution front relative to the carbonate mineral dissolution fronts resulted in less aggressive waters contacting the carbonate minerals and Al-phase minerals and therefore in higher retardation factors.

Influence of the aluminum mineral allowed to precipitate on the evolution of the low-pH waters. The choice of Al-bearing phase allowed to precipitate was the third major determining factor controlling the relative retardation of the rhodochrosite and Al-phase dissolution fronts in the simulations without Ca and Mg silicate dissolution. The simulations that allowed $AlOHSO_4$ to precipitate, instead of amorphous $Al(OH)_3$, all exhibited significantly greater retardation factors for the rhodochrosite and Al-phase dissolution fronts. Remarkably, the simulations that used the lower solubility product for $AlOHSO_4$ ($10^{-3.23}$) resulted in much higher R values for the $AlOHSO_4$ dissolution front, but did not result in significantly different R values for the rhodochrosite dissolution front, when compared to the values obtained in simulations with the less stable $AlOHSO_4$ phase. More generally, significant differences in retardation factors (for a given initial carbonate concentration) between the $Al(OH)_3$ and the $AlOHSO_4$ simulations occurred only in simulations with CMR ratios above 3/2. The exact reason for this behavior is not clear to us at the present time, but is probably related at least in part to the effect of the MnO_2 dissolution front moving faster than the rhodochrosite dissolution front. In any case, the precipitation of $Al(OH)_3$ generates 3 times more protons than that of $AlOHSO_4$, and would therefore result in significantly more aggressive waters and faster carbonate mineral dissolution, explaining the generally smaller retardation factors found in the

simulations with $Al(OH)_3$:

$$Al^{3+} + SO_4^{2-} + H_2O \Leftrightarrow AlOHSO_{4,s} + H^+$$
$$Al^{3+} + 3\,H_2O \Leftrightarrow Al(OH)_{3,am} + 3\,H^+$$

Table 9. Rhodochrosite dissolution-front retardation factors as a function of initial carbonate concentration (in mol/kg H_2O) and for various reaction models. All models except one had a dispersivity of 0 meters. The models all allowed precipitation of rhodochrosite and of one of four possible Al-bearing phases. The specified reaction models have an index that refers to the allowed Al-bearing phase. These indices and the meanings of the various reaction models are discussed in the table notes and in the text.

Reaction Model	Initial Carbonate Mineral Concentration ($x10^{-2}$)							
	0.525	1.05	2.1	3.0	4.2	8.4	16.8	33.2
Basic reaction model, (1)	1.6	2.3	3.7	5.0	12.6	34.1	65.6	128.9
Dispersivity, (1), PHREEQM	1.5	2.3	3.7	4.5	12.7	35.1	67.7	133.0
Dispersivity, (1), PHREEQC	1.5	2.2	3.6	4.5	12.5			
Low CEC, (1)	1.6	2.3	3.8	5.1	11.8	33.7	65.4	128.6
High CEC, (1)	0.0	3.5	5.1	6.5	8.8	31.3	63.0	126.3
CO_2, log pCO_2= -0.9865, (1)	1.4	2.1	3.5	5.0	12.2	32.5	56.5	104.5
CO_2, log pCO_2 = -1.33,(1)	1.5	2.2	3.7	5.9	15.2	37.5	68.8	131.4
Basic reaction model, (3)	1.6	2.3	3.6	4.9	14.7	42.3	81.4	159.4
Basic reaction model, (4)	1.6	2.3	3.6	4.8	14.5	41.3	80.9	160.2
Low CEC, (3)	1.6	2.3	3.7	5.0	13.6	41.8	80.9	158.9
High CEC, (3)	0.0	3.5	5.0	6.4	8.6	38.0	77.2	155.4
Surf. Complex., (3), no Cu,Zn,Co,Ni		3.4	4.7	12.3	22.5	47.4	86.8	165.4
Surf. Complex., (3), with Cu,Zn,Co,Ni	2.7	3.4	4.6	7.8	19.8	46.4	79.5	140.8
Tremolite, mod. 2, (1)	Rhodochrosite accumulates!							
Tremolite, MnO_2, mod. 2, (1)	7.3	10.9	18.2	24.3	32.6	61.6	119.4	235.3
Biotite/K-mont/An, mod. 7, (1)	Rhodochrosite accumulates!							
Biotite/K-mont/An, MnO_2, mod. 7, (1)	12.1	17.9	29.8	40.1	53.9	101.7	197.5	388.9
Biotite/K-mont/An., mod. 7, (3)	Rhodochrosite accumulates!							

Note: the identity of the Al bearing phase is indexed as follows for each reaction model. (1) $Al(OH)_3$, (2) kaolinite, (3) $AlOHSO_4$ with log K_{sp} = -2.2, (4) $AlOHSO_4$ with log K_{sp} = -3.2).

Guide to reaction model abbreviations and meanings.
Dispersivity: basic reaction model with dispersivity of 560 m;
CO_2: column open to a specified fixed pCO_2
Low CEC: low cation exchange capacity (1 meq/100g);
High CEC: high cation exchange capacity (10 meq/100g);
Surf. Complex.: surface complexation model
Tremolite, mod. 2: irreversible tremolite dissolution (model 2 in Table 5);
Tremolite, MnO_2, mod. 2: as above but with zero-order MnO_2 dissolution;
Biotite/K-mont/An, mod. 7: irreversible biotite and anorthite dissolution and K-montmorillonite precipitation (model 7 in Table 5);
Biotite/K-mont/An, MnO_2, mod. 7: same as above but with zero-order MnO_2 dissolution;

The precipitation of $Al(OH)_3$ (or of $AlOHSO_4$) generally occurred as a result of the increase in pH of the infilling water caused by the dissolution of the carbonate minerals. Reaction with the more acidic infilling waters eventually caused redissolution of the Al-

bearing phases. In the case of the simulations with low initial carbonate concentrations and with $AlOHSO_4$ (solubility product: $10^{-2.2}$) or with $Al(OH)_3$ allowed to precipitate, complete consumption of the Al-bearing phase occurred at least twice during the simulations. The retardation factors for the Al-phase dissolution fronts given in Table 11 refer only to the last and presumably final dissolution front in the simulations.

Effects of the irreversible dissolution of Ca- and Mg-silicates on the evolution of low-pH Fe(II)-rich waters. Several simulations were conducted using some of the reactions specified in the PHREEQC inverse Models 2 and 7 (Table 5). In addition to allowing secondary $Al(OH)_3$, $Fe(OH)_3$, and rhodochrosite to precipitate, and in addition to specifying initial amounts of calcite (or dolomite) also allowed to react to equilibrium, these simulations forced the dissolution of a fixed number of moles of Ca- and Mg-silicate minerals into each cell and at each time step, thereby simulating a 0-order kinetic dissolution process that matched (over the length of the 10-cell 5.6 km column) the net amount of Ca- and Mg-silicate minerals dissolved between wells 402 and 503 according to PHREEQC inverse Models 2 and 7 in Table 5. Irreversible dissolution of tremolite was specified in the simulations following Model 2 (Fig. 13). Irreversible dissolution of biotite and anorthite and removal from solution of K-montmorillonite was specified in the simulations following Model 7. The silicate dissolution processes would certainly have been more correctly simulated with a pH-dependent rate law, but this capability was not present in the PHREEQC code used. An inexhaustible supply of silicate minerals was also assumed available to all cells throughout the course of the simulations. Despite the crudeness and fallacy of these assumptions, it was hoped that these simulations would nevertheless contribute some insights as to the importance of silicate mineral dissolution in governing the pH evolution of acidic contaminated waters such as those found at the Pinal Creek site. [Ongoing investigations on the occurrence and kinetics of silicate mineral dissolution (and of carbonate and Al, Mn and Fe oxyhydroxide reactions) at the Pinal Creek site will hopefully result in more "realistic" models in the future.]

The Ca- and Mg-silicate dissolution simulations specified an essentially infinite amount of initial chalcedony. This mineral was allowed to react to equilibrium. Following the results of Models 2 and 7 in Table 5, gypsum precipitation was excluded from the simulations. (a few simulations were run allowing gypsum precipitation but the results of those simulations were not significantly different and are not presented here). Although an initial fixed amount of MnO_2 of 2×10^{-2} mol/kg H_2O was specified in most simulations, two sets of simulations specified instead a zero-order dissolution process for MnO_2, according to the amounts determined by Models 2 and 7 in Table 5. Finally, one set of simulations conducted tried to follow Model 7 (Table 5) but allowed $AlOHSO_4$ to precipitate instead of $Al(OH)_3$.

All the simulations that specified a fixed initial MnO_2 concentration (of 2×10^{-2} mol/kg H_2O) invariably resulted in rhodochrosite precipitation and accumulation (Table 9, Fig. 13a). A rhodochrosite dissolution front never formed, presumably because the continuous proton consumption caused by the dissolution of the silicate minerals and the high initial Mn and TDIC concentrations in the infilling water (from well 402) were sufficient to ensure that the infilling water never became undersaturated with respect to rhodochrosite. In contrast, the simulations that allowed the irreversible zero-order dissolution of MnO_2 did produce rhodochrosite dissolution fronts (Fig. 13b), probably because of the constant generation of acidity caused by the oxidation of dissolved Fe(II) and consequent precipitation of $Fe(OH)_3$. The retardation factors for the rhodochrosite dissolution fronts increased almost linearly as a function of the initial carbonate mineral content, nearly doubling for each doubling of the initial carbonate concentration, but only in

simulations with carbonate concentrations above 4.2×10^{-2} mol/kg H_2O (at lower initial carbonate concentrations rhodochrosite R values increased only by 50% or less).

The two sets of simulations with irreversible tremolite dissolution (with and without fixed initial MnO_2 concentrations) also generated calcite dissolution fronts (Table 10, Fig. 13). In contrast, out of the three sets of simulations that tried to emulate inverse Model 7, only the one that also allowed continuous zero-order dissolution of MnO_2 (and consequent production of acidity) also generated calcite dissolution fronts. Interestingly, the calcite R values increased nearly linearly with increasing initial carbonate concentration in the simulations that allowed continuous MnO_2 zero-order dissolution, but did not do so in the set of simulations (with tremolite dissolution) that specified a fixed initial MnO_2 amount. In that set of simulations the calcite R value increased from 4.3 to 97.7 (a factor of 23!) although the initial calcite amount specified increased only from 4.2×10^{-2} to 8.4×10^{-2} mol/kg H_2O. This probably occurred because in the simulation with the higher initial carbonate concentration the calcite dissolution front started moving more slowly than the MnO_2 dissolution front (R value = 4.7). Even higher initial carbonate concentrations resulted in a tripling of the calcite R value for each doubling of the initial calcite concentration. In the set of simulations that also used a fixed initial MnO_2 concentration (2×10^{-2} mol/kg H_2O) but attempted to emulate inverse Model 7, any initial dolomite dissolution was always followed eventually by dolomite precipitation and accumulation. Because of the additional contribution of Fe(II)-containing biotite, a retardation factor of 4.5 was obtained for the MnO_2 dissolution front in those simulations.

Most of the simulations with Ca- and Mg-silicate dissolution did not produce an Al-phase dissolution front (or produced only a temporary one). The proton consumption caused by the silicate dissolution reactions instead caused the continuous precipitation of $Al(OH)_3$ from the infilling water (Table 11). The set of simulations with irreversible tremolite dissolution and zero-order MnO_2 dissolution did however generate an $Al(OH)_3$ dissolution front, again probably because of the acidity generated by the continuous addition of MnO_2 and its reaction with dissolved Fe(II) in the infilling water. The set of simulations emulating Model 7, but allowing $AlOHSO_4$ to precipitate instead of $Al(OH)_3$ also produced a $AlOHSO_4$ dissolution front. Surprisingly, the R value for that front actually decreased as the initial carbonate concentration increased to 4.2×10^{-2} mol/kg H_2O and then increased with higher initial carbonate concentrations.

The pH values obtained during the evolution of the well 402 water during the simulations with irreversible Ca- and Mg-silicate dissolution (Fig. 13) were fairly close to the pH values predicted for the various mineral assemblages in Table 8, but only when carbonate minerals (rhodochrosite or calcite) were still present and when MnO_2 was either being added or was still present. The first 10 shifts of the simulations show a rather dramatic increase in the pH of cell 10 because of the constant forced dissolution of Ca- and Mg-silicates into the background water, which takes 10 shifts to flush out.

The effect of not allowing rhodochrosite precipitation. One set of simulations, without Ca- and Mg-silicate dissolution, was conducted using a low cation exchange capacity (1 meq/100 g), but disallowing rhodochrosite precipitation. Comparison with a similar set of simulations that did allow rhodochrosite precipitation shows that while the retardation factors (R values) for the calcite dissolution front were greater in the simulations without rhodochrosite precipitation, they were nevertheless up to two times smaller than the R values for the rhodochrosite dissolution front in the runs that allowed the mineral to precipitate. The pH values attained after complete dissolution of calcite in the simulations without rhodochrosite precipitation closely match the low-pH values attained after complete rhodochrosite dissolution in the simulations that allowed precipitation of that

Table 10. Calcite dissolution-front retardation factors. See Table 9 caption and notes for explanation of headings and abbreviations. One additional set of simulations reported here was performed with a CEC of 1 meq/100g but with no rhodochrosite allowed to precipitate (low CEC, no rhodo.).

*All simulations referring to Model 7 in Table 5 have initial dolomite instead of calcite.

Reaction Model	Initial Carbonate Mineral Concentrations ($x10^{-2}$)							
	0.525	1.05	2.1	3.0	4.2	8.4	16.8	33.2
Basic reaction model, (1)	1.2	1.5	2.2	2.7	3.4	8.0	22.7	52.0
Dispersivity, (1), PHREEQM	1.0	1.3	2.0	2.5	3.3	8.0	23.0	53.0
Dispersivity, (1), PHREEQC	1.0	1.3	2.0	2.5	3.3			
Low CEC, (1)	1.5	1.9	2.5	3.1	3.8	8.2	22.9	52.3
High CEC, (1)	2.5	3.5	4.9	5.9	6.9	10.7	25.4	54.8
CO_2, log pCO_2 = -0.9865, (1)	1.1	1.4	2.1	2.6	3.3	7.3	18.4	40.8
CO_2, log pCO_2 = -1.33, (1)	1.2	1.5	2.2	2.8	3.6	8.8	23.0	51.2
Low CEC, no rhodo., (1)	1.5	2.1	3.0	3.9	5.0	13.8	32.4	69.5
Basic reaction model, (3)	1.2	1.6	2.2	2.7	3.4	8.7	24.7	56.7
Basic reaction model, (4)	1.3	1.6	2.2	2.7	3.5	8.9	25.6	59.1
Low CEC, (3)	1.5	1.9	2.6	3.1	3.8	8.9	25.0	57.0
High CEC, (3)	2.5	3.5	4.9	5.9	7.0	11.4	27.4	59.5
Surf. Complex., (3), no Cu,Zn,Co,Ni		2.1	2.7	3.2	3.9	10.2	26.3	58.4
Surf. Complex., (3), with Cu,Zn,Co,Ni	1.7	2.0	2.6	3.1	3.8	8.9	22.2	48.2
Tremolite, mod. 2, (1)	1.5	1.9	2.8	3.5	4.5	**113.7**	**353.5**	**>500**
Tremolite, MnO_2, mod. 2, (1)	1.6	2.2	3.3	4.3	5.5	10.0	18.9	36.8
Biotite/K-mont, mod. 7, (1)	No calcite specified. Dolomite accumulates!							
Biotite/K-mont, MnO_2, mod. 7, (1)	1.6*	2.2*	3.2*	4.2*	5.4*	9.7*	18.4*	35.7*
Biotite/K-mont., mod. 7, (3)	No calcite specified. Dolomite accumulates!							

mineral (Table 8). Therefore for proper comparison, the *R* values for the calcite dissolution front in the simulations without rhodochrosite precipitation can only be compared to the *R* values for the rhodochrosite dissolution fronts in the other simulations. In simulations with low initial carbonate (2.1×10^{-2} mol/kg H_2O and lower), the faster movement of the $Al(OH)_3$ dissolution front relative to the rhodochrosite dissolution front meant that the complete dissolution of rhodochrosite led to a large pH decrease (Fig. 11a). In simulations with higher initial carbonate concentrations, the $Al(OH)_3$ final dissolution front traveled more slowly than the rhodochrosite front and therefore the disappearance of rhodochrosite resulted in a relatively small decrease in pH (Figs. 11b and 12). The *R* values for the $Al(OH)_3$ final dissolution-front were smaller (by as much as 1/3 in the runs with high initial carbonate concentrations) in the simulations without rhodochrosite precipitation relative to the $Al(OH)_3$ *R* values obtained in the simulations that allowed rhodochrosite to precipitate. For simulations with the three lowest initial carbonate concentrations (5.25×10^{-3}, 1.05×10^{-2} and 2.1×10^{-2}), however, differences in the *R* values between the simulations that did or did not include rhodochrosite precipitation were relatively small. It should also be remembered that the discretization error inherent in the lower *R* values is much greater than for the higher *R* values (resulting from higher initial carbonate concentrations). Indeed, for greater accuracy all the simulations with low *R* values (for any of the mineral fronts) should have been run with a greater number of cells (and consequently a greater number of time steps and a smaller cell length).

Table 11. Retardation factors for the final aluminum phase dissolution-front. See Table 9 caption and notes for explanation of headings and abbreviations. One additional set of simulations reported here was performed with a CEC of 1 meq/100g but with no rhodochrosite allowed to precipitate (low CEC, no rhodo.). In some cases, the aluminum phase was never exhausted during the 5000 time steps allowed for a simulation.

Reaction Model	Initial Carbonate Mineral Concentrations ($x10^{-2}$)							
	0.525	1.05	2.1	3.0	4.2	8.4	16.8	33.2
Basic reaction model, (1)	1.4	1.8	2.6	6.5	22.3	69.6	143.3	290.8
Dispersivity, (1), PHREEQM	1.3	1.8	2.7	8.4	25.3	78.9	162.7	330.3
Dispersivity, (1), PHREEQC	1.2	1.7	2.7	7.6	23.3			
Low CEC, (1)	1.7	2.2	3.2	3.9	20.6	68.8	142.6	290.1
High CEC, (1)	2.7	3.7	5.3	6.9	9.1	62.6	136.8	284.5
CO_2, log pCO_2 = -0.9865(1)	1.3	1.9	3.2	5.3	20.8	61.9	113.6	217.3
CO_2, log pCO_2 = -1.33, (1)	1.5	2.3	3.9	13.9	39.6	106.4	203.9	399.0
Low CEC, no rhodo., (1)	1.6	2.2	3.3	4.2	8.6	37.7	91.4	198.6
Basic reaction model, (3)	0.0	2.3	3.6	7.9	30.3	89.1	171.3	335.5
Basic reaction model, (4)	1.8	2.7	4.5	>500	>500	>500	>500	>500
Low CEC, (3)	1.6	2.3	3.7	5.0	27.5	87.6	169.9	334.1
High CEC, (3)	0.0	0.0	0.0	6.4	8.8	76.0	158.5	323.3
Surf. Complex., (3), no Cu,Zn,Co,Ni		3.5	7.4	24.7	45.9	96.8	176.6	335.8
Surf. Complex., (3), with Cu,Zn,Co,Ni	2.9	3.5	8.8	31.6	48.1	102.8	172.3	300.8
Tremolite, mod. 2, (1)	$Al(OH)_3$ accumulates!							
Tremolite, MnO_2, mod. 2, (1)	8.2	12.5	21.1	28.4	38.2	72.6	141.1	278.4
Biotite/K-mont, mod. 7, (1)	$Al(OH)_3$ accumulates!							
Biotite/K-mont, MnO_2, mod. 7, (1)	$Al(OH)_3$ accumulates!							
Biotite/K-mont, mod. 7, (3)	9.2	8.0	6.9	6.5	5.0	5.8	6.6	7.3

The CO_2 open system simulations. A few simulations were conducted assuming that the 1-dimensional column was allowed to equilibrate with an infinite gaseous CO_2 reservoir with a fixed partial pressure of either $10^{-1.33}$ (the pCO_2 value used by Brown, 1996, a value representative of equilibrium with a measured dissolved-CO_2 concentration for well 503) or $10^{-0.9865}$ (a pCO_2 value representative of the unsaturated zone pCO_2 at site 500 in Nov. 1991). Opening the system up to CO_2 did affect the retardation of the calcite, rhodochrosite and $Al(OH)_3$ dissolution fronts, particularly in the simulations with at least 3×10^{-2} mol/kg of initial calcite (i.e. with CMR ratios of 3/2 and above). The simulations conducted under the higher fixed pCO_2 value ($10^{-0.9865}$) generally resulted in lower R values for the calcite, rhodochrosite and $Al(OH)_3$ dissolution fronts, compared to the values determined in the basic reaction model simulations. In contrast, the simulations conducted under the lower fixed pCO_2 value ($10^{-1.33}$) resulted in higher R values for all three mineral dissolution fronts, compared to the values determined in the basic reaction model simulations. The relevance of these simulations to the migration of the acidic ground waters at Pinal Creek field site is questionable, although the magnitude of the CO_2 equilibration effect clearly warrants further study and confirmation that it is actually not significant at the field site.

The effect of longitudinal dispersion. Assuming a longitudinal dispersivity (α) of 560 m, 10% of the distance between wells 402 and 503, as opposed to a dispersivity

of 0 m, did not significantly affect the retardation of the calcite or rhodochrosite dissolution fronts, except for the simulations with the lowest initial carbonate concentrations (3×10^{-2} mol/kg H_2O and lower, corresponding to CMR ratios below 3/2). Dispersion typically has little effect on the propagation of sharp fronts, caused by simple mineral dissolution reactions, especially if the initial mineral concentrations are high enough to significantly retard the propagation of the fronts. At the limit, dispersion would have absolutely no effect on the retardation of a mineral dissolution front for which an infinite initial mineral concentration had been specified. Of course, using a dispersivity of 560 m has a tremendous effect on the spreading of non-reacting solutes, and can also be expected to affect the propagation of mineral dissolution fronts moving close to the advective speed of the water. The spreading of a conservative solute can easily be calculated after a given travel time, or travel distance, using the following equation (Appelo and Postma, 1993):

$$\sigma_x = \sqrt{2\alpha vt} = \sqrt{2\alpha x} \tag{17}$$

or if α = 560 m and x = 5600 m, the distance between wells 402 and 503, σ_x = 2504 m. σ_x represents a distance between two specific points in a 1-D homogeneous column. At those two specific points, a conservative tracer injected continuously at the beginning of the column (i.e. at well 402), with a relative concentration c/c_0 of 100%, would have achieved relative concentrations of 50% and 16%, respectively. Essentially, σ_x represents the spreading of the solute mass due to longitudinal dispersion. Longitudinal dispersion implies that portions of the tracer move both faster and slower than the average ground-water velocity. When the relative concentration of a conservative tracer reaches 50% at well 503, 5600 m downgradient from well 402, the 16% relative concentration level has already moved ahead by 2504 m. In contrast, the 84% relative concentration level would be 2504 m upgradient from well 503. The above analysis assumes steady-state flow through a porous medium with homogeneous physical properties and also assumes that there are no "dead-water" zones into which the conservative tracer can diffuse.

The simulations that included longitudinal dispersion were conducted with both the PHREEQM code and with an unpublished version of the PHREEQC v. 2 code (obtained courtesy of Tony Appelo and David Parkhurst). PHREEQC v. 2 allows the simulation of longitudinal dispersion, using an algorithm similar to the one used in PHREEQM. Although efforts were made to try to ensure that the two thermodynamic databases were identical, particularly as concerns Al speciation data, some minor differences may still remain, although we are not aware of any such differences at the present time. The database used in the PHREEQC v. 2 runs was identical to that used in all the other PHREEQC runs (those without dispersion). Unfortunately, we were unable to make PHREEQC v. 2 converge for the entire set of simulations.

The influence of ion exchange and surface-complexation sorption processes. The reader is referred to Appelo (this volume), Appelo and Postma (1993), Dzombak and Morel (1990) and Davis and Kent (1990) for excellent descriptions of the theories of ion exchange and surface-complexation sorption processes. The ion exchange conventions used in the PHREEQM and PHREEQC codes are described in Appelo and Postma (1993). PHREEQC's simulation of surface complexation sorption processes largely follows the diffuse double-layer surface-complexation model presented by Dzombak and Morel (1990) and is fully described in Parkhurst (1995).

Allowing ion exchange with a cation exchange capacity (CEC) of 1 meq/100g did not result in major changes in the rhodochrosite and calcite retardation factors (Tables 9, 10). The ions allowed to exchange were the following: Al^{3+}, Fe^{2+}, Mn^{2+}, Ca^{2+}, Mg^{2+}, Sr^{2+}, Ba^{2+}, Na^+, K^+. Proton exchange was also simulated. The selectivity coefficients used

were the default values present in the PHREEQC thermodynamic database (close to a set of values given in Appelo and Postma, 1993). A CEC of 1 meq/100g [equivalent to 52.2 meq/kg H_2O given the porosity and bulk density of the Pinal Creek alluvial sediments] appears to be a reasonable order of magnitude estimate for the Pinal Creek sediments, given their low content of organic matter and their relative coarseness. The empirical formula given by Breeuwsma et al. (1986) relating the CEC to the <2μm clay fraction and to the organic carbon content is assumed applicable (cited in Appelo and Postma, 1993):

$$\text{CEC (meq/100g)} = 0.7\ (\%\ \text{clay}) + 3.5\ (\%\ \text{C}) \tag{18}$$

Direct measurements of the CEC of Pinal Creek sediments, and of the exchangeable ion composition of the sediments, would certainly be preferable to using an empirical formula. The purpose of our simulations, however, was to determine the effect of including ion exchange processes on the evolution of the low-pH and high-Fe(II) contaminated ground waters at the site. Therefore, simulations were also conducted using an unrealistically high CEC of 10 meq/100g, a CEC that would be applicable to sediments with more than 10% clay content. As discussed earlier, these high CEC simulations resulted in a doubling of the retardation of the MnO_2 dissolution front (from 4.7 to 9.2 for an initial MnO_2 concentration of 2×10^{-2} mol/kg H_2O). The high CEC ion-exchange simulations also generally increased the retardation factors for the calcite dissolution front but did not result in a uniform increase in the retardation of the rhodochrosite or of the Al-phase dissolution fronts (as a function of initial carbonate). At low initial carbonate concentrations, the high CEC simulations did not result in any rhodochrosite precipitation. Nevertheless, at initial carbonate concentrations of 2.1×10^{-2} and 3.0×10^{-2} mol/kg H_2O, the simulations that allowed $Al(OH)_3$ precipitation and a high CEC had higher retardation factors for the rhodochrosite dissolution front. The retardation factors were lower than those of the simulations with no ion exchange, however, at the higher initial carbonate concentrations. The retardation factors for the $Al(OH)_3$ dissolution front also exhibited this complex behavior with increasing initial carbonate concentration.

The PHREEQC simulations that included a diffuse double-layer surface-complexation sorption model resulted in retardation factors for the rhodochrosite, calcite and $AlOHSO_4$ dissolution fronts that were generally higher than the R values determined in simulations without sorption. Surface protonation and deprotonation reactions were incorporated into the sorption model, along with surface complexation of Mn, Ca, Mg, Cu, Zn, Co, Ni and SO_4 at weak and strong surface sites. Cu (36.2 mg/L), Zn (4.97 mg/L), Co (4.14 mg/L) and Ni (1.57 mg/L) concentrations measured in the well 402 water were added to one set of simulations. Another set of simulations was also conducted without those elements. This second set of simulations resulted in higher R values for the rhodochrosite and calcite fronts, but in slightly lower R values for the $AlOHSO_4$ front except in the simulations with the two highest initial carbonate concentrations.

The thermodynamic model was based on the compilation of intrinsic constants for hydrous ferric oxide published by Dzombak and Morel (1990) and used by default in PHREEQC. The number of weak and strong sorption sites used (1.5×10^{-2} and 3.8×10^{-4} respectively) and the amount of surface area per kg of H_2O used (4032 m^2) were identical to the values used by Brown (1996) in his 1-D simulation of reactive transport at the Pinal Creek site, and also in his PHREEQC simulation-fit of a column experiment conducted by Stollenwerk (1994). In his experiment, Stollenwerk (1994) eluted acidic contaminated ground water from the Pinal Creek site through an 80-cm column containing uncontaminated alluvial sediments also taken from the site. Using a higher number of sorption sites in our simulations would probably have resulted in much more significant effects on the retardation of the mineral dissolution fronts.

Other minor effects on the evolution of the low-pH waters. The effects of specifying an initial concentration of dolomite in addition to calcite, and separately of allowing kaolinite to precipitate instead of $Al(OH)_3$ or $AlOHSO_4$ was tested in several simulations. All the simulations specified the same initial carbonate mineral concentration (8.4×10^{-2} mol/kg H_2O) and initial MnO_2 concentration, concentrations identical to the those used in the simulation of Glynn et al. (1991). Including or excluding dolomite did not, in and of itself, affect the retardation of the low-pH waters, as can be seen from the resulting retardation factors for the rhodochrosite dissolution front (Table 12). The important variable was the total moles of solid carbonate, whether in the form of calcite or dolomite.

Table 12. Calcite, dolomite and rhodochrosite retardation factors (R) for various simulations with 8.4×10^{-2} mol/kg H_2O of initial carbonate. The simulations may include dolomite and may allow kaolinite precipitation instead of $Al(OH)_3$ or $AlOHSO_4$ precipitation. See Table 9 caption and notes for explanation of the row headings. "1/2 dolomite" means that half of the initial solid-phase carbonate was provided by dolomite.

Reaction Model	Calcite	Dolomite	Rhodochrosite	Al-phase
basic reaction model, (1)	8.0		34.1	69.6
basic reaction model, (2)	7.6		26.4	>500
basic reaction model, 1/2 dolomite, (1)	7.7	4.5	33.6	68.3
dispersivity, (1), PHREEQM	8.0		35.1	78.9
dispersivity, (2), PHREEQM	7.6		27.8	>34
dispersivity, 1/2 dolomite, (1), PHREEQM	7.8	4.3	34.6	77.7
Low CEC, (1)	8.2		33.7	68.8
Low CEC, (2)	7.9		26.2	>500
Low CEC, 1/2 dolomite, (1)	8.0	4.8	33.2	67.6
High CEC, (1)	10.7		31.3	62.6
High CEC, (2)	10.4		24.3	488.2
High CEC, 1/2 dolomite, (1)	10.5	0.0	30.9	61.6
High CEC, 1/2 dolomite, (2)	10.2	0.0	24.0	480.2
CO_2, log pCO_2 = -0.9865, (1)	7.3		32.5	61.9
CO_2, log pCO_2 = -0.9865, (2)	7.1		25.5	>500
CO_2, log pCO_2 = -0.9865, 1/2 dolomite, (1)	6.9	4.5	31.8	60.4
Low CEC, no rhodo., (1)	13.8			37.7
Low CEC, no rhodo., (2)	13.0			305.3
Low CEC, no rhodo., 1/2 dolomite, (1)	13.6	4.9		37.0
Low CEC, no rhodo., 1/2 dolomite, (2)	12.8	4.9		299.6
High CEC, (3)	11.4		38.0	76.0
High CEC, 1/2 dolomite, (3)	11.2	0.0	37.4	74.8
High CEC, 2/3 dolomite, (3)	11.1	6.5	37.3	74.6

Allowing kaolinite to precipitate instead of $Al(OH)_3$ resulted in slightly lower retardation factors for the calcite and rhodochrosite dissolution fronts (Table 12). In contrast, the R values obtained for the final kaolinite dissolution front were generally much greater than those obtained for the final $Al(OH)_3$ dissolution front. These effects were both due to the greater stability of kaolinite in the presence of acidic water.

Comparison of the reactive transport simulation results with observations at the Pinal Creek site. Although ground water samples at the Pinal Creek site have been collected and analysed by the U.S. Geological Survey since 1984 until now (1996), the large scale of the basin and of the contaminant plume, and limited financial resources, have prevented the emplacement of a large density of wells. The sparseness of the available spatial information have made it difficult to determine the exact location and especially the movements of the low-pH and high-Fe(II) ground waters (Fig. 14). The width of the fronts (and especially of the Fe(II) front), which might give valuable information on reaction kinetics, has also been difficult to determine exactly.

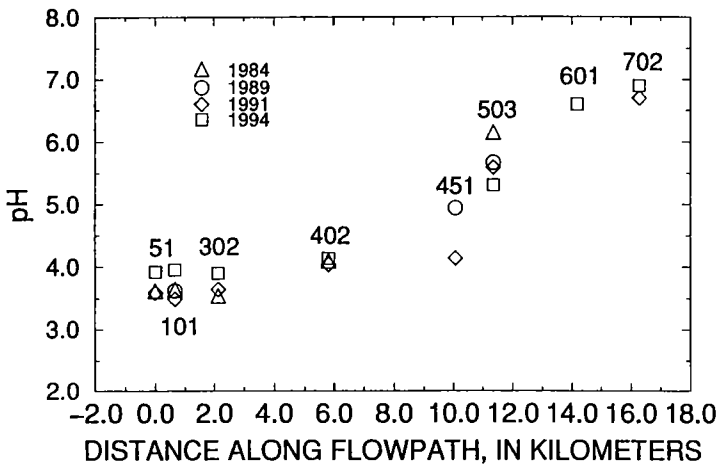

Figure 14. pH profiles along an aquifer flowpath based on the most contaminated wells in the Pinal Creek alluvial aquifer. Well 451 was emplaced in December 1988 and torn away during the floods of spring 1993, and therefore only January 1989 and November 1991 pH data are presented for that well. Note the large pH decrease at well 451 between those dates (actually, most of the decrease occurred between March and August 1989).

Nevertheless some estimates of the velocity of the low-pH front can be made, primarily because the breakthrough of low-pH waters (from a pH of 4.96 in March 1989 to a pH of 4.24 in August 1989) was observed at well 451 only a few months after its emplacement (December 1988). If we assume that the creation of Webster Lake in 1940, approximately 18.5 km upgradient from well 451 provided the principal source of acidic contaminated waters, then an effective velocity of about 1 m/day can be estimated for the low-pH front over that section of the aquifer. This velocity can be compared to an estimated average ground-water velocity of 8.4 m/day between Webster Lake and well 451, giving an estimated retardation factor of about 8.4 for the movement of the low-pH waters. This retardation factor estimate is thought to be a maximum estimate, because the applicable ground water velocity could actually be as low as 5 m/day. Eychaner (1991) and Glynn et al. (1991) estimated that a lower value of R of 5 would be reasonable for the movement of the pH front from Webster Lake to well 451.

Similarly, a low-pH (4.0 to 4.5) high-Fe(II) water was found to be already present during drilling (in February 1995) of a group of wells (LPC wells) emplaced by the Pinal Creek Group (a consortium of copper companies) slightly west of well 503 (on the other side of the creek bed). Given the distance of the LPC wells downgradient from well 451 (1.3 km), the minimum velocity of the low-pH front is estimated to be greater than 0.65

m/day. Comparing this velocity with an estimated average ground-water velocity of about 5 m/day (between 451 and 503) results in a maximum retardation factor of about 7.7 for the velocity of the low-pH front (between well 451 and the LPC well site). The acidity of the well 451 water in August 1989 was ~2 times lower than that of the well 402 water used in our simulations, although the potential acidity (see discussion of Table 7) of the well 451 water did increase with time until a maximum acidity, ~1/3 lower than that of well 402, was reached in November 1991.

In comparison to this field evidence, results of a column elution experiment conducted by Stollenwerk (1994), using water from well 51 (of composition similar to that presented in Table 7), indicated that the velocity of the low-pH front was about 2.5 times slower than that of the water. Many factors can explain the approximately 3 times lower retardation factor found in the column experiment, relative to the field-determined values. The pH front retardation factors estimated from the field evidence incorporate significant effects of dilution (Figs. 3 and 4, Table 7), which also are not accounted for in our transport simulations. The acidity of the initial solutions used in determining those retardation factors also needs to be taken into account if comparisons are to be made. The Webster Lake waters were certainly more acidic than those of well 51 used in Stollenwerk's column experiment. The potential acidity of the well 51 water was 4.5 times greater than that of the well 402 water used in our simulations. As a result, the retardation factor of 2.5 determined by Stollenwerk (1994) should translate to an retardation factor of approximately 7.8, $(2.5 - 1) \times 4.5 + 1 = 7.75$, had well 402 water been used in his column experiments. Equation (15) is used to crudely normalize these results, assuming that *DM* is proportional to the acidity of the low-pH solution and that the field and laboratory experiments both had identical homogeneous mineral concentrations and reactions. Similarly, considering that the water from well 451 in August 1989 was about 2 times less acidic than the water used in our simulations, the retardation factor of 7.7 determined between 451 and the LPC site would correspond to an *R* value of 4.35, if normalized to the acidity of the well 402 water (89/1/12). Comparing these normalized retardation factors (4.4 and 7.8) with the *R* values reported for the rhodochrosite dissolution front in Table 9, in the simulations without irreversible dissolution of Ca- and Mg-silicates, indicates that initial carbonate mineral concentrations between 2.1×10^{-2} and 4.2×10^{-2} mol/kg H_2O and certainly no lower than 1.05×10^{-2} mol/kg H_2O would give reasonable simulated retardation factors. This assumes that an MnO_2 concentration of 2×10^{-2} mol/kg H_2O was also reasonable. A lower MnO_2 concentration would result in a higher CMR ratio and therefore could increase the simulated retardation factors. Consequently, initial carbonate concentrations would have to be adjusted slightly downward in order to match the estimated lab and field retardation factors. A higher MnO_2 concentration would probably not, however, have any significant effect on the simulated pH front *R* values (for initial carbonate mineral concentrations between 1.05×10^{-2} and 3.0×10^{-2} mol/kg H_2O).

In the simulations with Ca- and Mg-silicate dissolution, the retardation factors for the rhodochrosite front are so high that an initial carbonate concentration of 5.25×10^{-3} or lower would have to be used to match the observed retardation of the pH front in Stollenwerk's experiments and in the field, if we assume that the disappearance of rhodochrosite controls the low-pH front. Such a low initial carbonate concentration is not really realistic given our knowledge of the alluvial sediments at the site, and we therefore conclude that the simulations with irreversible dissolution of Ca- and Mg-silicate should probably be conducted again using a finite (as opposed to an inexhaustible) source of these silicates. Further field information on the concentration, and on the rate of dissolution of silicate minerals at the Pinal Creek site, will however be needed. We note however, that the calcite *R* values obtained in our forward simulations of inverse Model 2 (Table 5), were reasonable but only for initial calcite concentrations below 4.2×10^{-2} mol/kg H_2O. The

disappearance of calcite did not by itself, however, result in a sufficient pH decrease to match the pH 4.0 to 4.5 values (or lower) that we associate with the pH "front" in the field (Fig. 14).

The question of which secondary aluminum phase actually precipitates out, and its rate of redissolution, are also important considerations. Table 8 shows that the most acidic waters (below a pH of 5) can only be obtained if $Al(OH)_3$ is not present (or if its rate of dissolution is slow relative to the movement of the water). If we assume that it is present and that the Local Equilibrium Assumption is reasonable, then our simulations show that initial carbonate concentrations would have to be lower than 3.0×10^{-2} mol/kg H_2O to match the retardation of the pH front observed in the field and in Stollenwerk's laboratory columns.

There has been until now, to our knowledge, no direct observation of the breakthrough of the high-Fe(II) waters at the Pinal Creek site. Waters from wells 451 and the LPC site (near 503) were already found to have high Fe(II) concentrations during the emplacement of those wells (in November 1991 and February 1995 respectively). The fact that dissolved Fe(II) was present at well 451 before the low-pH breakthrough suggests that the Fe(II) front is moving faster than the low-pH front, or at least had progressed further than the low-pH front until that point in time. If we again use the creation of Webster Lake as an initial condition, retardation factors between 5 and 8.4 can be estimated for the high-Fe(II) front, between Webster Lake and well 451. Similarly, the evidence based on data from well 451 and from the LPC well site also suggests a maximum retardation factor of 7.7 over that section of the aquifer. The latter factor is equivalent to a maximum retardation factor of about 3.2 in our simulations, after having corrected for the three times higher Fe(II) concentration of well 402 relative to that of well 451 (in August 1989).

In his laboratory column experiments, Stollenwerk (1994) observed retardation factors of approximately 2 for the high-Mn(II) spike, and 2.5 for the high-Fe(II) front (Fig. 10 gives an example of a dispersion-affected Mn(II) spike and of the associated Fe(II) front). The lag in the Fe(II) front suggests that the rate of $Fe(OH)_3$ precipitation was delayed relative to the rate of MnO_2 dissolution. Normalizing those retardation factors to an infilling solution with 4.7 times less dissolved Fe(II) (for well 402) results in equivalent retardation factor of between 5.7 and 8.1.

Therefore, after normalization to the infilling water used in our simulations, the field and laboratory determined retardation factors for the high-Fe(II) front encompass a range of about 3.2 to 8.1. This range compares favorably with the retardation factor of 4.7 determined for most of the simulations presented here. Furthermore, although the MnO_2 dissolution front may be moving a little bit faster than that of the low-pH waters, according to field and laboratory observations, it probably is not moving much faster, and therefore the CMR ratio is probably close to 3/2.

The pH values determined for the various pH-plateaus in our simulations (Table 8, Figs. 11, 12, 13) are within the range of the values observed in the field (Fig. 14) and therefore the belief expressed in our simulations that the complete dissolution of secondary rhodochrosite occurs after the dissolution of calcite and is accompanied by a significant decrease in pH (in the absence of $Al(OH)_3$) is not inconsistent with the field evidence.

CONCLUSIONS

The basic theory and assumptions of inverse geochemical modeling were presented. Although much less commonly used than reactive transport modeling, particularly in investigations of ground-water contamination, inverse geochemical modeling can provide a

powerful tool in such investigations by helping the user identify the possible reactions that may be affecting the chemical and isotopic evolution of contaminated ground waters. This information can then be incorporated into a geochemical transport model and used to conduct a sensitivity analysis on the transport of various reactive contaminants of concern, as a function of the reaction models identified earlier by inverse modeling. This approach was demonstrated for the case of a site of acidic heavy-metal ground-water contamination in the Pinal Creek Basin, Arizona. The interactive inverse geochemical modeling code NETPATH was first used to construct a series of inverse models that quantified observed differences in chemical composition between an initial acidic Fe(II)-rich water and an evolutionary, partially-neutralized Fe(II)-poor water, according to sets of postulated reactions. Each inverse model created was proposed and evaluated according to our knowledge of the geochemistry of the aquifer and according to our knowledge of the thermodynamic and kinetic feasibility of its reactions. Once an apparently suitable and irreducible set of inverse models had been identified, the PHREEQC inverse modeling code was used to further refine and evaluate our set of possible inverse models. Unlike NETPATH, PHREEQC takes account of uncertainties in the analytical data and additionally maintains alkalinity-balance, charge-balance and water-balance constraints in its solution of possible inverse models.

Inverse modeling with NETPATH and with PHREEQC allowed us to quantify the reaction processes responsible for the evolution of an acidic Fe(II)-rich ground water into a partially neutralized Fe(II)-poor water at the Pinal Creek site. The principal reaction processes appear to be the reductive dissolution of solid MnO_2 by aqueous Fe(II), the consequent precipitation of $Fe(OH)_3$, the dissolution of calcite and/or dolomite, the precipitation of an aluminum phase, $Al(OH)_3$ or $AlOHSO_4$, and the possible precipitation of chalcedony. Results of the inverse modeling simulations also led us to conclude that:

(1) Ca- and Mg-silicate dissolution must be an important process during the neutralization of the low-pH waters, given that CO_2 exsolution probably does not occur.

(2) Dilution of the acidic ground waters does occur and can be quantified using Cl, Na and SO_4 concentrations as conservative constituents, constituents that do not undergo significant heterogeneous mass-transfer reactions. The PHREEQC models revealed that SO_4 could be considered a conservative constituent given its associated analytical uncertainty.

(3) Rhodochrosite precipitation (or possibly an MnO_2-$Mn(OH)_3$ electron-transfer or Mn^{2+} sorption mechanism) must be responsible for the lower than expected increase in dissolved Mn(II) concentrations caused by the aqueous Fe(II) reduction of MnO_2 solids.

After a brief review of the status of reactive transport modeling at the Pinal Creek site, the results of some new forward simulations were presented. These geochemical transport simulations explored the effect of the reactions identified through the previous inverse modeling simulations, and also of reactions previously mentioned by other researchers, on the chemical evolution of an acidic Fe(II) rich water from the Pinal Creek site. The purpose of the PHREEQC and PHREEQM transport simulations was to determine the relative rates of movement of the Fe(II)-rich and low-pH ground waters and to determine how the retardation of these contaminated waters was affected by the various postulated reaction processes.

The only factors affecting the retardation of the Fe(II)-rich waters and the propagation of the MnO_2 dissolution front in our simulations were the initial specified concentration of MnO_2 and the concentration of Fe(II) in the inflowing contaminated water. As we

demonstrated, the rate of movement of the MnO_2 front could have easily been calculated by hand, but only in the absence of ion-exchange or other processes affecting the Fe(II) concentration of the inflowing water. Simulations conducted with a high ion-exchange capacity of 10 meq/100g resulted in a doubling of the retardation factor for the MnO_2 dissolution front.

The propagation of the various pH fronts caused by the complete dissolution of carbonate and aluminum minerals could not, however, have been so easily predicted. The use of a geochemical transport code such as PHREEQM or PHREEQC does seem to be required to determine the retardation factors applicable to each mineral dissolution front. The initial amount of carbonate (calcite and/or dolomite) specified in each simulation was the primary factor determining the movement of the low-pH waters. Other important factors were: the ratio of initial carbonate to initial MnO_2, the type of Al phase allowed to precipitate, and whether or not rhodochrosite was allowed to precipitate. High initial carbonate to MnO_2 ratios, allowing rhodochrosite precipitation and allowing $AlOHSO_4$ precipitation instead of $Al(OH)_3$ precipitation resulted in higher retardation factors for the movement of the low-pH waters. Allowing the irreversible dissolution of Ca- and Mg-silicates so as to match the mass-transfer amounts determined in a few of our inverse models, resulted in unrealistically high retardation factors for the rhodochrosite and $Al(OH)_3$ dissolution fronts, although the retardation factors determined for the calcite dissolution front were reasonable. More field and laboratory information is required on the abundance and rates of reaction of these silicate minerals if more "realistic" transport simulations are to be conducted.

Inclusion of ion-exchange processes did not have a significant effect on the movement of the pH fronts at low cation exchange capacities (1 meq/100g) but did have a significant effect at higher cation exchange capacities (10 meq/100g). Because of surface-protonation, allowing surface-complexation reactions generally resulted in higher retardation factors for the carbonate and $AlOHSO_4$ dissolution fronts. Allowing equilibrium with a pCO_2 of $10^{-0.9865}$ resulted in lower retardation factors for the carbonate and $Al(OH)_3$ dissolution fronts particularly at initial carbonate concentrations greater than 3×10^{-2} mol/kg H_2O. Allowing equilibrium with a lower fixed pCO_2 of $10^{-1.33}$ resulted instead in generally higher retardation factors for the carbonate and $Al(OH)_3$ dissolution fronts. Simulation of longitudinal dispersion was not an important factor controlling the movement of the calcite and rhodochrosite disssolution fronts except at very low initial carbonate concentrations. Longitudinal dispersion would also have had an effect on the rate of movement of the Fe(II)-rich waters at very low initial MnO_2 concentrations had such simulations been conducted. Including dolomite in addition to calcite in the background aquifer, and allowing kaolinite to precipitate instead of $Al(OH)_3$ did not significantly affect the propagation of the low-pH fronts associated with the dissolution of calcite and rhodocrosite.

Identifying knowledge gaps and critical data needs, preventing us from more accurately determining the identity and importance of the reactions occurring at the Pinal Creek site, was one of the most important results of the inverse and reactive transport modeling simulations conducted in this paper.

A preliminary comparison of the retardation factors for the low-pH and high-Fe(II) fronts determined in our local equilibrium simulations with retardation factors estimated from field evidence and from Stollenwerk's (1994) laboratory column elution tests suggests that an initial carbonate concentration between 2.1×10^{-2} and 4.2×10^{-2} mol/kg H_2O may be reasonable and that the initial MnO_2 concentration of 2×10^{-2} mol/kg H_2O used in our simulations was also reasonable. Finally, pH values obtained during the course of our local equilbrium simulations are reasonable given the pH values observed in the field.

The retardation factors determined for the mineral dissolution fronts as a result of our various simulations will be of use not only in estimating the rate of movement of the low-pH and high-Fe(II) ground waters at the Pinal Creek site, but will also be useful in identifying the most important chemical parameters controlling the movement of these contaminated waters. The results of our simulations also may provide information on the possible rate of movement of acidic metal-rich waters at other similar ground-water contamination sites, after adjustments are made for the pH and dissolved metal (Al, Fe, Mn) concentrations in the contaminated waters and for the mineralogical characteristics of the particular site.

This paper presents and demonstrates an approach for the investigation of the evolution and movement of contaminated ground waters: the use of inverse geochemical modeling to identify important possible reaction processes, followed by geochemical transport simulations that incorporate the possible reactions previously determined and a range of possible aquifer characteristics. Such an approach results in an improved understanding of the processes that may control the future evolution of contaminated ground waters. This information may then lead to better predictability of the transport of highly reactive contaminants and may be used for more effective mitigation of contaminated ground waters at sites with sparse spatial information.

How to obtain U.S. Geological Survey computer codes and the PHREEQM code

The latest USGS gechemical codes can be obtained by anonymous ftp to the following internet site, brrcrftp.cr.usgs.gov, or may be obtained along with other USGS hydrologic modeling codes, via the World Wide Web (WWW) at URL http://h2o.usgs.gov/software, or by anonymous ftp to h2o.usgs.gov. Codes and documentation may also be ordered from U.S. Geological Survey, Branch of Information Services, Box 25286, Denver CO, 80225-0286 (*Telephone:* 303 202-4700, *Fax:* 303 202-4693). PHREEQM may be purchased for a modest fee from: A.A. Balkema Publishers, P.O. Box 1675, 3000 BR Rotterdam, The Netherlands (*Fax:* 31-10-4135947).

ACKNOWLEDGMENTS

We are deeply grateful to David Parkhurst for helping us understand the power and intricacies of inverse modeling with his latest very powerful geochemical code, PHREEQC. We also greatly appreciate the extensive help of Joseph Vrabel, who conducted many of the reactive transport simulations presented in this paper. We extend our sincere appreciation to Carl Steefel, Eric Oelkers and Don Thorstenson, who managed to review this paper on very short notice and still provided very significant comments that led to distinct improvements in the paper. Finally, I thank Paul Ribbe for his patience and skill in editing this manuscript.

REFERENCES

Appelo CAJ, Willemsen A (1987) Geochemical calculations and observations on salt water intrusions I. A combined geochemical/mixing cell model. J Hydrol 94:313-330

Appelo CAJ, Postma D (1993) Geochemistry, groundwater and pollution. A.A. Balkema, Rotterdam, The Netherlands, 536 p

Breeuwsma A, Wösten JHM, Vleeshouwer JJ, Van Slobbe AM, Bouma J (1986) Derivation of land qualities to assess environmental problems from soil surveys. Soil Sci Soc Am J 50:186-190

Brown JG (1996) Movement of metal contaminants in ground water in the Pinal Creek basin, Arizona: Model assessment and simulation of reactive transport, MSc Thesis, Dept Hydrology and Water Resources, Univ Arizona, Tucson, 236 p

Brown JG, Harvey JW (1994) Hydrologic and geochemical factors affecting metal-contaminant transport in Pinal Creek basin near Globe, Arizona. In: Morganwalp DW, Aronson DA (eds) U S Geol Surv Toxic Substances Hydrology Program—Proc Technical Mtg, Colorado Springs, CO, September 20-24, 1993: U. S Geol Surv Water Resources Invest Rpt 94-4015 (in press)

Davis JA, Kent DB (1990) Surface complexation modeling in aqueous geochemistry. In: Mineral-Water Interface Geochemistry, Hochella MF Jr, White AF (eds) Rev Mineral 23:177-260

Dria MA, Bryant SL, Schechter RS, Lake LW (1987) Interacting precipitation dissolution waves: the movement of inorganic contaminants in groundwater. Water Resources Res 23:2076-2090

Dzombak DA, Morel FMM (1990) Surface Complexation Modeling: Hydrous Ferric Oxide. Wiley & Sons, New York, 393 p

Engesgaard P, Kipp (1992) A geochemical transport model for redox-controlled movement of mineral fronts in groundwater flow systems: a case of nitrate removal by oxidation of pyrite. Water Resources Res 28:2829-2843

Eychaner JH (1989) Movement of inorganic contaminants in acidic water near Globe, Arizona, In: Mallard GE, Ragone SE (eds) U S Geol Surv Toxic Substances Hydrology Program—Proc Technical Mtg, Phoenix, Arizona, September 26-30, 1989: U S Geol Surv Water Resources Invest Rpt 89-4220:567-575

Eychaner JH (1991) The Globe, Arizona, research site—Contaminants related to copper mining in a hydrologically integrated environment. In: Mallard GE, Aronson DA (eds) U S Geol Surv Toxic Substances Hydrology Program—Proc Technical Mtg, Monterey, California, March 11-15, 1991: U S Geol Surv Water Resources Invest Rpt 91-4034:475-480

Eychaner JH, Stollenwerk KG (1985) Neutralization of acidic ground water near Globe, Arizona, In: Schmidt KD (ed) Groundwater Contamination and Reclamation. Proc of a Symposium, Tucson, Arizona, August 14-15, 1985. Bethesda, Maryland: Am Water Resources Assoc p 141-148

Ficklin WH, Love AH, Papp CSE (1991) Solid-phase variations in an aquifer as the aqueous solution changes, Globe, Arizona, In: Mallard GE, Aronson DA (eds), U S Geological Survey Toxic Substances Hydrology Program - Proc Technical Mtg, Monterey, California, March 11-15, 1991: U S Geol Surv Water Resources Invest Rpt 91-4034:475-480

Glynn PD (1991) Effect of impurities in gypsum on contaminant transport at Pinal Creek, Arizona In: Mallard GE, Aronson DA (eds), U S Geol Surv Toxic Substances Hydrology Program - Proc Technical Mtg, Monterey, California, March 11-15, 1991: U S Geol Surv Water Resources Invest Rpt 91-4034:466-474

Glynn PD, Engesgaard P, Kipp KL (1991) Use and limitations of two computer codes for simulating geochemical mass transport at the Pinal Creek toxic-waste site, In: Mallard GE, Aronson DA (eds) U S Geol Surv Toxic Substances Hydrology Program—Proc Technical Mtg, Monterey, California, March 11-15, 1991: U S Geol Surv Water Resources Invest Rpt 91-4034:454-460

Glynn PD, Busenberg E (1994a) Dissolved gas and chlorofluorocarbon content of ground waters in the Pinal Creek Basin, Arizona. In: Morganwalp DW, Aronson DA (eds), U S Geol Surv Toxic Substances Hydrology Program—Proc Technical Mtg, Colorado Springs, CO, September 20-24, 1993: U S Geol Surv Water Resources Invest Rpt 94-4015 (in press)

Glynn PD, Busenberg E (1994b) Unsaturated zone diffusion of carbon dioxide and oxygen in the Pinal Creek Basin, Arizona. In: Morganwalp DW, Aronson DA (eds) U S Geol Surv Toxic Substances Hydrology Program—Proc Technical Mtg, Colorado Springs, CO, September 20-24, 1993: U S Geol Surv Water Resources Invest Rpt 94-4015 (in press)

Hill M (1992) A computer program (MODFLOWP) for estimating parameters of a transient, three-dimensional, ground-water flow model using nonlinear regresssion.U S Geological Survey Open-File Report 91-484, 358 p

Hydro Geo Chem Inc. (1991) Investigation of acid water contamination along Miami Wash and Pinal Creek, Gila County, Arizona: Claypool, Arizona, Cyprus Miami Mining Corporation, 140 p

LeBlanc DR (1984) Sewage plume in a sand and gravel aquifer, Cape Cod, Massachusetts. U S Geological Survey Water Supply Paper 2218, 28 p

Lichtner PC (1985) Continuum model for simultaneous chemical reactions and mass transport in hydrothermal systems. Geochim Cosmochim Acta 49:779-800

Lichtner PC (1988) The quasi-stationary state approximation to coupled mass transport and fluid-rock interaction in a porous medium. Geochim Cosmochim Acta 52:143-165

Lind CJ, Stollenwerk KG (1994) Alteration of alluvium of Pinal Creek, Arizona by acidic ground water resulting from copper mining. In: Morganwalp DW, Aronson DA (eds), U.S. Geological Survey Toxic Substances Hydrology Program - Proc Technical Mtg, Colorado Springs, CO, September 20-24, 1993. U S Geol Surv Water Resources Invest Rpt 94-4015 (in press)

Mackay DM, Freyberg DL, Roberts PV, Cherry JA (1986) A natural gradient experiment on solute transport in a sand aquifer—1. Approach and overview of plume movement. Water Resources Res 22:2017-2029

Neaville CC, Brown JG (1993) Hydrogeology and hydrologic system of Pinal Creek Basin, Gila County, Arizona. U S Geol Surv Water Resources Invest Rpt 93-4212

Nordstrom DK, Plummer LN, Langmuir D, Busenberg E, May HM, Jones BF, Parkhurst DL (1990) Revised chemical equilibrium data for major water-mineral reactions and their limitations. In: Melchior DC, Bassett RL (eds), Chemical Modeling in Aqueous Systems II, Am Chem Soc Symp Series 416:398-413

Ortoleva P, Auchmuty G, Chadam J, Hettmer J, Merino E, Moore CH, Ripley E (1986) Redox front propagation and banding molalities. Physica 19D:334-354

Parkhurst DL, Plummer LN, Thorstenson DC (1982) BALANCE—A computer program for geochemical calculations. U S Geol Surv Water Resources Invest Rpt 82-14

Parkhurst DL, Plummer LN (1993) Geochemical models. In: Alley WM (ed) Regional Ground-Water Quality. Van Nostrand Reinhold, New York, Chapter 9:199-225

Parkhurst DL (1995) User's guide to PHREEQC—A computer program for speciation, reaction-path, advective-transport, and inverse geochemical calculations. U S Geol Surv Water Resources Invest Rpt 95-4227

Parkhurst DL (1996) Including uncertainties in geochemical mole-balance modeling. (In preparation)

Petersen NP (1962) Geology and ore deposits of the Globe-Miami district, Arizona. U S Geol Surv Prof Paper 342, 151 p

Pollock DW (1989) Documentation of computer programs to compute and display pathlines using results from the U.S.Geological Survey modular three-dimensional finite-difference ground-water flow model. U S Geol Surv Open File Report 89-381, 188 p

Plummer LN, Parkhurst DL, Thorstenson DC (1983) Development of reaction models for ground-water systems. Geochim Cosmochim Acta 47:665-686

Plummer LN, Prestemon EC, Parkhurst DL (1991) An interactive code (NETPATH) for modeling Net Geochemical Reactions along a flow path. U S Geol Surv Water Resources Invest Rpt 91-4078

Ransome FL (1903) Geology of the Globe copper district, Arizona. U S Geol Surv Prof Paper 12, 168 p

Revesz K, Coplen TB, Baedecker MJ, Glynn PD, Hult M (1995) Methane production and consumption monitored by stable H and C isotope ratios at a crude oil spill site, Bemidji, Minnesota. Applied Geochem 10:505-516

Robertson FN (1991) Geochemistry of ground water in alluvial basins of Arizona and adjacent parts of Nevada, New Mexico, and California. Regional Aquifer-System Analysis-Southwest Alluvial Basins, Arizona and Adjacent States. U S Geol Surv Prof Paper 1406-C.

Stollenwerk KG, Eychaner JH (1987) Acidic ground water contamination from copper mining near Globe, Arizona. In: Franks BJ (ed) U S Geol Surv Toxic Substances Hydrology Program—Proc of the 3rd technical meeting, Pensacola, Florida, March 23-27, 1987: U.S. Geol Surv Open File Report 87-109:D19-D24

Stollenwerk KG (1994) Geochemical interactions between constituents in acidic groundwater and alluvium in an aquifer near Globe, Arizona. Applied Geochem 9:353-369

Tolle S, Arthur GV (1991) Aquifer restoration under the clean water act. In: Mallard GE, Aronson DA (eds), U.S. Geological Survey Toxic Substances Hydrology Program—Proc Technical Mtg, Monterey, California, March 11-15, 1991: U S Geol Surv Water Resources Invest Rpt 91-4034:520-523

Winograd IJ, Robertson FN (1982) Deep oxygenated ground water: anomaly or common occurrence? Science 216:1227-1230